REMOVAL OF NICKEL, CYANIDE, AND ETHYLENE DIAMINE TETRAACETIC ACID FROM ELECTROPLATING WASTEWATER BY IRON MEDIA: MECHANISM AND APPLICATION

A Dissertation

by

CHENG ZHANG

Submitted to the Graduate and Professional School of
Texas A&M University
in partial fulfillment of the requirements for the degree of

DOCTOR OF PHILOSOPHY

Chair of Committee,	Yongheng Huang
Committee Members,	Kung-Hui Chu
	Xingmao Ma
	Zong Liu
Head of Department,	John Tracy

May 2022

Major Subject: Biological and Agricultural Engineering

Copyright 2022 Cheng Zhang

ABSTRACT

This study presented and discussed the results from batch and continuous flow experiments of nickel, cyanide, and Ethylene Diamine Tetraacetic Acid (EDTA) treatment using iron-based media. The removal mechanisms of all three contaminants have been investigated. The activated iron media (AIM) system can be further applied to the electroplating wastewater treatment for the removal of nickel, cyanide, and EDTA.

Nickel removal is possible for both the Zero-Valent Iron (ZVI) and AIM systems. The removal mechanism in the ZVI system is mostly contributed by the reductive reaction. Fe^0 on the iron particle surface reduces the dissolved Ni^{2+} ions to insoluble Ni^0, while oxidizes itself and releases as Fe^{2+}. In the AIM system, it is the replacement reaction that dominates the removal mechanism. The labile Fe(II) from surface CPs are substituted by dissolved Ni^{2+} ions resulting in the change of the FeO_x structure. The X-Ray Photoelectron Spectroscopy (XPS) and X-Ray Diffraction (XRD) spectra of the sediments indicated the detection of Ni^0 in the ZVI system and the formation of $NiFe_2O_4$ (trevorite) in the AIM system. These evidences support the reductive and replacement mechanisms, which also agreed with the difference in final dissolved Fe^{2+} concentration in the two systems. The results of the continuous batch and Continuous Stirred-Tank Reactor (CSTR) experiments show that the AIM system was sustainable and more efficient than the ZVI system. Therefore, the AIM system would be a robust and time-tested treatment procedure for nickel removal.

The removal of cyanide was not preferable in anoxic condition. In the iron-precipitation process, cyanide forms ferrocyanide with dissolved Fe^{2+} and further to

insoluble ferrous ferrocyanide. However, the process is reversible and the sediments are unstable. The anion exchange procedure allows cyanide ions to exchange with ions in iron media, which reduced the aqueous cyanide concentration. The cyanide ions, whereas can be exchanged back to the solution by ions with higher binding affinity. Therefore, this process is hard to operate and maintained. Cyanide treatment can be feasible in the oxic environment. The oxic AIM system can produce a notable amount of hydroxyl radicals, which oxidized cyanide. Cyanide and iron-chelated cyanide can be converted to nitrogen gas step by step. With the quantification of the intermediate products (ferricyanide, cyanate, and ammonia) and comparison of the inhibited system, the AIM system was proven to treat cyanide irreversibly with no other reagent needed. The continuous batch test further implied the reliability, efficiency, and sustainability of the system. Therefore, the oxic AIM system would be a trustworthy treatment procedure for cyanide-containing wastewater.

EDTA can be removed by the adsorption process in both ZVI and AIM systems. In the anoxic environment, only a certain amount of EDTA can be adsorbed due to the limited surface loading of both media. It is not sustainable and reliable. EDTA treatment is feasible in the oxic AIM system by the oxidative process. Hydroxyl radicals, produced in the oxic AIM system, are able to break down the long-chain EDTA molecule to the smaller molecule products. The detection of iminodiacetic acid (IMDA), nitrilotriacetic acid (NTA), glycine, and ammonia has proved that EDTA was degraded through the 'glycine's pathway' during the process. Additional H_2O_2 injection leads to the efficiency improvement of the EDTA treatment in the oxic AIM system. H_2O_2 performs Fenton

reactions with dissolved Fe^{2+} in the system, which expedites the hydroxyl radical's production. In the H_2O_2-AIM system, the final EDTA removal was increased. The continuous batch experiment proves the H_2O_2-AIM has higher removal efficiency than AIM itself. Therefore, the H_2O_2-AIM system would be a possible treatment procedure for wastewater containing EDTA.

The reduction of cyanide and EDTA were nearly unaffected when they combined with nickel. However, due to the strong chelating effect with EDTA, the nickel treatment was limited. The addition of H_2O_2 accelerates the decomposition of cyanide and EDTA, which consequently improves nickel treatment. In the H_2O_2-AIM system, with the increased amount of additional H_2O_2, the dissolved nickel concentration dropped faster than it in the AIM-only system. The continuous batch and CSTR experiment proved the H_2O_2-AIM system can simultaneously treatment of nickel, cyanide, and EDTA. Therefore, the H_2O_2-AIM system can be a reliable and sustainable process for simultaneous treatment of nickel, cyanide, and EDTA in industrial wastewater.

ACKNOWLEDGMENTS

I would like to express my deepest appreciation to my advisor and committee chair, Dr. Yongheng Huang for accepting me as his student, guiding me throughout the whole research. Without his enormous support and profound understanding, my doctoral study and this dissertation would not be possible. His comprehensive knowledge in this field brings me a unique experience of innovative technology.

I would also like to thank the other members of my committee, Dr. Kung-Hui Chu, Dr. Xingmao Ma, and Dr. Zong Liu for their advice and support throughout the course of this research.

I wish to thank Dr. Joseph H. Reibenspies in the X-ray Diffraction Laboratory, Dr. Yordanos Birsrat, and Dr. Jing Wu in Material Characterization Facility. Their help and assistance for XRD, SEM, and XPS analysis bring great benefits to my study.

I want to express my thanks to Ashlea P. Schroeder, Cheryl L. Yeager, and Stormy Kretzschmar for their effort to perfectly maintain my record. I may have been missed a lot of things without your reminder and forwarded information.

Thanks also go to my all friends, colleagues, faculty, and staff from our department and the Graduate and Professional School for this great experience during my time here at Texas A&M University.

Finally, thanks to my parents for their encouragement. Furthermore, I dedicate this dissertation to my beloved wife, Vivi. Without her company, support, and endless love, this could not be done.

NOMENCLATURE

$\cdot OH$	Hydroxyl Radicals
μM	microMolar
AIM	Activated Iron Media
BET	Brunauer, Emmett, and Teller
$C_6H_5CO_2H$	Hydroxybenzoic Acid
Ca^{2+}	Calcium Ion
Cd^{2+}	Cadmium Ion
Cl^-	Chloride Ion
Cl_2	Chlorine Gas
CN^-	Cyanide Ion
$CNCl_2$	Cyanogen Chloride
Cr^{6+}	Chromium Ion
CSTR	Continuous Stirred-Tank Reactor
CT	Carbon Tetrachloride
Cu^{2+}	Copper Ion
d	Day(s)
DDI	Deoxygenated Deionized
DI	Deoxygenated Deionized
EDTA	Ethylenedinitrilotetraacetic Acid
Fe^0	Zero-Valent Iron
Fe^{2+}	Ferrous Iron

Fe^{3+}	Ferric Iron
$Fe(CN)_6^{3-}$	Ferricyanide Ion
$Fe(CN)_6^{4-}$	Ferrocyanide Ion
$Fe_2Fe(CN)_6$	Ferrous Ferrocyanide
$Fe_4[Fe(CN)_6]_3$	Ferric Ferrocyanide
Fe_3O_4	Magnetite
$Fe(OH)_2$	Ferrous Hydroxide
$FeCl_2$	Ferrous Chloride
FeOx	Iron Oxides
$FeSO_4$	Ferrous Sulfate
FE-SEM	Field Emission Scanning Electron Microscope
g	Gram(s)
h	Hour(s)
H^+	Hydrogen Ion
H_2	Hydrogen Gas
H_2O	Water
H_2O_2	Hydrogen Peroxide
HPLC	High-Performance Liquid Chromatography
H_2SO_4	Sulphuric acid
H_2SO_5	Peroxymonosulphuric acid
HRT	Hydraulic Rentention Time
IARC	International Agency of Research on Cancer

IC	Ion Chromatography
ICP-MS	Inductively Coupled Plasma Mass Spectrometry
L	Liter
mg/g	Milligrams Per Gram
mL	Milliliter
mg/L	Milligrams Per Liter
N_2	Nitrogen Gas
Na_2SO_4	Sodium Sulfate
$NaNO_3$	Sodium Nitrate
NaCN	Sodium cyanide
NF	Nanofiltration
NH_3	Ammonia
Ni^0	Zero-Valent Nickel
Ni^{2+}	Di-Valent Nickel Ion
$NiCl_2$	Nickel Chloride
$NiCl_2$	Nickel Chloride
$NiFe_2O_4$	Trevorite
$Ni(OH)_2$	Nickel Hydroxide
O_2	Oxygen Gas
O_3	Ozone Gas
OCN^-	Cyanate Ion
OH^-	Hydroxyl Ion

PCBs	Polychlorinated Biphenyls
PCE	Perchloroethene
Pd^{2+}	Lead Ion
RO	Reverse Osmosis
SO_2	Sulphur Dioxide
SO_4^{2-}	Sulfate Ion
TCE	Trichloroethylene
TiO_2	Titanium Dioxide
UF	Ultrafiltration
USEPA or EPA	U.S. Environmental Protection Agency
XPS	X-Ray Photoelectron Spectroscopy
XRD	X-Ray Diffraction
UV	Ultraviolet
UV-VIS	Ultraviolet-Visible Spectrophotometry
WAD	Weak Acid Dissociable
Zn^{2+}	Zink Iron
ZVI	Zero-Valent Iron

TABLE OF CONTENTS

Page

LIST OF FIGURES

Page

LIST OF TABLES

Page

CHAPTER I. INTRODUCTION

Water pollution caused by industrial activities is a global environmental issue, which poses a serious threat to the earth's ecosystem and human health. Wastewater of metal finishing and electroplating industry, often laden with high concentrations of various heavy metals, represents one of the most prevalent and challenging wastewater pollution sources (graBlais, Djedidi et al. 2008, Salcedo, Ballesteros et al. 2016). Depending on purpose and processes, electroplating wastewater may contain one or a mix of metal elements including Cr, Ni, Cu, Zn, Cd, As, Ag, and Pd. These heavy metals are listed among the priority pollutants around the world (Chen 2004, Barakat 2011, Fu and Wang 2011). Unlike many organic pollutants that may be degraded into non-toxic substances through biological or chemical processes over time, heavy metal elements cannot be destructed. Moreover, they are typically bio-accumulative to many organisms. When exposed to heavy metals, living organisms including humans may absorb these elements into their bodies through water intake and food consumption. Over time, the body accumulation of these metals reaches an excessive level that becomes detrimental to their health. Therefore, heavy metal discharge often causes long-term or permanent environmental damages, which are extremely difficult to reverse and remediate.

Nickel, like many other heavy metals, has both short- and long-term hazardous effects toon human health (Repo, Warchoł et al. 2013, Liu, Li et al. 2014, Al-Shannag, Al-Qodah et al. 2015, Ghaedi, Hajjati et al. 2015). In electroplating factories, supplementary reagents (i.e., metal complexing/chelating reagents, buffering chemicals, surfactants, and organics) are commonly used. Nickel often bonds with reagents like

cyanide and ethylenediaminetetraacetic acid (EDTA), forming nickel complexes that can remain soluble and chemically stable under broad conditions. These metal complexes are much more difficult to degrade or precipitate than the metal ions alone. Therefore, wastewater treatment in the electroplating industry has become one of the most challenging tasks.

Various methods have been studied extensively for the removal of nickel, cyanide, and EDTA, namely: biological degradation, chemical oxidation, adsorption, precipitation, ion exchange, and membrane filtration processes (Botz, Mudder et al. 2005, Dash, Gaur et al. 2009, Barakat 2011, Fu and Wang 2011, Coman, Robotin et al. 2013, Al-Shannag, Al-Qodah et al. 2015). Although many of these treatment techniques are suitable for nickel, cyanide, and EDTA separately, no cost-effective method is available to treat strongly-chelated nickel-cyanide-EDTA compounds in their co-presence. A very complex, multi-step system is needed for treating such a waste stream, resulting in high chemical and energy consumption. The cost for such systems is often too high. Even then, the industry often reported failures to meet discharge limits, particularly for the nickel and COD limits.

Zero-valent iron (ZVI) is an environmental-friendly material of excellent reductive capacity and relatively inexpensive cost. It was widely used to remove all kinds of pollutants including organic compounds (Lowry and Johnson 2004, Li, Li et al. 2016), inorganic anions (Sohn, Kang et al. 2006) and heavy metal ions (Yang, Shan et al. 2016). For most of the contaminant removals, ZVI can activate various reactions (i.e., redox, precipitation, and absorption) to reduce elements to their corresponding lower

toxic products. In particular, other metals can be spontaneously participated in an electrochemical process that includes the reduction of the more positive potential species by the more negative potential metal (Dries, Bastiaens et al. 2005).

The activated iron media (AIM) technology, which employs the reactivity of a mixed media of metallic iron powder along with iron oxides of designed compositions to react, transform and immobilize various contaminants, was found highly effective for removing virtually all heavy metals in free forms commonly encountered in wastewater. The effectiveness of the AIM for removing heavy metals in form of strongly-chelated metal complexes, however, has not been evaluated. How the AIM would interact with cyanide and the organic chelating reagents is not known. In light of various mechanisms and chemistries the AIM could initiate to tackle different types of contaminants, it is not unthinkable that an AIM-based system might be able to achieve simultaneous treatment of different types of contaminants (cyanide, heavy metals, and organic chelating reagents) found in electroplating wastewater.

Research Hypothesis

Most research on ZVI technologies and their use for environmental applications focus on exploiting the reductive reactivity of ZVI and the related intermediate products from the ZVI corrosion process such as H_2, aqueous Fe^{2+}, surface-bound Fe^{2+} and green rusts that may give away electrons and chemically reduce various contaminants such as nitrate, selenate, Cu^{2+}, halogenated compounds, TNT, etc. Similarly, our group's previous research has invariably centered on understanding the nature of ZVI's capability to release electrons and the roles of the iron corrosion products in facilitating

such electron transfer toward the contaminants of interest and the reductive transformation, degradation, and immobilization of these contaminants. The contaminants we previously investigated include nitrate, selenate, molybdate, Hg^{2+}, $Cu^{2,+}$ and so on, all of which can be classified as oxidant and can be reductively transformed and immobilized.

In this study, we aim to explore the potential of the AIM system as an oxidizing reactive system. We postulate that the AIM system, with ZVI as the core material and the electron-conducting magnetite-like iron oxides in form of surface coating on the ZVI grain surface or discrete particulate FeO_x crystalline, could also facilitate the formation of highly reactive radicals, particularly hydroxyl radicals under certain controlled conditions. This oxidative reactivity could be exploited and used as a novel type of advanced oxidation process (AOP) for contaminant breakdown and removal.

One direct evidence that supports our thinking was from our previous laboratory and field pilot study on using the AIM system to treat selenium-contaminated stripped sour water (SSW) of the refinery. In the stripped sour water, selenium is in form of selenocyanate ($SeCN^-$), which is a reduced form with Se in the oxidation state of -2. We discovered that in a rigorously oxygen-free AIM system, $SeCN^-$ could not be removed by the AIM. When air or O_2 was introduced into the AIM system, $SeCN^-$ could be effectively removed, for example decreasing from 10 ppm to below 0.01 ppm in 6-hour treatment. Selenium was found to be incorporated into the iron oxide structure in the forms of either Se^0 or Se^{2-}. The overall pieces of evidence suggested that $SeCN^-$ removal by the AIM involves oxidation of $SeCN^-$ before selenium was severed with CN and

incorporated into FeO_x structure. The presence of O_2 and its interaction with the AIM is responsible for the $SeCN^-$ breakdown, and removal.

Recent understandings of heterogeneous Fenton reactions also suggest the possibility of an advanced oxidation process occurring in the AIM system. Traditional Fenton reactions involve mixing H_2O_2 with aqueous Fe^{2+} or Fe^{3+} in an acidic environment to produce hydroxyl radicals ($OH\cdot$) to react with target contaminants; whereas for a heterogeneous Fenton reactive system, H_2O_2 is mixed with iron oxides in solid form (e.g., magnetite), on which H_2O_2 can be catalytically utilized to generate hydroxyl radicals. The AIM contains highly reactive iron oxides with flexible and electron-conducting structures. When H_2O_2 (or even just O_2) is introduced into the AIM system, it is not inconceivable that H_2O_2 would interact with the reactive surface and result in the production of hydroxyl radicals. These hydroxyl radicals could be used to oxidize contaminants. Therefore, the AIM system could be expanded to include an advanced oxidation process on top of other mechanisms (reductive reactivity, surface adsorption, and lattice substitution) that can be used for environmental applications.

Hence, the main hypotheses of this study are that the AIM is not only a reactive system capable of providing electrons for reductive transformation and breakdown of certain contaminants, but also capable of generating highly oxidative radicals in conjunction with supplementary oxidants such as O_2 or H_2O_2 to oxidatively transform and remove contaminants.

In the context of treating highly complicated and challenging electroplating wastewater characterized with a mix of different heavy metals, cyanides, and other chelating/supplemental reagents represented as recalcitrant organic compounds, we propose to evaluate feasibility of using a single AIM process to tackle all three key types of contaminants, i.e., heavy metals, cyanides, organic chelating compounds. In this study, we choose Ni as the target heavy metal, because Ni is considered more difficult than the other three major heavy metals Zn, Cu, Cr to be treated for compliance purposes. We choose cyanide as one of the target pollutants because it is often used as a chelating reagent in the electroplating industry. We also chose EDTA as another target compound. EDTA is one of the strongest chelating reagents used in the industry and also one of the most difficult compounds resistant to most conventional physical and chemical treatments. For nickel removal, we will focus on the mechanism of nickel removal and evaluate how and to what extent the two potential mechanisms, the direct reduction of Ni^{2+} to Ni^0 by Fe^0 ($Ni^{2+} + Fe^0 \rightarrow Fe^{2+} + Ni^0$) or incorporation of Ni^{2+} into the FeO_x structure, contribute to the removal of nickel. For cyanide and EDTA removal, we will explore the mechanism(s), kinetics, and pathways of removal by the AIM; we will evaluate factors of the AIM system affecting cyanide and EDTA removal; most importantly, how the introduction of O_2 could facilitate the treatment process.

Specifically, for nickel removal by the AIM system, we hypothesize that: Direct reduction of Ni^{2+} to Ni^0 by Fe^0 could contribute in part to the removal of nickel from water, but not adequate to decrease nickel to a low concentration in compliance with strict nickel limits. Theoretically, Fe^0 could reduce Ni^{2+} into Ni^0 in a ZVI reactive

system, but such reaction could not be completed because nickel possesses a more positive standard reduction potential (-0.24 V) than that of Fe^{2+} (-0.44 V) (Li and Zhang 2006, Dong, He et al. 2016, Li, Dong et al. 2017). Rather, lattice substitution of Ni^{2+} into the structure of the FeO_x in the AIM is responsible for achieving low nickel concentration in the treated wastewater.

For cyanide removal, we postulate that introduction of O_2 into the AIM reactive system could significantly accelerate cyanide removal through the production of highly reactive radicals that oxidize CN^- to OCN^-, which further breakdown to carbonate and NH_4^+. We will evaluate the capability of the AIM system to directly break apart the Ni-CN complex and remove both Ni^{2+} and CN^- simultaneously.

For EDTA removal, similar to cyanide, we postulate that highly reactive radicals could be produced from the interaction of externally added H_2O_2 with the AIM and that the radicals could facilitate the removal of EDTA through oxidative transformation.

The reactivity of the AIM system is normally dependent on the chemical compositions and impurities in the iron oxide phase in the reactive media. The different chemical compositions of iron oxide could lead to distinct physical and chemical properties with unique morphology, pore structure, surface area, ion strength, electrical conductivity, adsorption capacity, and cation/anion exchange capacity. These properties could affect the reactivity of the AIM system for the removal of contaminants from different wastewaters.

Research Objectives

The overall objective of this study is to evaluate the feasibility of applying AIM technologies to treat electroplating wastewater featuring strong metal-chelating complexes. Our goal is to develop a simple, yet cost-effective chemical treatment process that can tackle one of the most challenging waste streams. From this study, we aim to advance our understanding of the fundamental chemistry of the AIM system in several key aspects: how the AIM interact with nickel and what chemical processes are responsible for nickel removal; for the first time, evaluate if and how a reduced compound like cyanide could be transformed and removed by an AIM system—a predominantly reducing reactive system; and to evaluate if the AIM could be modified to incorporate advancing oxidation process into its mechanism for removal of ETDA.

From this research, we will understand how the complex water matrix, especially the metal-complexing reagents, would affect the AIM performance. To advance our knowledge on nickel, cyanide, and EDTA reduction mechanisms as well as the roles of magnetite, ZVI, and hydroxyl radicals, both batch, and CSTR experiments will be performed. The detailed objectives will be pursued as follows:

1. Evaluate the effectiveness of the AIM technology for nickel removal. Develop an understanding of the main mechanism(s) of nickel removal: chemical reduction of Ni^{2+} to Ni^0 or lattice substitution and incorporation of nickel into iron oxide structure. (CHAPTER II)
2. Evaluate the effectiveness of the AIM-only system and AIM assisted with supplemental oxidants (O_2 from aeration) to treat cyanide in water. Develop an

understanding of the main mechanism of the cyanide oxidation process. (CHAPTER III)

3. Evaluate the feasibility of the AIM assisted with supplemental oxidants (O_2 or H_2O_2) as a novel advanced oxidation process for EDTA breakdown and transformation in water. (CHAPTER IV)
4. Evaluate the effectiveness of the AIM for simultaneous removal of nickel, cyanide, and EDTA in a single treatment system. Determine the operational conditions (pH, aeration intensity, nitrate dosage, and/or H_2O_2), system configurations (one or multiple stage treatment systems), and required treatment time. (CHAPTER V)

CHAPTER II. NICKEL TREATMENT

Introduction

Nickel, usually in form of divalent nickel (Ni^{2+}) in water, is commonly found in electroplating industry wastewaters (Salcedo, Ballesteros et al. 2016). The discharge of this heavy metal element into the environment brings detrimental effects on the biosphere. According to the International Agency of Research on Cancer (IARC), nickel is categorized as a carcinogen to humans. Research has also shown that exposure to high concentration nickel compounds can severely endanger human health with serious diseases including allergies, contact dermatitis, cardiovascular diseases, and kidney disorders (Kasprzak, Sunderman et al. 2003). World Health Organization (WHO) recommends the maximum acceptable nickel concentration in drinking water to be 0.1 mg/L. However, nickel in industrial wastewaters has been reported to be over 4,000 ppm (Martín-Lara, Blázquez et al. 2014). If not properly treated, the discharge of nickel-contaminated wastewater into the environment could pose significant long-term risks to the safety of our drinking water sources. Therefore, the US Environmental Protection Agency (USEPA) has set a maximum nickel discharge concentration of 2.6 mg/L for the electroplating industry, whereas China has an even stricter nickel discharge limit, at 0.1 mg/L (China GB 21900-2008).

Many conventional treatment methods have been proven effective for removing nickel from water. Adsorption, among the commonly used techniques, is attractive for its high removal efficiency, cost-effectiveness, and simplicity in operation. A wide range of adsorbents can be chosen (Barakat 2011, Fu and Wang 2011). Adsorption used in metal

removal is a mass transfer procedure by which metals are transferred and accumulate at the interface between liquid-solid phases. Many recent review papers describe and summarize technologies dealing with heavy metal adsorption from wastewater using zeolite, multi-walled carbon nanotubes, protonated rice bran, chitosan-coated PVC beads, and orange peel. The adsorption capacities of adsorbents in described examples above for nickel removal are ranging from 49 to 158 mg/g (Ajmal, Rao et al. 2000, Mavrov, Erwe et al. 2003, Kandah and Meunier 2007, Popuri, Vijaya et al. 2009, Zafar, Abbas et al. 2009). However, the adsorption capacities are often affected by the unstable surface loading of adsorbents. Therefore, the process is not always efficient. Various studies were done for its alternate (Bhatnagar and Sillanpää 2010).

Chemical precipitation is also a widely used method for nickel removal (Bartzas, Komnitsas et al. 2006, Blais, Djedidi et al. 2008). Chemical precipitation of nickel can be achieved by raising the system pH to 9 to 10, where the nickel is transformed into the highly insoluble nickel hydroxide [$\mathrm{Ni(OH)_2}$] as Equation 1.

$$Ni^{2+} + OH^{-} \rightleftharpoons Ni(OH)_2 \downarrow \quad (1)$$

Using this mechanism, many researchers have reported good removal rates for nickel ranging from 95% to 99.8% (Sist and Demopoulos 2003, Giannopoulou and Panias 2008). However, most chemical precipitation processes become ineffective for nickel removal in the co-presence of cyanide or EDTA, mainly because the solubility of nickel increases dramatically by forming nickel-cyanide, or nickel-EDTA complexes. Therefore, direct precipitation is not a viable method for removing metals in chelated complexes (Madden, Datye et al. 1997).

Ion exchange is a water treatment technique that replaces undesirable ions in the water with environmentally harmless ions. It is one of the most frequently applied treatments for heavy metal wastewaters (Dąbrowski, Hubicki et al. 2004, Kurniawan, Chan et al. 2006), often showing advantages of high treatment capacity and fast kinetics. Various ion exchange resins and zeolites were shown effective for nickel removal (Argun 2008, Alyüz and Veli 2009, Priya, Basha et al. 2009). However, regenerations of exhausted ion exchange resins often consume extra chemical reagents and release a waste stream laden with even higher concentrations of nickel, which would require additional treatment for disposal to avoid serious secondary pollutions. Besides, ion exchange may be cost-effective for treating wastewaters with high-concentrated heavy metals, but it would become much more expensive if treating low concentration water streams (Fu and Wang 2011).

Membrane filtration processes with different types of membranes like ultrafiltration (UF), nanofiltration (NF), and reverse osmosis (RO) were also reportedly used for heavy metal removal. Membrane technologies show great promise for metal removal with advantages of high efficiency, easy operation, and space-saving. Since UF membranes have the size of the pores typically larger than metal ions and metal complex, direct use of UF may not achieve the needed removal efficiency. Modified UF processes such as the micellar enhanced UF (Akita, Castillo et al. 1999, Yurlova, Kryvoruchko et al. 2002, Danis and Aydiner 2009), polymer enhanced UF (Molinari, Poerio et al. 2008, Barakat and Schmidt 2010), and complexation-UF (Borbély and Nagy 2009) were proposed and tested to obtain a higher rejection efficiency. The pore size of

the NF membrane falls between that of UF and RO. NF was demonstrated capable of achieving high nickel removal rates (Ahn, Song et al. 1999, Mohammad, Othaman et al. 2004, Murthy and Chaudhari 2008), effective for wide pH ranges (2-10) and concentrations ranging from 5 ppm to 1000 ppm. RO processes use semi-permeable membranes with the finest pores capable of retaining a wide range of dissolved materials, including most metal pollutants (Qin, Wai et al. 2002, Ipek 2005, Mohsen-Nia, Montazeri et al. 2007). Major drawbacks of these membrane technologies include high operation costs, complexity in maintenance, low permeate flux, and membrane fouling problems. Most importantly, like ion exchange, how to safely dispose or handle the rejected streams with high concentrations of heavy metals and other pollutants is a major issue. These challenges limit the application of membrane technologies in heavy metal treatment.

ZVI is an environmental-friendly material of excellent reductive capacity and relatively inexpensive cost. It was widely used to remove all kinds of pollutants including organic compounds (Lowry and Johnson 2004, Li, Li et al. 2016), inorganic anions (Sohn, Kang et al. 2006) and heavy metal ions (Yang, Shan et al. 2016). It can activate various reactions for most of the contaminant removal (i.e., redox, precipitation, and absorption) to reduce the elements to their corresponding products with less toxicity. In particular, other metals can spontaneously participate in an electrochemical process that includes the reduction of the more positive potential species by the more negative potential metal (Dries, Bastiaens et al. 2005).

However, due to the iron surface passivation problem, the feasibility of these processes is dramatically suppressed. ZVI loses its reactivity fast in reactions. In order to reduce the impact of ZVI surface passivation and enhance ZVI reactivity and longevity, it is common to add some additives among reactive species like Fe_3O_4 (magnetite) and Fe^{2+}. They form a combined system towards specific contaminant removal (Noubactep 2008, Tang, Huang et al. 2016).

Building on the understanding of the unique roles of magnetite and Fe^{2+} in sustaining the ZVI system's reactivity and overcoming ZVI surface passivation for contaminants removal, an AIM system was developed (Huang, Zhang et al. 2003). The effectiveness of ZVI-related processes for metal removals is well-established (Huang, Tang et al. 2012, Huang, Peddi et al. 2013, Huang, Peddi et al. 2014, Tang, Huang et al. 2016). However, the nickel removal mechanism by the iron media system is not fully understood. The potential of AIM for nickel removal and the underlying mechanisms needs to be evaluated.

Materials and Methods

Materials

Chemicals used in this study were all analytical reagent grade. Nickel chloride ($NiCl_2 \cdot 6H_2O$, >99%, Alfa Aescar), ferrous sulfate ($FeSO_4 \cdot 4H_2O$, J.T. Baker), and sodium nitrate ($NaNO_3$, Alfa Aescar) were used. Oxygen and nitrogen supply were ultra-purity grades from Airgas. ZVI grain of 325-mesh (>99.2%, Johnson Matthey) has a specific surface area of 0.073 m^2/g by BET nitrogen absorption analysis (Autosorb-6, Quantachrome).

Anoxic and oxic environment

Chemicals for an anoxic experiment will be prepared into the anaerobic chamber. The atmosphere of the anaerobic chamber is approximately 95% N_2 and 5% H_2 with a palladium catalytic O_2 removal system (Coy Laboratory). The chamber is monitored by an oxygen/hydrogen analyzer to indicate the gas components. All oxygen-free stock solutions will use deoxygenated deionized (DDI) water. The DDI water is prepared by bubbling nitrogen gas in deionized (DI) water (E-Pure D4641, Barnstead, USA) at a flow rate of 10 L/min for 1 h to eliminate the dissolved oxygen (DO) and maintained 24 h in the chamber before use.

In the anoxic experiment, the system was remaining sealed from oxygen. In the oxic experiment, the gas in the headspace of the reactor was drawn out 3 mL using a syringe (10-mL, Air-Tite) and replaced with pure oxygen every 30 min to maintain oxygen pressure.

Batch experiment procedure

Batch experiments were performed using the 12-mL serum bottles at ambient temperature (22 ± 1 °C) controlled by central air-conditioning in the laboratory. Reactors were prefilled with 0.5 g ZVI or AIM in the anaerobic chamber. Designed volumes of the stock solutions and DDI water were added by single-channel variable volume pipettes (Eppendorf), to ensure the total volume of 10 mL and media concentration of 50 g/L. Rubber stoppers and aluminum crimps were used to seal the reactors tightly. The

reactors would then be placed in a rotary tumbler for complete mixing at 30 rpm in the dark. At predetermined time intervals (0.1 h, 0.5 h, 1 h, 2 h…), three reactors were removed from the tumbler for evaluating (average of result) pH, cations of Ni^{2+}, Fe^{2+}, Fe^{3+}, and anions of.

CSTR experiment procedure

The CSTR experiments were conducted using a self-designed bench-top single-stage unit reactor (Figure 1). The reactor has an effective volume of 6 L. An overhead-motorized mixer (OS20-S overhead stirrer, Scilogex) with a propeller operated at 1500 rpm was used to fluidize the reactor. Within the reactor, an internal settling zone of about 3 L was designed to achieve solid/liquid separation and to retain reactive solids. A peristaltic pump (model 7528-30, Masterflex) transports the influent at the flow rate of 1 L/h. The corresponding hydraulic retention time of the reactor is 6 h. The initial ZVI concentration was controlled at 100 g/L. The reactor was sealed by a plastic cover to create the anoxic environment. The effluent was sampled and analyzed following the same sampling procedure in the batch experiment.

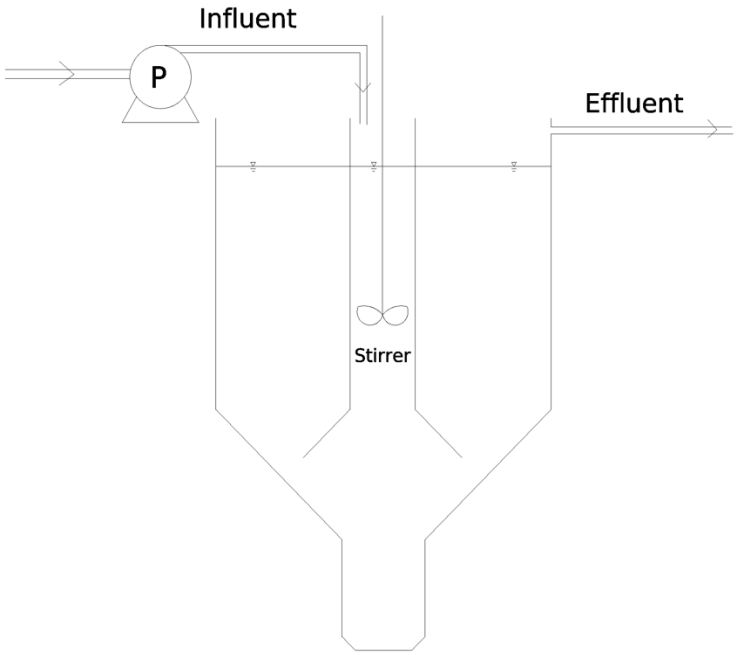

Figure 1. Schematic drawing of the single-stage benchtop treatment system.

Production of the AIM system

The AIM system is converted from the ZVI system using a nitrate-Fe^{2+} pretreatment method. According to a similar ZVI/nitrate-Fe^{2+} system (Huang, Zhang et al. 2003), Fe^{2+} and nitrate can be rapidly reduced by ZVI, and magnetite was formed following Equation 2:

$$NO_3^- + 0.75\ Fe^{2+} + 2.82\ Fe^0 + 2.25\ H_2O \rightarrow NH^{4+} + 1.19\ Fe_3O_4 + 0.5\ OH^- \quad (2)$$

At the end of the process, magnetite was created both as discrete particulate FeO_x crystalline particles and the surface-bonding form on the ZVI grain. The iron surface morphology under the two conditions was photo using a scanning electron microscope (SEM). The surface of the ZVI grain was smooth with a small number of cavities (Figure 2a). After pretreating, granular crystal growth on the iron surface was observed

(Figure 2b). These granular crystals are corrosion products (CPs) consisting of electron-conducting magnetite-like iron oxides, which have a multi-layer structure of anion-cation intercalation.

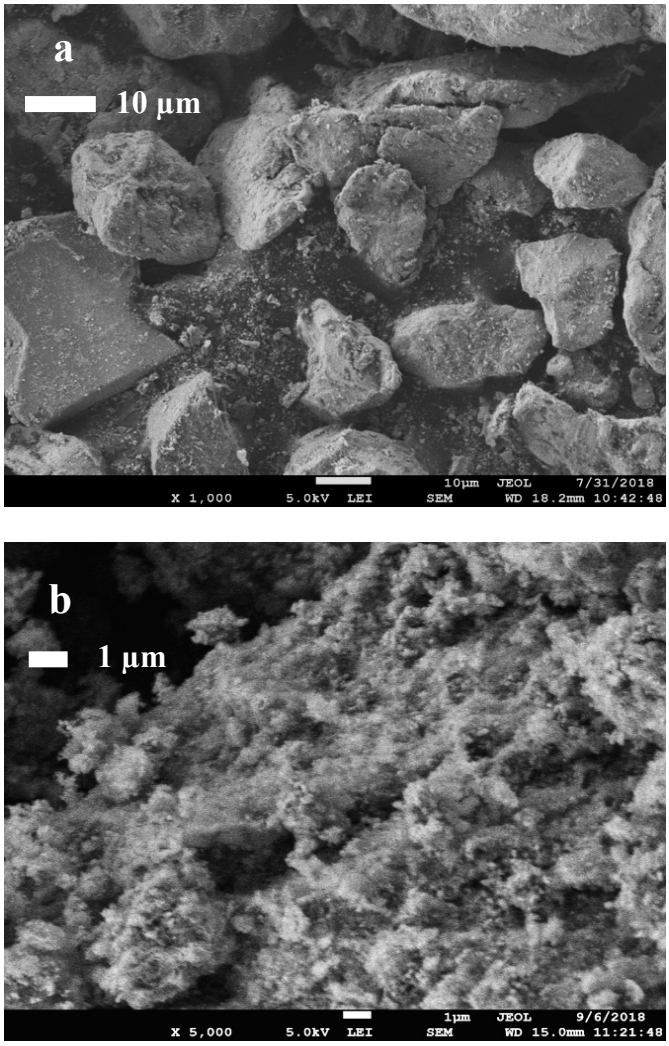

Figure 2. The SEM images of the iron media surface a) ZVI, b) AIM.

Analytical Methods

The filtrate was collected in sampling vials through a membrane filter (0.45-µm Polyethersulfone syringe filter, VWR) for analysis. Dissolved nickel concentration was

determined using Inductively Coupled Plasma Mass Spectrometry (ICP-MS) (Agilent). Dissolved Fe^{2+} and Fe^{3+} were tested on an ultraviolet-visible (UV-VIS) spectrophotometer (T80, PG Instruments) colorimetrically using the 1,10-phenanthroline method at the wavelength of 510 nm (Method 3500-Fe-D). Nitrate was measured using the Ion Chromatography (IC) (DX-500, Dionex) equipped with an AS-22 separation column (Method 4110 B). ORION pH meter was used for pH measurement.

Solid characterization

The reactive particles and solids were analyzed and characterized using microscopic and spectroscopic instruments, including FE-SEM, X-ray diffraction (XRD), and X-ray photoelectron spectroscopy (XPS), all of which were conducted in the X-ray Diffraction Laboratory and the Material Characterization Facility at Texas A&M University.

Samples for FE-SEM, XPS, and XRD analysis were prepared individually following the batch procedure discussed above. The analyzed samples were first washed three times to remove dissolved salts from the solid surface, then filtrated through a 0.2-μm membrane filter in the anaerobic chamber. The filer was subsequently dried for 72 h in the anoxic environment before analysis.

The FE-SEM photos were taken by JEOL JSM-7500F at magnifications of 1000X and 5000X.

XPS test was done using a Kratos Axis Ultra Imaging X-ray photoelectron spectrometer with a monochromatized Al Kα X-ray source ($hv = 1486.6$ eV) operating at the power of 300 W. The base pressure in the analytical chamber was $1 \times (10^6 \sim 10^7)$

Pa. To control the charging of the samples, a charge neutralizer was used. For high-resolution spectra, the pass energy was set at 40 eV and the step size of 0.05 eV for individual core levels. The binding energy was corrected by assigning the C 1s peak to 284.8 eV. The peak was integrated using CasaXPS software.

XRD analysis was performed using a powder X-ray diffractometer (Bruker D8) equipped with a monochromatized Cu Kα radiation.

Results and Discussions

Blank comparison

To understand the roles of different components in the AIM, both ZVI and AIM systems were blank tested under anoxic conditions using DI water for 72 hours. The nitrate concentration was zero in both systems, the dissolved Fe^{3+} concentration was negligible (<0.5 mg/L). As shown in Figure 3, in anoxic tests, both ZVI and AIM would initially release some dissolved Fe^{2+} and slightly lower the pH over time: about 16 mg/L Fe^{2+} in the ZVI system vs. 13 mg/L in the AIM system. For ZVI, one reaction could proceed as: $Fe^0 + 2H_2O \rightarrow Fe^{2+} + H_2 + 2OH^-$. The observed pH decrease may be a result of forming FeO_x coating on the ZVI surface. In the case of AIM, no direct contact between Fe^0 and H_2O, but rather between FeO_x and H_2O; the release of Fe^{2+} could be the result of a new equilibrium between $Fe^0/FeO_x/H_2O$.

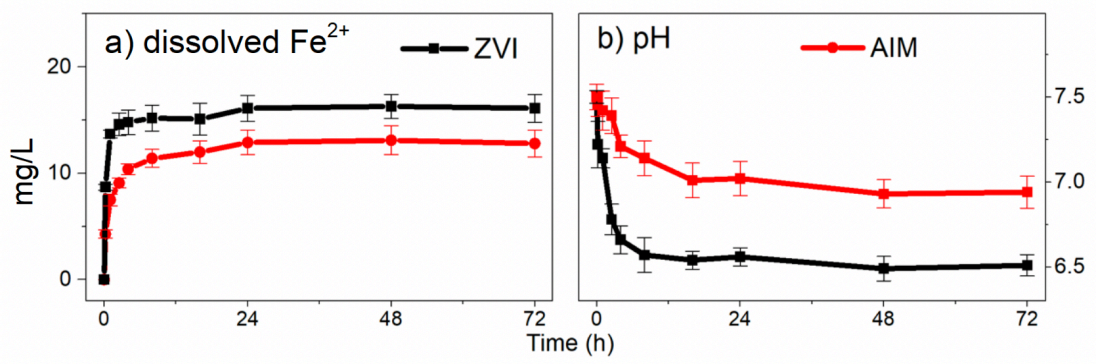

Figure 3. The concentration profile of dissolved Fe^{2+} and pH in the blank anoxic a) ZVI and b) AIM batch system.

The reductive process by ZVI

Figure 4 showed the dissolved nickel concentration (in log scale) during the anoxic and oxic ZVI system batch test with the initial nickel concentration of 50, 100, and 200 mg/L. In the oxic environment, the dissolved nickel concentration declined to 25.2, 51.2, and 111.2 mg/L within the first hour, dropped to 4.84, 12.5, and 37.5 mg/L after eight hours, and finally reached over 99.3% removal (to 0.16, 0.37, and 1.31 mg/L) after 72 hours.

In the oxic ZVI system, the decrease of nickel concentration follows a similar trend. The nickel treatment rate was a little slower than it was in the anoxic environment. For all three initial dosages, the nickel concentration declined to 27.9, 53.9, and 128.4 mg/L within the first hour, dropped to 6.32, 13.5, and 38.9 mg/L after eight hours. However, it finally reached a similar removal percentage (to 0.15, 0.36, and 1.38 mg/L) as the anoxic batch after 72 hours. The system pH dropped from an initial 7.5 to around 6.5 in all the batches.

In both conditions, all three dosages achieved the EPA's limit with good removal efficiency, but failed to comply with the restrict China's limit of 0.1 mg/L.

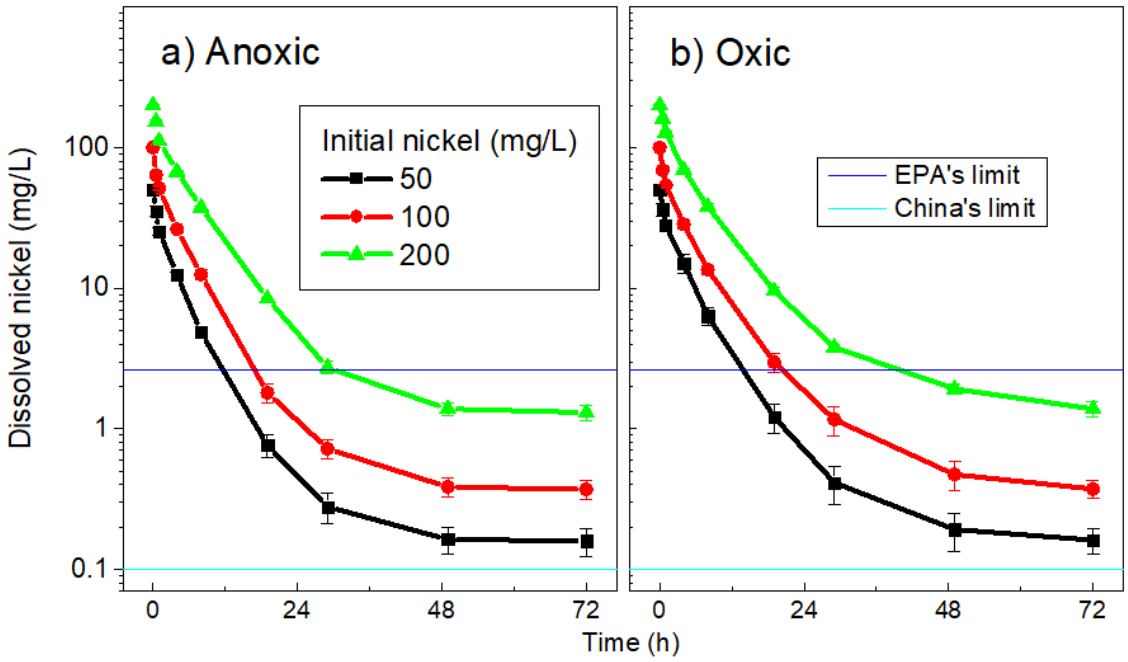

Figure 4. The concentration profile of dissolved nickel in the a) anoxic and b) oxic ZVI batch system.

The solid sample products from the 200-mg/L batch test at 1, 8, and 72 h were carefully examined by XPS to investigate the valent state of the removed nickel (Figure 5). The photoelectron peaks were assigned (at ~855.8 and ~852.1 eV) to the $2p_{3/2}$ binding energies of Ni^{2+} and Ni^0 respectively (Li and Zhang 2006, Ling and Zhang 2014). Both zero-valent and divalent nickel were detected in the samples, with different peak areas. The ratio of Ni^0 to the total removed Ni^{2+} rises from 12% to 58%, finally to 74%. The increasing ratio of Ni^0/Ni_{tot}, indicates the ongoing reduction reaction of Ni^{2+} to Ni^0.

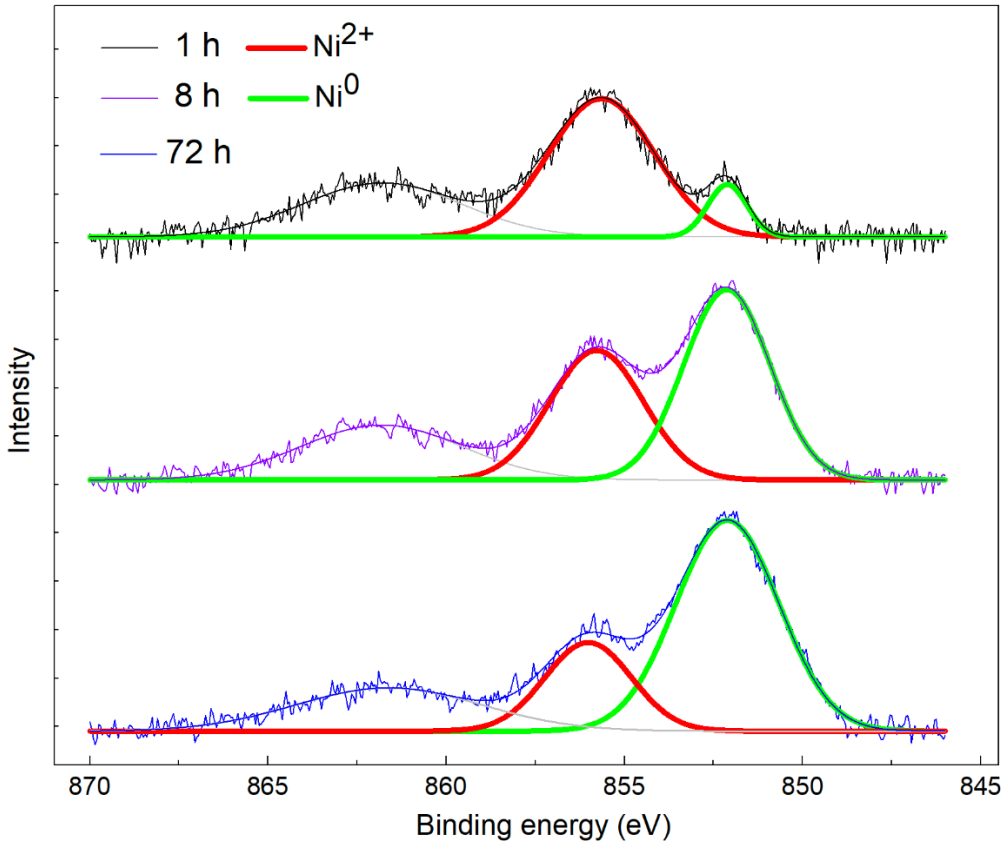

Figure 5. The XPS spectra of nickel 2p3/2 for the products in the anoxic ZVI batch system.

In the first hour 200-mg/L batch, only 12% of the removed nickel was Ni^0. This indicates the nickel removal process is the first adsorption. The dissolved Ni^{2+} ions were first absorbed to the ZVI surface and got in contact with Fe^0. According to the ZVI's reductive property in the water system, it then reduces from divalent nickel to zero-valent nickel (Noubactep 2008, Noubactep 2013, Li, Dong et al. 2017). The oxidized Fe^0 was released as aqueous Fe^{2+} ions and Ni^0 was fixed into the iron structure (Equation 3 or 4). The Gibbs free energy change (ΔG) in Equation 5 is -33.3 kJ/mol, indicating a spontaneous reaction in the room temperature (Robie and Hemingway 1995). The

slightly slower treatment reaction in the oxic ZVI system may be due to a series of reactions between FeO_x and dissolved oxygen. However, the removed Ni^0 would not be oxidized back to Ni^{2+} by oxygen at room temperature. The final nickel removal was similar for both conditions.

$$\equiv Fe^0 + Ni^{2+} \rightarrow \equiv Fe^0 \cdot Ni^{2+} \rightarrow \equiv Fe^{II} \cdot Ni^0 \rightarrow Fe^{2+} + Ni^0 \quad (3)$$

$$\equiv Fe^0 + Ni^{2+} \rightarrow Fe^{2+} + Ni^0 \quad (4)$$

The reduction of Ni^{2+} to Ni^0 would produce more Fe^{2+} than the blank system. In order to better evaluate the contribution of reduction reaction to the nickel removal, we further investigate the generation of Fe^{2+} during nickel removal in the ZVI process (Figure 6). The test was conducted in anoxic conditions to avoid complications of Fe^{2+} with oxygen. When nickel was introduced, the dissolved Fe^{2+} concentration gradually increased while the nickel concentration decreases and reached a platform after 30 h (99% of nickel exhausted). The final dissolved Fe^{2+} concentrations were 47.7, 88.7, and 161.9 mg/L. The increased dissolved Fe^{2+} indicated that at least 60% of the Ni^{2+} was reduced to Ni^0.

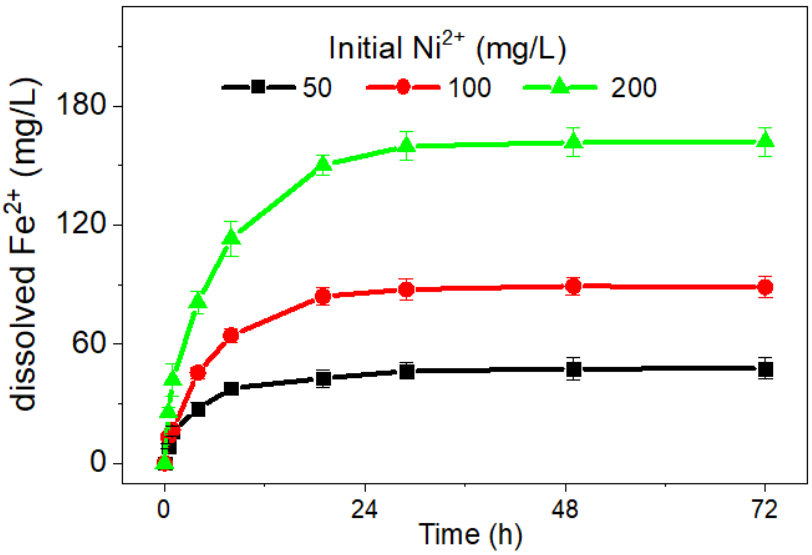

Figure 6. The concentration profile of dissolved Fe^{2+} in the anoxic ZVI batch system.

Therefore, the reductive mechanism contributes to the main effort of the total nickel removal in the ZVI system.

The lattice substitution process by AIM

Figure 7 showed the nickel concentration during the AIM batch with the same initial nickel concentrations in both anoxic and oxic conditions. In the anoxic condition, the dissolved nickel concentration declined to 17.9, 42.9, and 90.9 mg/L within the first hour, decreased to 2.3, 5.5, and 15.4 mg/L after eight hours, and finally achieved more than 99.6% removal (to 0.07, 0.16, and 0.69 mg/L) after 72 hours.

In the oxic condition, the treatment reaction was slower. The required time to reach EPA's limit doubled. The dissolved nickel concentration declined to 37.8, 75.7, and 141.5 mg/L within the first hour, decreased to 7.92, 15.8, and 31.7 mg/L after eight hours. However, the final nickel concentration was similar at 0.105, 0.331, and 0.961 mg/L (over 99.5% removal).

In both conditions, all the three dosages achieved the EPA's limit with good removal efficiency, The AIM system can achieve China's limit when the initial nickel concentration is below 50 mg/L. The system pH was decreased from an initial 7.5 to around 6.5 in all the batches.

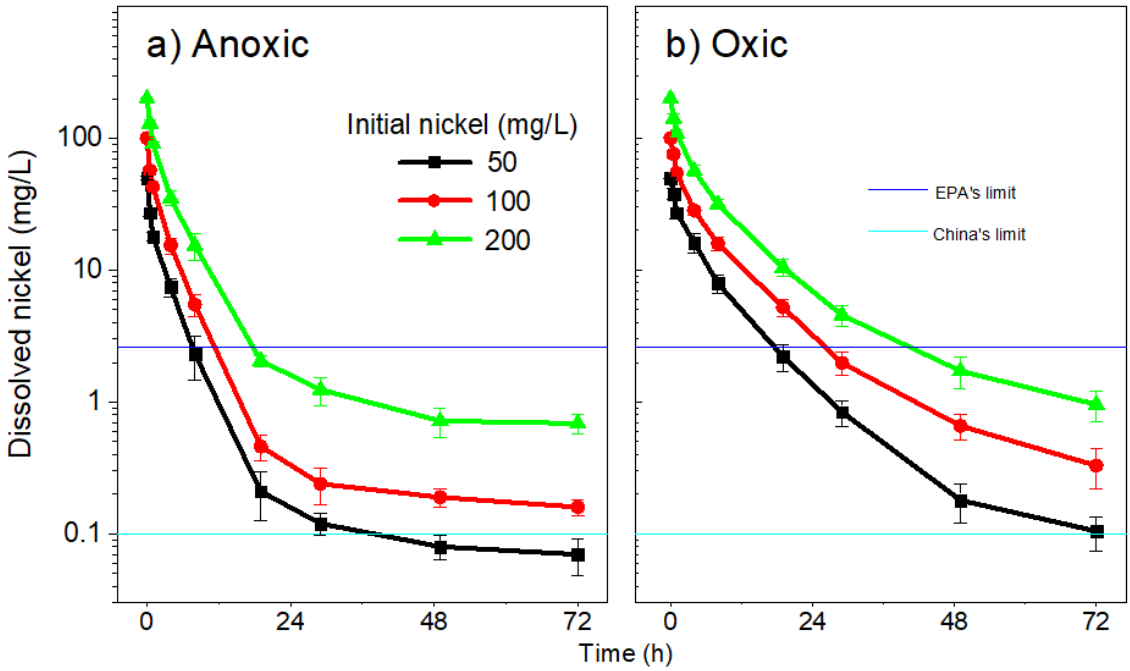

Figure 7. The dissolved nickel concentration of the (a) anoxic and (b) oxic AIM batch system.

Similarly, the samples in the anoxic AIM system from the 200-mg/L batch at 1 and 72 h were analyzed by XPS (Figure 8). The photoelectron peak at ~855.8 EV was assigned to the $2p_{3/2}$ binding energies of Ni^{2+} (Noubactep 2008, Li, Dong et al. 2017). The XPS spectra indicated only divalent nickel implying that Ni^{2+} did not reduce to Ni^0 in the AIM system (or Ni^0 mass was lower than detect limit).

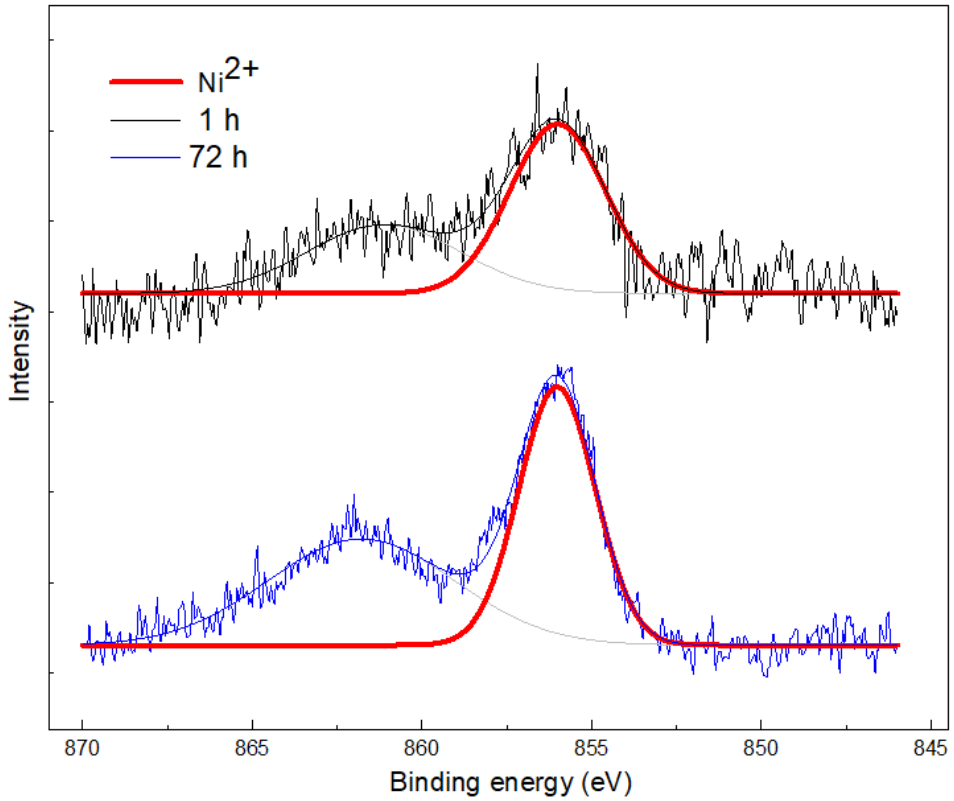

Figure 8. The XPS spectra of nickel 2p3/2 for the products in the AIM batch system.

In order to better investigate the nickel removal mechanism in the AIM system, an XRD analysis was performed. Figure 9 presents the XRD spectra comparison of the same batch samples as the XPS test. From 0 h to 72 h, the pattern of magnetite peaks remained, but the intensity was slightly decreased. Smaller peaks appeared about one degree to the right of the magnetite peaks. According to Bragg's law, the diffraction angle of the XRD spectrum was determined by the crystal radius of the ion. The decrease of ion radius would increase the diffraction angle (Whittig and Allardice 1986). Ni(II) has a smaller crystal radius (0.83 Å) than Fe(II) (0.92 Å). The small portion of peaks with increased angle can be the result of a Ni(II)-iron structure that is similar to magnetite. According to the literature, $NiFe_2O_4$ shares a similar crystal structure but

smaller lattice parameter (8.337 Å) than magnetite (8.394 Å) (Gorter 1954, Shannon 1976, Fleet 1981, Laetsch and Downs 2006, Smith, Taylor et al. 2015, Smith, Um et al. 2016). XRD spectra reveal a possible formation of $NiFe_2O_4$.

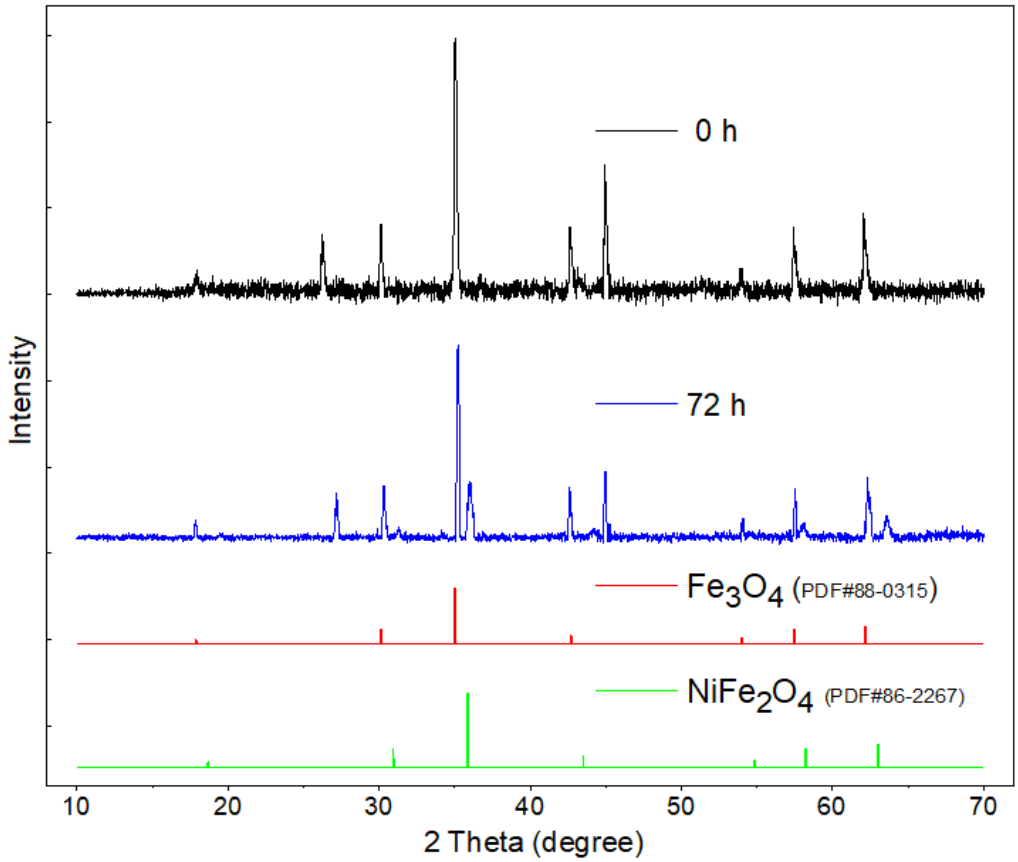

Figure 9. The XRD spectra of the samples in the AIM batch system.

The dissolved Ni^{2+} ions were first adsorbed to the AIM surface, then incorporated into the FeO_x structure and possibly formed $NiFe_2O_4$ while releasing Fe^{2+} (Equation 5 or 6). The Gibbs free energy change (ΔG) in Equation 7 is 6.2 kJ/mol indicating the replacement reaction is slow but possible at room temperature (Kurepin, Kulik et al. 2002). Therefore, the lattice substitution of Ni^{2+} into the FeO_x structure in the AIM is the major nickel removal mechanism.

$$\equiv Fe^{II} + Ni^{2+} \rightarrow \equiv Fe^{II} \cdot Ni^{2+} \rightarrow \equiv Ni^{II} \cdot Fe^{2+} \rightarrow \equiv Ni^{II} + Fe^{2+} \quad (5)$$

$$Fe^{II}Fe_2^{III}O_4 + Ni^{2+} \rightarrow Ni^{II}Fe_2^{III}O_4 + Fe^{2+} \quad (6)$$

We further examined the concentration of dissolved Fe^{2+} in the anoxic AIM system (Figure 10), for purpose of better comparing it with the ZVI system. With nickel injection, dissolved Fe^{2+} concentration increased with the reaction and stayed steady after 20 hours (after 99% of nickel consumed). The final concentrations were 34.3, 69.0, and 134.7 mg/L respectively. The lower Fe^{2+} concentration may be due to the better ferrous balancing ability of AIM than ZVI.

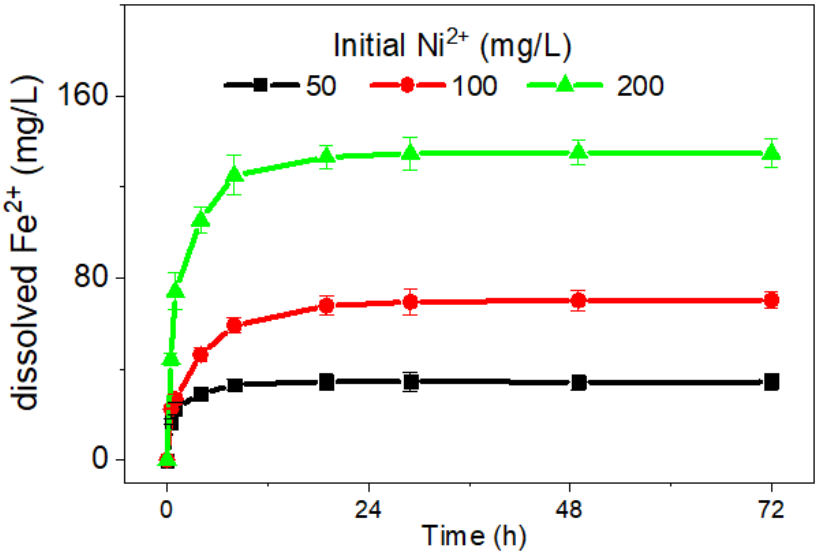

Figure 10. The concentration profile of dissolved Fe^{2+} in the anoxic AIM batch system.

Continuous batch experiments

The continuous anoxic batch experiment was conducted to further assess the efficiency of the two systems (Figure 11). The next dose was added when the nickel concentration was below the EPA's limit (2.6 mg/L). For each dosage, nickel concentration was 50, 100, and 200 mg/L in the 96-hour experiment. The AIM system

can treat 4, 3, and 2 batches with the removed nickel concentration over 198, 340, and 592 mg/L. The ZVI system, compared to that, can only treat 2 batches with the removed nickel concentration around 146, 275, and 480 mg/L. The continuous batch test implied that the nickel removal in the AIM system was more efficient and sustainable than it in the ZVI system.

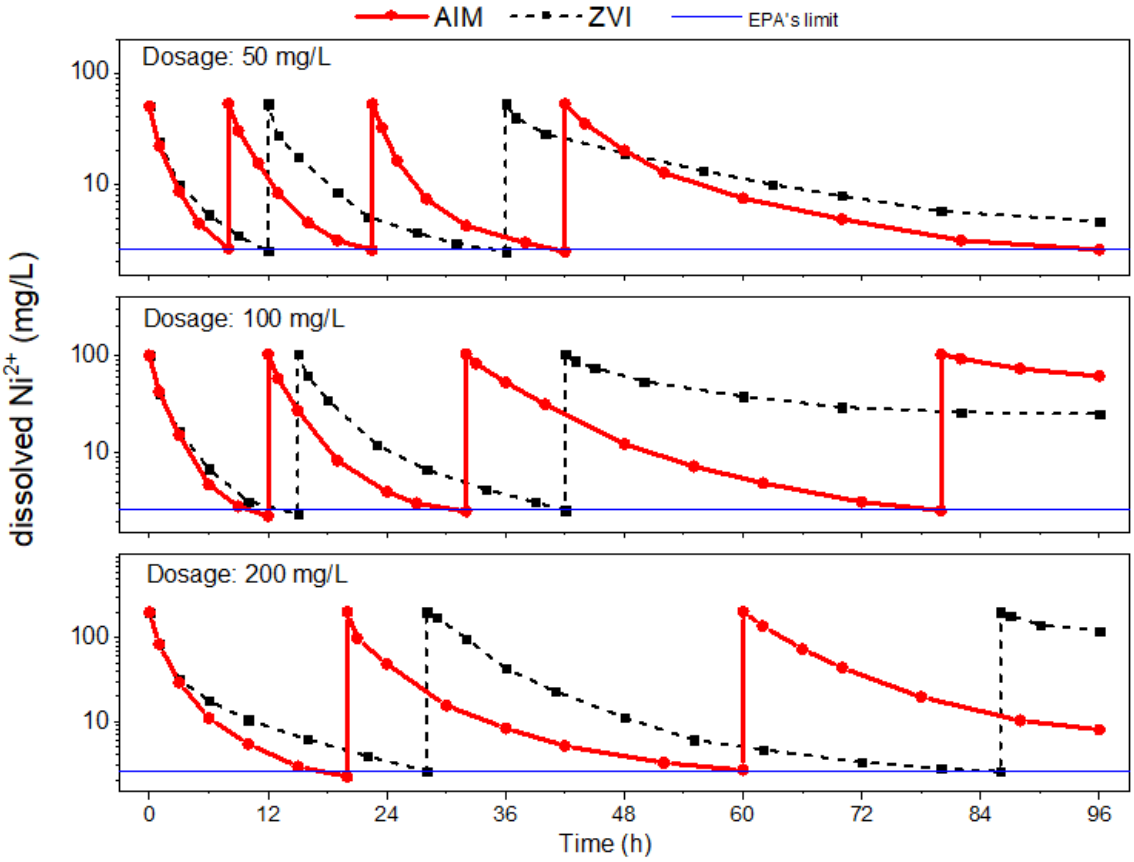

Figure 11. The nickel concentration of the continuous anoxic ZVI and AIM batch system.

CSTR experiments

The CSTR experiment was also performed to simulate the field application with an influent of 100 mg/L nickel. An additional 21 mg/L of nitrate was fed into the AIM

system. For the hydraulic retention time of 6 h, effluent nickel, Fe^{2+}, and nitrate concentration were monitored daily (Figure 12). In the ZVI system, the effluent nickel concentration was stable for 44 days. It maintained an average of 3 mg/L and fluctuated from 1 to 4 mg/L. The ZVI system failed after day 44 and effluent nickel concentration rockets to 60 mg/L. The AIM system, however, was able to achieve better nickel removal and maintained it. The nickel concentration started and was maintained from 0.1 to 0.4 mg/L (average of 0.25 mg/L) throughout the 50 days.

The Fe^{2+} concentration in the ZVI system was a lot higher (average of 75 mg/L) than the AIM system (average of 0.5 mg/L). Almost all the dissolved Fe^{2+} and the additional nitrate in the AIM system were utilized. The released Fe^{2+} and additional nitrate were quickly exhausted by the reduction process as Equation 2, which allows the passivated iron media in the system to reform and reactivate.

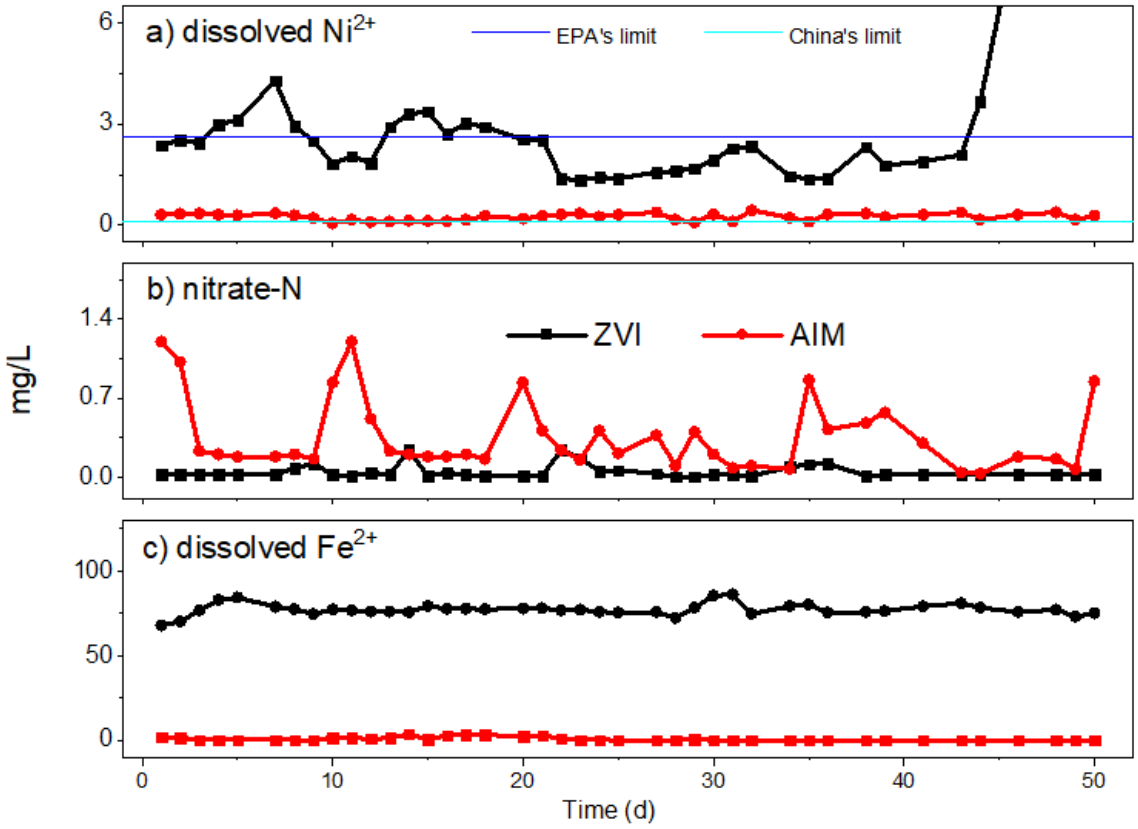

Figure 12. The concentration profile of a) dissolved nickel, b) nitrate, and c) dissolved Fe^{2+} in the anoxic ZVI and AIM CSTR system.

Therefore, AIM can continuously react with influent nickel, making it a feasible, sustainable, and reliable nickel treatment process.

Summary

We found in the nickel treatment research that the removal of nickel was achievable in both ZVI and AIM systems (>99.3% removal). In the ZVI system, the removal process is dominated by the reductive reaction, while most of the nickel was reduced to Ni^0 by Fe^0. In the AIM system, the lattice substitution reaction controlled the removal mechanism, while nickel react with the CPs and replace labile Fe(II) in the

structure of the FeO_x. The XPS and XRD spectra showed two different removal mechanisms of the two systems.

The continuous batch test proves the AIM system has higher removal efficiency than the ZVI system. The CSTR comparison further indicates that the AIM system is more reliable and sustainable for nickel treatment.

CHAPTER III. CYANIDE TREATMENT

Introduction

Cyanide (CN^-) is a carbon-nitrogen compound that can be found in a wide variety of organic and inorganic materials. All forms of cyanide are toxic at high levels, but free cyanide is the deadliest form of the toxins. Cyanide-bearing materials, solutions, and waste streams require special handling and management. Cyanide compounds are readily absorbed through the skin or lungs from dust or vapor (Hanson 1979). At short-term exposure, free cyanide causes rapid breathing, tremors, and other neurological effects. Long-term exposure to cyanide would result in weight loss, thyroid effects, nerve damage, and death (US 2001). Thus, USEPA has proposed a limit of 50 μg/L for total cyanide (free and complexed cyanides) in drinking water (Dash, Balomajumder et al. 2008). Cyanide has been extensively used in the metal finishing industry for decades. The use of cyanide in plating and stripping solutions is born of its ability to complex many metals. The high affinities of metals for CN^- can be attributed to its negative charge, compactness, and ability to form π-bonding. The cyanide complexes with nickel, iron, and cobalt are highly stable and difficult to destroy. Therefore, conventional water treatment processes often report problems with these complexes (Gallerani 2001). Total cyanide is also regulated in electroplating discharge at 1 mg/L by the USEPA. The Chinese national standard for that is 0.2 mg/L.

Cyanide-contaminated wastewater was once widely treated by biological process (Patil and Paknikar 2000, Dash, Gaur et al. 2009). Aerobic biological treatment processes with a large population of bacteria can convert free cyanide into energy, cell

mass, and less toxic by-products. The biologically-mediated cyanide oxidation reaction can be represented as Equation 7.

$$CN^- + 0.5O_2 + 3H_2O \rightarrow NH_4^+ + HCO_3^- + OH^- \quad (7)$$

Biological systems can handle cyanide in low to medium concentrations (Figueira, Ciminelli et al. 1996, Desai, Ramakrishna et al. 1998, Given, Dixon et al. 1998, Annachhatre and Amornkaew 2001). It was found very effective for treating free cyanide and weak acid dissociable (WAD) cyanide (Ingles and Scott 1987, Zaidi and Whittle 1987, Wedl and Fulk 1991). However, the strong metal-cyanide complexes (i.e. nickel cyanide and iron cyanide) are unable to be oxidized biologically (Botz, Mudder et al. 2005).

Chemical oxidation methods are the oxidation processes of cyanide to the lesser toxic products, which are being used widely worldwide. The procedures are usually categorized by alkaline chlorination, copper-catalyzed hydrogen peroxide, sulfur dioxide and air, and Caro's acid.

The destruction reactions of cyanide in the alkaline chlorination process involve two steps. The first step is the conversion of cyanide and chlorine (Cl_2) to cyanogen chloride (CNCl). The second step is the hydrolysis of cyanogen chloride to cyanate (OCN^-). Cyanate is further hydrolyzed to yield ammonia (NH_4^+). If sufficient chlorine is available, the reaction continues through breakpoint chlorination, in which ammonia is oxidized to nitrogen gas (N_2) (Equation 8, 9, 10, and 11).

$$CN^- + Cl_2 \rightarrow CNCl + Cl^- \quad (8)$$

$$CNCl + H_2O \rightarrow OCN^- + Cl^- + 2H^+ \quad (9)$$

$$OCN^- + 3H_2O \rightarrow NH_4^+ + HCO_3^- + OH^- \quad (10)$$

$$NH_4^+ + 3Cl_2 \rightarrow N_2 + 6Cl^- + 8H^+ \quad (11)$$

The process is carried out at a pH higher than 10.5 to maintain the hydrolysis reaction rate. The usage of chlorine is 3 to 8 grams per gram of cyanide (Botz, Mudder et al. 2005). However, it is ineffective for treating strong metal-cyanide complexes (Dash, Gaur et al. 2009).

The copper-catalyzed hydrogen peroxide (H_2O_2) process utilizes H_2O_2 instead of Cl_2. Soluble copper is required as a catalyst in the reaction and the product is cyanate (Equation 12). Cyanate further hydrolyzed to ammonia as Equation 10.

$$CN^- + H_2O_2 \xrightarrow{Cu^{2+}\ Catalyst} OCN^- + H_2O \quad (12)$$

The process typically uses 2 to 8 grams of H_2O_2 to treat each gram of cyanide. It is effective for the treatment of free and weak acid dissociable (WAD) cyanides (Mudder, Botz et al. 2001). Alkaline chlorination and hydrogen peroxide treatment process were once the most widely used for the removal of cyanide. Due to the high reagent usages in the process operation, they are now only used occasionally and have been gradually replaced by other processes (Ingles and Scott 1987, Mudder, Botz et al. 2001, Botz, Mudder et al. 2005). Besides, the chemical residues in the treated water are toxic to aquatic life. Residues like chlorine can react with natural organic matters forming carcinogenic byproducts, causing more problems (Bougeard, Goslan et al. 2010).

The sulfur dioxide and air process have similar reaction chemistry to alkaline chlorination and copper-catalyzed hydrogen peroxide process, but cheaper chemicals (SO_2 and O_2) are used instead of H_2O_2 and Cl_2 (Equation 13).

$$CN^- + SO_2 + O_2 + H_2O \xrightarrow{Cu^{2+}\ Catalyst} OCN^- + SO_4^{2-} + 2H^+ \quad (13)$$

The SO_2 usage ranges from about 3.5 to 5 grams per gram of cyanide oxidized in practice. The primary application of sulfur dioxide and air process is for slurry tailings, but they are also effective for the treatment of free and WAD cyanides (Patterson 1985, Ingles and Scott 1987, Lee, Kwon et al. 2004).

Caro's acid or Peroxymonosulphuric acid (H_2SO_5) is typically produced with H_2SO_4 and H_2O_2 (Norcross 1996) (Equation 14). Due to the instability of Caro's acid, it is produced on-site and used immediately to detoxify cyanide to cyanate (Equation 15).

$$H_2SO_4 + H_2O_2 \rightarrow H_2SO_5 + H_2O \quad (14)$$

$$CN^- + H_2SO_5 \rightarrow OCN^- + SO_4^{2-} + 2H^+ \quad (15)$$

The process uses 5 to 15 grams H_2SO_5 to oxidize one gram of cyanide. Caro's acid is normally used where the copper catalyst is not desirable. It can be applied to the wastewater containing low to moderate levels (between 10 and 50 ppm) of cyanide (Botz, Mudder et al. 2005).

The iron-cyanide precipitation process use Fe^{2+} or Fe^{3+} to bind with free and WAD cyanides to form precipitates and remove cyanide from the water (Sharma, Rivera et al. 1998, Ghosh, Dzombak et al. 1999). Cyanide reacts with Fe^{2+} or Fe^{3+} to produce a variety of Fe-CN complexes including soluble compounds ferrocyanide ($Fe(CN)_6^{4-}$) and insoluble compounds including ferrous ferrocyanide ($Fe_2Fe(CN)_6$) and ferric

ferrocyanide ($Fe_4[Fe(CN)_6]_3$). The iron-cyanide precipitation process has the limitation that requires careful control of the precipitation reactions as well as proper separation and disposal of the precipitated solids. The need for further treatment represents a major disadvantage of this process (Adams 1992, Dzombak, Dobbs et al. 1996).

Hydroxyl radical is capable of independent existence and possesses unpaired electrons (Gomes, Fernandes et al. 2005). With the highest oxidation potential, it is a strong oxidant and can be used to oxidize and degrade various organic species (Tai, Gu et al. 2002, Tchobanoglous, Burton et al. 2003). Hydroxyl radicals attack organic pollutants mainly through four pathways: radical addition, hydrogen abstraction, electron transfer, and radical combination (Deng and Zhao 2015). Their reactions with organic compounds produce carbon-centered radicals (R· or R-OH). With O_2, these carbon-center radicals may be transformed into organic peroxyl radicals (ROO·). All these radicals further react with the formation of more reactive species such as H_2O_2 and superoxide ($O_2^{\bullet-}$), leading to chemical degradation. Because hydroxyl radicals have a very short lifetime, they are only in situ produced during application through many different methods, including a combination of oxidizing agents (such as H_2O_2 and O_3), UV light, and catalysts (such as Fe^{2+} and TiO_2). Many studies have attempted to investigate the role of hydroxyl radical in the decolorization of dyes, the cleavage of naphthalene and benzene rings, the oxidation of organic compounds, the remediation of As^{3+} contaminated water, and decompose pollutants like cyanide and EDTA (Lee, Yoon et al. 2004, Dutta, Pehkonen et al. 2005, Song, Xu et al. 2007, Li, Crittenden et al. 2009, Wang, Xu et al. 2012, Yang, Shan et al. 2016).

The effectiveness of ZVI-related processes for metal removals is well-established (Huang, Zhang et al. 2003, Huang, Tang et al. 2012). Laboratory experiments and field pilot tests of the AIM technology result in remarkable efficiency of removing various heavy metals, metalloids, and nitrate from mining, electric power, and refinery wastewaters (Huang, Peddi et al. 2014). In the AIM system, a substantial mass of magnetite co-presences in forms of both a surface adhesion on ZVI grains and discrete magnetite particles, and various forms of surface-bound (i.e., hydroxyl and hydroxide radical), the multi-layer structure of anion-cation intercalation, colloidal, and dissolved Fe^{2+} species alongside with ZVI cores. Little has been reported about the potential of ZVI for cyanide treatment. While removal and breakdown of cyanide involve primarily oxidation process, ZVI as a reductive chemical may not be a good candidate for treating cyanide at first thought. Yet it is understood that ZVI-based processes may have a chance of generating radicals that might contribute to cyanide breakdown.

Therefore, developing and investigating specialized methods is needed in order to fully handle the treatment of cyanide.

Materials and Methods

Materials

All chemicals used in this study were all analytical reagent grade and pre-weighed before being transferred into the anaerobic chamber. Sodium cyanide (NaCN, >98%, Acros), ferrous sulfate ($FeSO_4 \cdot 4H_2O$, J.T. Baker), sodium nitrate ($NaNO_3$, Alfa Aesar), sodium sulfate (Na_2SO_4, Alfa Aesar), and hydroxybenzoic acid ($C_6H_5CO_2H$, Alfa Aesar) stock solutions were prepared using DDI water in the chamber.

Oxygen and nitrogen supply were ultra-purity grade from Airgas. ZVI of 325-mesh (>99.2%, Johnson Matthey) has a specific surface area of 0.073 m^2/g by BET nitrogen absorption analysis (Autosorb-6, Quantachrome).

Batch experiment procedure

Serum vials with 12 ml in volume were used as batch reactors. For each run, multiple reactors were prepared with the same designed initial conditions. Reactors were prefilled with 0.5 g AIM and then transferred to the anaerobic chamber. Designed amount of stock solutions and DDI water were filled in the reactor to a total volume of 10 mL. Rubber stoppers and aluminum crimps were used to seal the reactors tightly. The reactors would then be placed in a rotary tumbler for mixing at 30 rpm in the dark. In the anoxic experiment, the system was kept sealed. In the oxic experiment, the gas in the headspace of the bottle was drawn out 3 mL and replaced with pure oxygen every 30 min. At predetermined time intervals, three reactors were removed from the tumbler for measuring pH, cations of Fe^{2+}, Fe^{3+} and NH_4^+, anions of Cl^-, NO_3^-, SO_4^{2-}, CN^-, $Fe(CN)_6^{4-}$, and OCN^-.

Production of the AIM system

The nitrate-Fe^{2+} pretreatment method was used to convert original ZVI media into AIM. The detail of the pretreating process was described in Chapter II. More recent studies by Huang's group reveals that while Fe_3O_4 is the main iron corrosion product, the actual reaction is more complicated than described in the previous chapter, involving the formation of the Fe(II)-rich flexible FeO_x structure that may consist of a green-rust like structure as a precursor. These corrosion products (CPs) are mostly magnetite-like

iron oxides (FeO_x) with mixed Fe(II) and Fe(III) forming flexible structures with many-electron or lattice vacancies. In the AIM system, a substantial mass of FeO_x co-exists with ZVI in the forms of either a surface adhesion on ZVI grains or discrete FeOx particles to form a mixture of highly reactive media that not only could provide electrons to carry out redox transformation of contaminants, but also could immobilize contaminants through surface adsorption or ion exchanging via a multi-layer structure of anion-cation intercalation.

Oxygen consumption experiment procedure

In the oxygen consumption test, multiple reactors were prepared using the following procedures: (1) stock solutions were prepared by dissolving pre-weighted chemicals in deoxygenated DI water, (2) 8 ml of the stock solution was transferred to the reactor containing pre-weighted iron grains, (3) the reactor was immediately capped with a stopper, the headspace (3.5 ± 0.1 mL) was flushed with O_2 for 20 s by inserting two needles through the stopper and allowed the headspace pressure to equilibrate with the atmosphere so that the initial O_2 pressure in the headspace was 1.0 atm, (4) the reactors were placed in a rotary tumbler for mixing at 30 rpm in the dark, and (5) at selected times, one reactor was sacrificed for regular analyses of various parameters. In these experiments, only the initial conditions in the reactors were controlled.

The gas pressure in the 3.5 mL headspace of the batch reactor was measured with a method developed in this study as elaborated below. Since the headspace pressure was allowed to balance with the ambient atmospheric pressure, the initial headspace gas pressure in all tests was considered as 1 atm. As the reaction proceeded, the headspace

pressure was measured and calculated by the following steps: (1) submerge the reactor into the water a beaker filled with, with a water level of 2-cm above the top of the reactor cap; (2) poke a gas-tight syringe (50 μL capacity) through the rubber stopper, and then slowly withdraw 50 μL gas from the headspace so that the gas pressure in the syringe would be the same as that in the headspace of the reactor; (3) pull out the needle, but ensure the needle is still immersed in water. If the gas in the syringe has a pressure lower than 1 atm, water will be sucked into the syringe to equilibrate with the atmospheric pressure. The headspace pressure can be calculated from the volume of the water in the syringe. For example, 10 μL water in the syringe means that the headspace pressure is (50–10)/50 = 0.80 atm. Note that the smallest reliable reading of the syringe is 2 μL (equivalent to 0.04 atm).

Analytical Methods

Dissolved Fe^{2+}, Fe^{3+}, free cyanide, ferrocyanide, and ammonia were tested on a UV-VIS spectrophotometer (T80, PG Instruments). Fe^{2+} and Fe^{3+} were measured colorimetrically using the 1,10-phenanthroline method at the wavelength of 510 nm (Method 3500-Fe-D). Free cyanide was tested using the chloramine-T and pyridine-barbituric method at the wavelength of 580 nm (Method 4500-CN-C). Ferrocyanide $[Fe(CN)_6^{4-}]$ was measured using the direct ultraviolet spectrophotometric method at 215 nm wavelengths (Method 9015). Ammonia was tested using the phenate method at the wavelength of 640 nm (Method 4500-NH_3-F). Chloride, nitrate, and cyanate were measured using the use IC (DX-500, Dionex) with IonPac AS22 and AS18 (Method

4110 B). ORION pH meter was used for pH measurement. The total cyanide concentration was the sum of free cyanide and ferrocyanide.

Solid characterization

The reactive particles and solids were analyzed and characterized using XRD, which was conducted at the Material Characterization Facility at Texas A&M University. XRD analysis was performed using a powder X-ray diffractometer (Bruker D8) equipped a monochromatized Cu Kα radiation. Samples for XRD analysis were prepared specially. The analyzed samples were initially filtrated through a 0.2-μm membrane filter in the anaerobic chamber. The filer was subsequently dried for 72 hours in the anoxic environment before analysis. All sample transportation was controlled in the sealed environment in order to minimize the contact of oxygen.

Results and Discussions

The iron-precipitation process

The blank test indicated that there are about 13 mg/L of dissolved Fe^{2+} in the anoxic AIM system. Free cyanide forms metal-complex with Fe^{2+} in aqueous system forming ferrocyanide $[Fe(CN)_6^{4-}]$ (Kyle 1997). The anoxic test was performed at neutral pH with 60 mg/L Fe^{2+} and initial cyanide of 0.769 and 1.538 mM (20 and 40 mg/L) as CN^- (Figure 13). The concentration of free cyanide, ferrocyanide, cyanate, nitrate, ammonia, and pH were monitored during the experiment. Shortly after cyanide introduction, free cyanide decreased rapidly to 0.019 and 0.304 mM while the ferrocyanide rocket to 0.419 and 0.820 mM. After two hours, both free cyanide and ferrocyanide dropped under the EPA's limit. The total cyanide concentration achieves

Chinese limit (0.008 mM) after 16 hours. The concentration of cyanate, nitrate, and ammonia was tested at zero and the system pH was between 6.2 and 6.6 during the test.

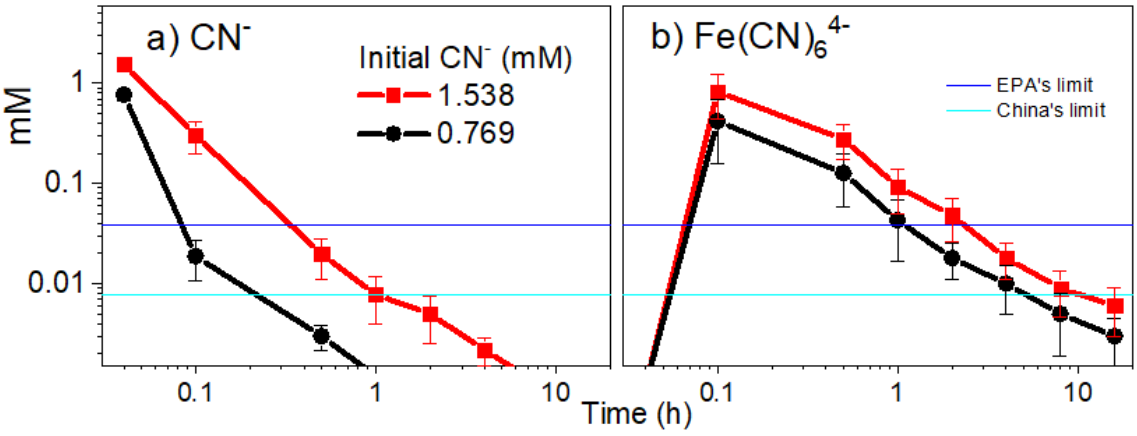

Figure 13. The concentration of (a) free cyanide and b) ferrocyanide in the anoxic Fe^{2+}-enriched AIM batch system.

The aqueous Fe^{2+} ions react with free cyanide ions to form a ferrocyanide complex (Adams 1992, Kyle 1997, Huang, Zhang et al. 2003, Chiang, Chang et al. 2010). Therefore, free cyanide dropped fast in the AIM system. With the excess of aqueous Fe^{2+} ions, ferrocyanide can be immobilized to an insoluble ferrous ferrocyanide $[Fe_2Fe(CN)_6]$ and precipitate slowly, known as Williamson's or Berlin's White. (Ghosh, Dzombak et al. 1999, Reguera, Fernández-Bertrán et al. 1999) (Equation 16 and 17)

$$Fe^{2+} + 6CN^- \rightarrow Fe(CN)_6^{4-} \quad (16)$$

$$2Fe^{2+} + Fe(CN)_6^{4-} \rightarrow Fe_2^{II}Fe^{II}(CN)_6 \downarrow \quad (17)$$

In order to better investigate the cyanide co-precipitation mechanism, we run an XRD test on the sediment. Figure 14 presents the XRD spectra of the samples in 24-hour 600-mg/L Fe^{2+}, 400-mg/L cyanide batch. The pattern of magnetite peaks remained but blended with the peaks of ferric ferrocyanide ($Fe_4[Fe(CN)_6]_3$, Prussian blue). Equation

18 describes the rapid oxidation reaction of ferrous ferrocyanide to ferric ferrocyanide, which was detected by XRD (Williams 1948, Botz, Mudder et al. 2005). The ferrous ferrocyanide in the sediment may have been oxidized to ferric ferrocyanide during the XRD examination.

$$3Fe_2^{II}Fe^{II}(CN)_6 + 4H^+ + O_2 \rightarrow 2Fe^{2+} + Fe_4^{III}[Fe^{II}(CN)_6]_3 \downarrow \quad (18)$$

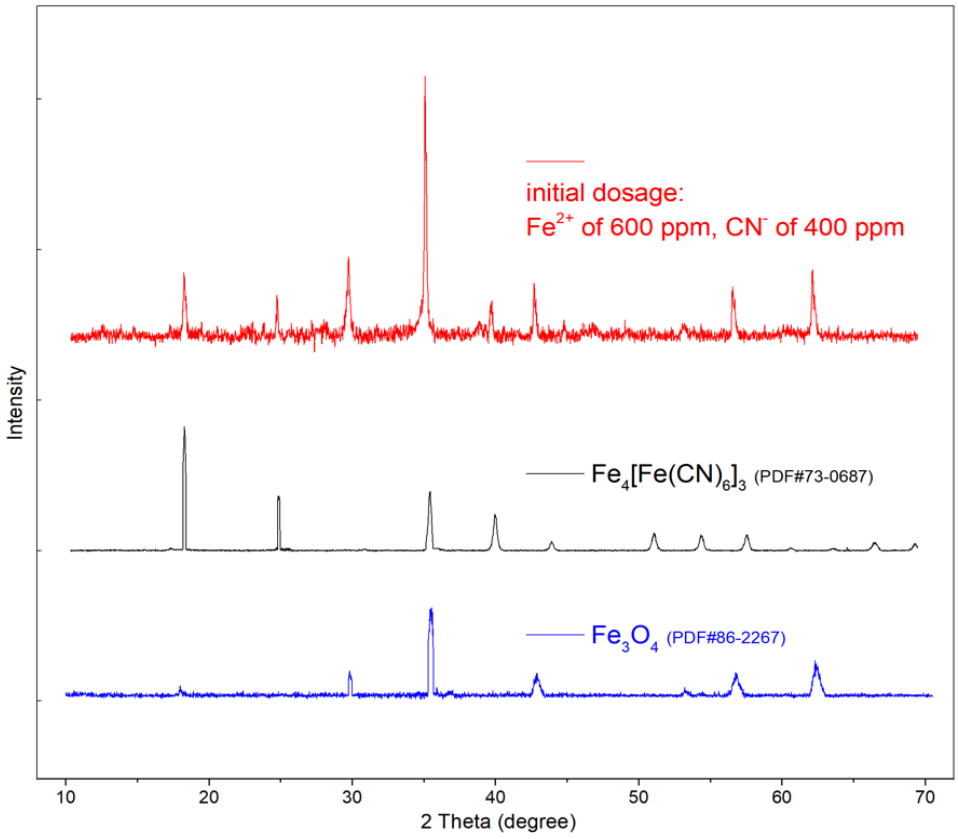

Figure 14. The XRD spectra of sediment samples in the anoxic Fe^{2+}-enriched AIM batch system.

To further analyze the precipitate's stability, after the 16-hour reaction, both reactors from the anoxic Fe^{2+}-enriched AIM batch were sonicated for 30 seconds. Figure 15 showed that free cyanide and ferrocyanide change after sonication. The ferrocyanide

concentration increased (from 3 and 6 µM to 34 and 64 µM), as well as a small increase of free cyanide (from 0.1 and 0.9 µM to 0.7 and 2.7 µM). According to the literature, ferrous ferrocyanide is unstable under conditions of changing temperature, low pH, ultraviolet light, and vibration (Griffith 1962, Zaidi and Carey 1984, Pohlandt 1985). A portion of ferrous ferrocyanide would be decomposed to Fe^{2+} and ferrocyanide ions back to the solution due to the 30-s sonication.

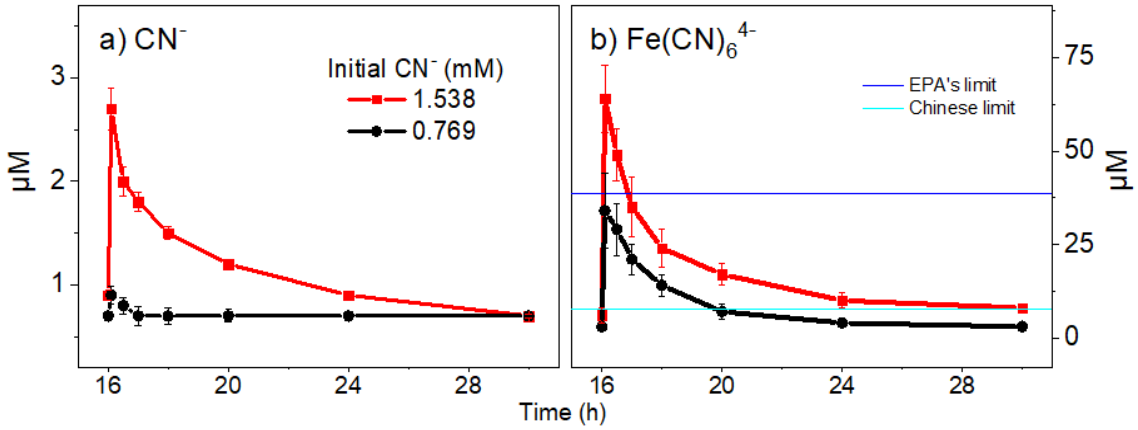

Figure 15. The concentration profile of the sediment stability test for a) free cyanide and b) ferrocyanide in the anoxic Fe^{2+}-enriched AIM batch system.

Therefore, the removal of cyanide follows the iron-precipitation mechanism in an anoxic Fe^{2+} enriched AIM system. Due to the unsteady property and required further treatment of the precipitate, an alternate process is needed to be evaluated.

The anion exchange process

Due to the ion exchanging ability of the AIM via the multi-layer structure of anion-cation intercalation (Huang, Peddi et al. 2014). We test the AIM system for cyanide exchangeability. However, the labile Fe(II) on the AIM surface balances with aqueous Fe^{2+} ions in a neutral pH (Tang, Huang et al. 2016). Cyanide will react with

Fe^{2+} forming ferrocyanide as long as aqueous Fe^{2+} exists. However, when the system's pH is over 8, ferrous hydroxide $[Fe(OH)_2]$ will dominate and the concentration of Fe^{2+} ion can be neglected (Morgan and Lahav 2007). Therefore, in order to avert the intervention of Fe^{2+} ion, sodium hydroxide was added to increase the system pH. We conducted the AIM batch experiment with initial cyanide of 0.769 mM and pH-controlled at 10 during the whole process. Figure 16 shows the result with monitoring chloride, sulfate, nitrate, free cyanide, and ferrocyanide. The ferrocyanide concentration was maintained at 0.023 mM. Free cyanide dropped from 0.769 to 0.004 mM, while chloride and nitrate concentration increased from 0.02 and 0.01 mM to 0.71 and 0.045 mM in 8 hours. An addition of 1.5 mM sodium sulfate was added after that. The ferrocyanide concentration was not increased due to the high pH. The concentration of free cyanide increased back from 0.004 to 0.715 mM. The sulfate concentration dropped from 1.5 to 1.148 mM.

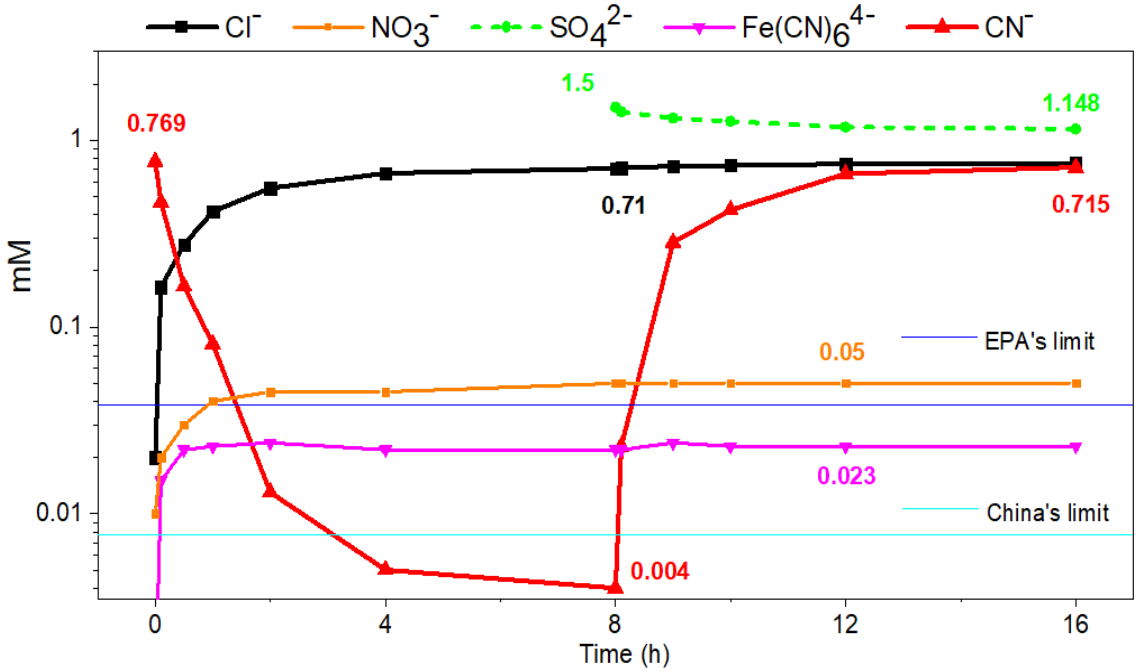

Figure 16. The concentration profile of ions during the anion exchange test in the pH-controlled anoxic AIM batch system.

Anions are differences in binding affinity and selectivity coefficient. The greater the selectivity coefficient is, the greater preference is for the ion to be exchanged (Pohl, Stillian et al. 1997). The overall anion selectivity order is $SO_4^{2-} \gg CN^- > NO_3^- > Cl^- \gg OH^-$ (Xu, Chen et al. 2010). Therefore, the chloride, nitrate, and hydroxide ions in the AIM can exchange with cyanide ions. The decrease of free cyanide concentration (0.765 mM) basically equals the combined increased concentration of chloride and nitrate (0.726 mM). However, sulfate has a larger affinity and selectivity coefficient than the other four species (CN^-, NO_3^-, Cl^-, and OH^-). Therefore, sulfate would exchange cyanide back to the aqueous system (Equation 19 and 20). the result reflects the anion exchange cyanide removal mechanism in the high pH anoxic AIM system. The decrease

of sulfate concentration (0.352 mM) basically represents half of the increased free cyanide concentration (0.711 mM).

$$CN^- \rightleftharpoons NO_3^- + Cl^- + OH^- \quad (19)$$

$$SO_4^{2-} \leftrightharpoons 2CN^- \quad (20)$$

In real industrial wastewater sources, higher binding affinity ions (like sulfate) usually exist, which would weaken the exchangeability of cyanide. Therefore, the anion exchange procedure can hardly be a robust treatment process for cyanide.

Blank comparison

The blank anoxic ZVI and AIM systems were tested in Chapter II. The result showed that the nitrate, ammonia, and ferric concentration was negligible. The dissolved Fe^{2+} concentration was about 16 and 13 mg/L.

We also experiment in the oxic condition for both systems. In the ZVI with O_2 system, the pH was around 7. The dissolved Fe^{2+} and Fe^{3+} concentrations were 18 and 0.5 mg/L, respectively (Figure 17a). Ammonia was negligible. In the AIM system, the pH was lower at around 6.5 and the final ammonia concentration was 1.12 mg/L (0.08 mM). The dissolved Fe^{2+} and Fe^{3+} concentration was 21.5 and 7.3 mg/L, respectively (Figure 17b). Here, the significant presence of Fe^{3+} from the oxic AIM system is the most intriguing: AIM promotes the formation of Fe^{3+} species, but ZVI does not. It must be noted that in this study, the reported Fe^{3+} is derived from total dissolved Fe subtracting dissolved Fe^{2+} as measured. More rigorously, the value should be reported as oxidized dissolved Fe species. The possibility of the presence of ferret ions cannot be excluded.

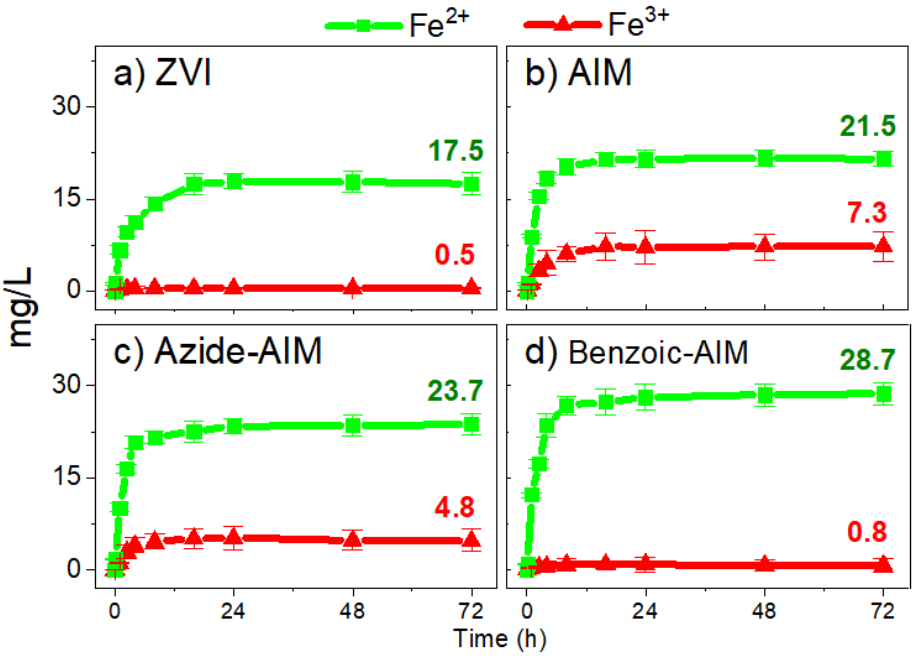

Figure 17. The concentration of dissolved Fe^{2+} and Fe^{3+} in the blank oxic a) ZVI, b) AIM, c) Azide-AIM, and d) Benzoic-AIM systems.

The unexpected presence of oxidized dissolved Fe species points towards a potential role of radical reaction involved in the AIM/Fe^{2+} + O_2 system. Azide has the fully quenching effect to singlet oxygen and can partially influence the generation of free radicals (Equation 21) (Harbour and Issler 1982, Britigan, Hassett et al. 1989, Li, Cline et al. 2001). Benzoic acid reacts with hydroxyl radicals (·OH) at the rate constant of 5.7×10^9, significantly faster than with Fe^{2+} ions at 3.4×10^8 (Ross and Ross 1977, Buxton, Greenstock et al. 1988) (Equation 22 and 23). Therefore, In many studies, benzoic acid was used as a universal radical scavenger in order to eliminate the radicals' oxidation effect of hydroxyl radicals (Haseloff, Blasig et al. 1990).

$$N_3^- + O{=}O \rightarrow \cdot N_3 + O_2^- \quad (21)$$

$$C_6H_5CO_2H + \cdot OH \rightarrow HOC_6H_5CO_2H \quad (22)$$

$$Fe^{2+} + \cdot OH \rightarrow Fe^{3+} + OH^- \quad (23)$$

The control tests with an oxic AIM system with an additional 5 mM sodium azide or benzoic acid were conducted to evaluate the potential role of radicals in the formation of dissolved Fe^{3+}. The system pH was adjusted to 6.5 (the same pH in the normal AIM system) with sodium hydroxide. As shown in Fig. 13c, no significant impact was found for the dissolved Fe^{3+} (4.8 mg/L) with the presence of azide. The dissolved Fe^{2+} concentration increased to 23.7 mg/L in the azide-AIM system. The mere impact to the system indicates the oxidation reactions in the oxic AIM system are not contributed by singlet oxygen. In the benzoic-AIM system, the dissolved Fe^{3+} concentration could hardly be monitored (0.8 mg/L), while the Fe^{2+} concentration increased to 28.7 mg/L. However, the total dissolved iron concentration was similar between AIM, azide-AIM, and benzoic-AIM systems, at around 28 mg/L.

Therefore, it could be inferred that the oxic AIM system might produce a notable amount of hydroxyl radical, which might be responsible for the formation of oxidized dissolved Fe^{3+} species. In contrast, an anoxic ZVI system does not form a significant amount of radicals under similar conditions.

Oxygen consumption

According to Dr. Huang's previous study, ZVI will react with dissolved oxygen forming iron oxide layers on the ZVI surface. The ongoing reactions will consume oxygen fast, resulting in the quick drop of the gas pressure in the reactors' headspace (Huang and Zhang 2005, Zhang and Huang 2006). We conducted the oxygen consumption experiment in the AIM system to better evaluate its oxidation potentials and the source of hydroxyl radicals. Figure 18 presents the oxygen consumption test in

the blank AIM system for 16 hours. With initial gas pressure of 1 atm, it drops rapidly to 0.50 atm at 2 h and to 0.22 at 4 h. The second dosage of oxygen (1 atm) was injected at 8 hours after the first dosage of oxygen was fully consumed. The gas pressure drops to 0.54 atm at 10 h and to 0.32 at 12 h. It decreased to around 0.04 after 16 hours of reaction. The oxygen consumption rate was almost the same for the two dosages.

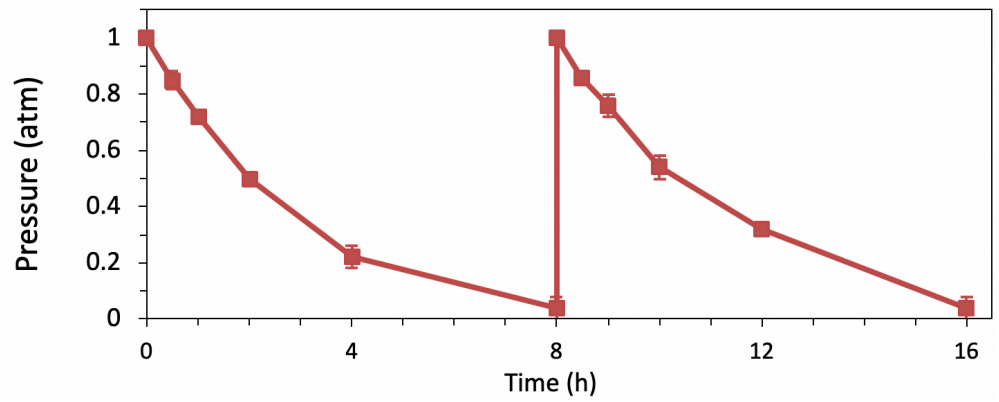

Figure 18. The gas pressure of the headspace in the blank AIM batch system.

This test indicates the continuous oxygen consumption of the AIM system during the oxic environment. It explains the source in the producing hydroxyl radicals during the reactions in the oxic AIM system.

The oxidative degradation process

The conventional chemical cyanide treatments like alkaline chlorination, Sulphur dioxide, hydrogen peroxide, ozone, and Caro's acid are all oxidation processes that can create the middle product of cyanate (OCN^-) and ammonia (NH_3) and the end product of nitrogen (N_2). The blank test of oxic AIM indicated the production of hydroxyl radicals. Therefore, a batch test of initial cyanide of 0.769 and 1.538 mM in the oxic AIM system was performed for 48 hours (Figure 19). The free cyanide concentration quickly dropped

below the limit in 1 h, while ferrocyanide concentration rise to peak at 0.427 and 0.927 mM. Ferrocyanide concentration then dropped steadily and the concentration was below limit after 8 h. Cyanate concentration increased to the peak (0.203 and 0.369 mM) at 2 to 3 h, then declined steadily. The ammonia concentration increased slowly at first, then rockets to the peak of 0.743 and 1.443 mM at 8 h followed by a decomposed trend. Tracing nitrogen element, the increasing amount of ammonia should be formed by the decreasing amount of total cyanide (0.764 and 1.533 mM). Ammonia may gradually decompose to nitrogen gas with a final concentration drop to 0.274 and 0.571 mM. The total cyanide removal was 99.3% and 99.6%. The dissolved Fe^{2+} concentration was maintained at around 14 and 25 mg/L and the dissolved Fe^{3+} concentration was about 6 and 7 mg/L.

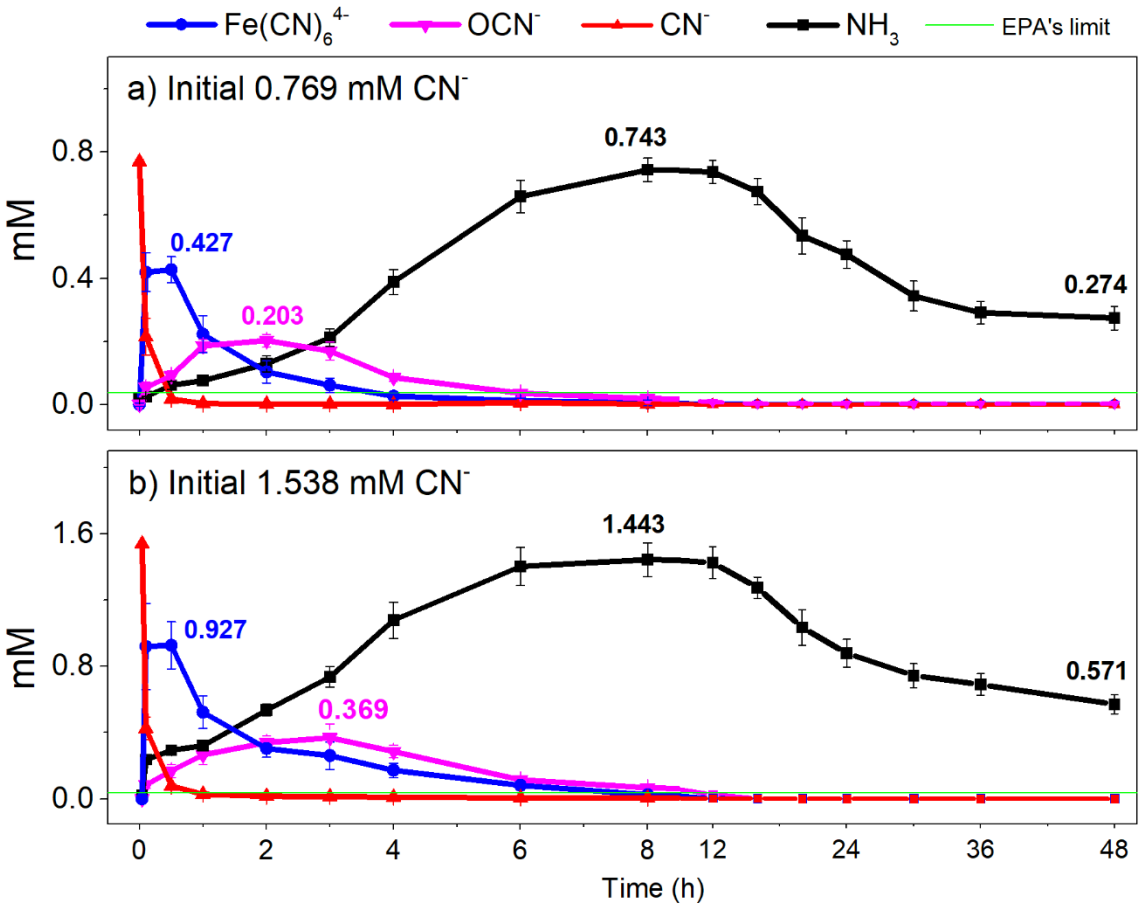

Figure 19. The concentration profile of cyanide, ferrocyanide, cyanate, and ammonia in the oxic AIM batch system with initial cyanide concentration of a) 0.769 mM and b) 1.538 mM.

Hydroxyl radicals can oxidize Fe^{2+} to Fe^{3+}, also ferrocyanide to ferricyanide following Equation 17 and 24 (Klein, Bhatia et al. 1975, Keenan, Sedlak et al. 2008). The cyanide oxidation procedure begins with hydroxyl radicals reacting with cyanide (both free and chelating form) to cyanate (Equation 25 and 26). The producing cyanate hydrolyzed with water to ammonium carbonate later (Equation 27) (Wen and Brooker 1994). Ammonia was then slowly oxidized to nitrogen gas following Equation 28 (Kim, Kim et al. 2005).

$$Fe^{II}(CN)_6^{4-} + \cdot OH \rightarrow Fe^{III}(CN)_6^{3-} + OH^- \quad (24)$$

$$CN^- + 2 \cdot OH \rightarrow OCN^- + H_2O \quad (25)$$

$$Fe^{III}(CN)_6^{3-} + 6 \cdot OH \rightarrow 6\, OCN^- + H_2O + Fe^{3+} \quad (26)$$

$$OCN^- + 3H_2O \rightarrow NH_4^+ + HCO_3^- + OH^- \quad (27)$$

$$NH_4^+ + 2 \cdot OH \rightarrow \frac{1}{2} N_2 + 2\, H_2O \quad (28)$$

Therefore, cyanide can be treated in the oxic AIM system following the oxidative degradation mechanism. It can transform to ferrocyanide, cyanate, ammonia, and finally emitted out of water.

System and media comparison

The comparison experiments were conducted for 24 hours in the no media and ZVI system under the oxic condition with initial cyanide of 1.538 mM (Figure 20). The cyanate and ammonia concentrations were not detected in both systems. The cyanide concentration in no media system remains unchanged with no sight of ferrocyanide. While in the ZVI system, the increase of ferrocyanide (0.931 mM) basically equals the decrease of free cyanide (1.065 mM). The result indicated that cyanide cannot be oxidized by dissolved oxygen alone nor in the oxic ZVI system.

To better categorize the radicals produced in the oxic AIM system, experiments were conducted using an additional 5 mM sodium azide, compared with 5 mM benzoic acid. The system's initial pH was adjusted to 6.5 and a dosage of 1.538 mM cyanide was added. Free cyanide, ferrocyanide, cyanate, and ammonia were monitored during the 8-hour test (Figure 21).

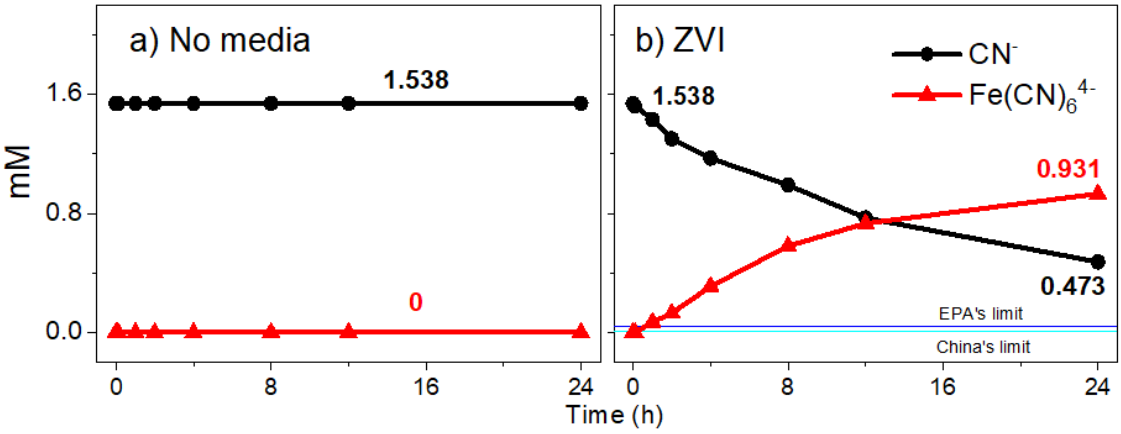

Figure 20. The concentration profile of a) no media system and b) ZVI system under oxic condition.

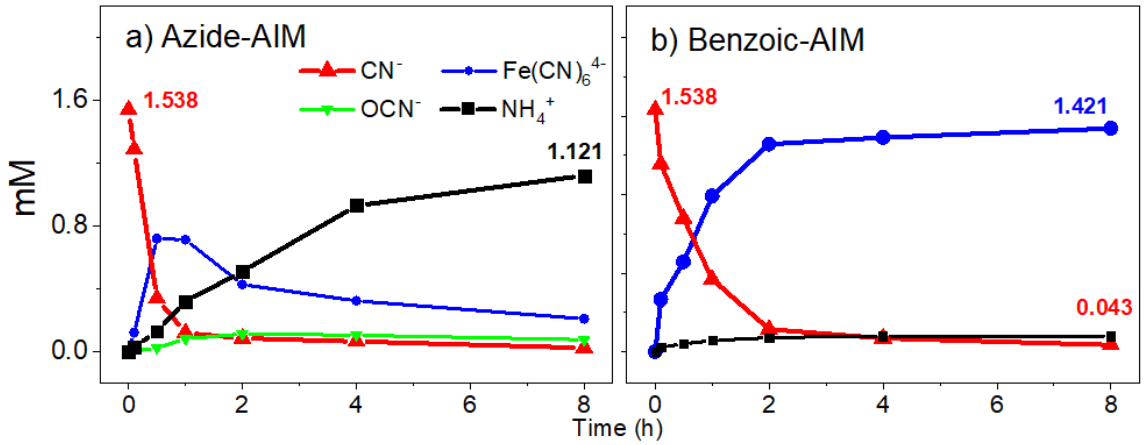

Figure 21. The concentration profile of a) azide-AIM and b) benzoic-AIM system.

In the azide-AIM system, although the oxidative degradation reactions occurred (transformation from cyanide to ammonia), the treatment efficiency was slower than the normal AIM system. The small impact to the system indicates the oxidative degradation process is not contributed by singlet oxygen.

In the benzoic-AIM system, no cyanate was found. Ammonia concentration was around 0.1 mM (similar to the blank oxic AIM system). The increase of ferrocyanide (1.421 mM) basically represents the decrease of free cyanide (1.495 mM) in the benzoic-

AIM system. As a radical scavenger, benzoic acid can totally consume all radicals including hydroxyl radicals (Klein, Bhatia et al. 1975, Haseloff, Blasig et al. 1990). Therefore, the scavenging effect stopped the cyanide oxidation process, inhibited the oxidation reactions. As a result, the oxidative degradation by hydroxyl radicals contributes to the main cyanide removal mechanism during the oxic AIM process.

Continuous batch experiments

The continuous batch experiment was conducted in order to further assess the removal efficiency of the oxic AIM system (Figure 22). The next dose was added when the cyanide concentration was below the EPA's limit (0.039 mM). Total cyanide and ammonia concentration were monitored. For each dosage, cyanide concentration was 0.769 and 1.538 mM. During the 96-h experiment, the oxic AIM system achieved 4 batches for the two different dosages, indicating 3.46 and 6.15 mM of cyanide was removed. The final ammonia concentration of 3.22 and 5.96 mM basically represented the reduced cyanide amount.

The results of the continuous batch experiments by the oxic AIM system indicated that cyanide can be irreversibly and steadily converted to ammonia and nitrogen gas. The procedure does not require additional reagents, further treatment, or complicated system control.

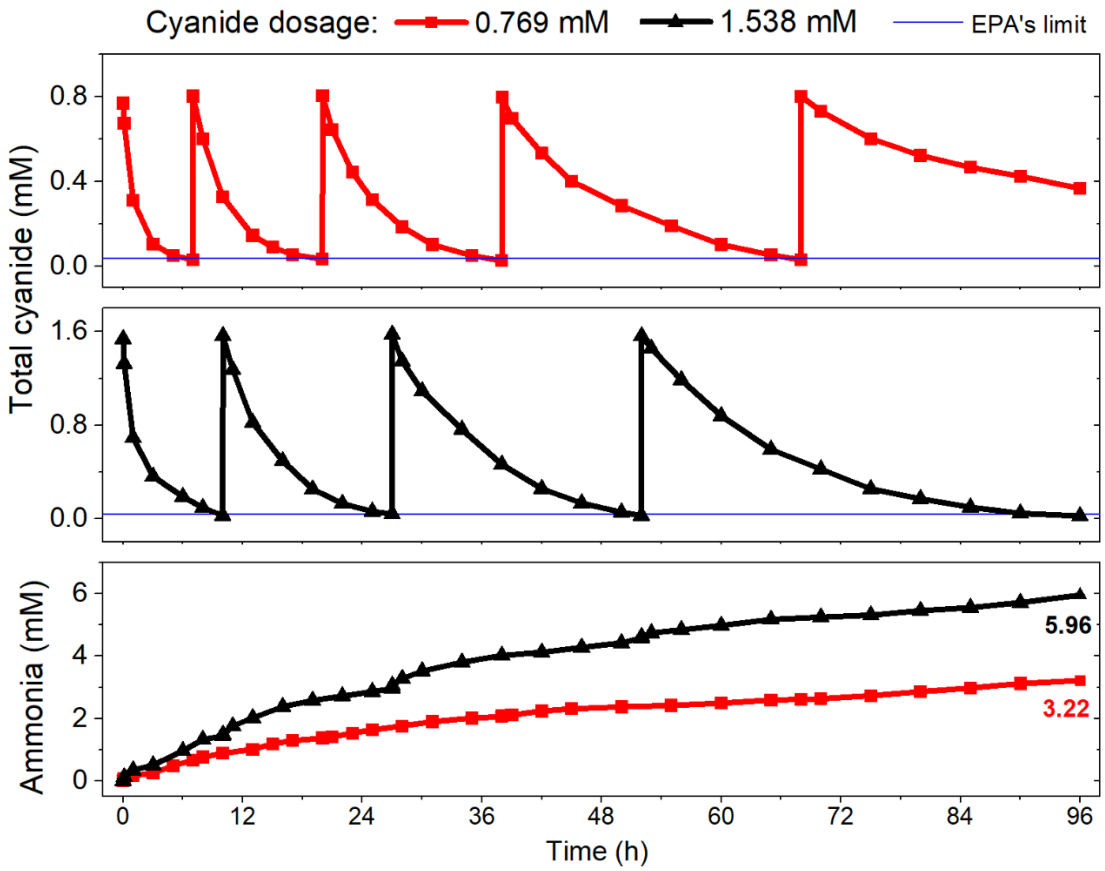

Figure 22. The total cyanide and ammonia concentration profile of continuous oxic AIM batch system with initial cyanide of 0.769 and 1.538 mM.

Summary

We found the removal of cyanide was not ideal in the anoxic environment. The anoxic iron-precipitation process transforms cyanide to ferrocyanide and then to insoluble ferrous ferrocyanide. However, the sediment is unstable and easy to decompose. The anoxic anion-exchange procedure allows cyanide exchange with ions in the iron media and is removed. It, whereas can be exchanged back by higher binding affinity ions. Thurs, it is hard to operate and maintained.

In the oxic environment, the AIM system becomes an oxidizing reactive system with highly reactive radicals. The oxygen consumption in the AIM system and the difference of the aqueous Fe^{3+} in the blank and inhibited system indicated the production of the hydroxyl radicals. The oxidizing reactive AIM system made it feasible for cyanide treatment. Cyanide and chelated cyanide can be converted to nitrogen gas step by step. With the quantification of the intermediate products (ferricyanide, cyanate, and ammonia) and comparison of the inhibited system, the oxic AIM system was tested to remove cyanide irreversibly (>99% removal).

The continuous batch test further implied the reliability and sustainability of the oxic AIM system without requiring additional reagents, further treatment, or complicated system control. Therefore, the oxic AIM system would be a feasible treatment procedure for cyanide-containing wastewater.

CHAPTER IV. EDTA TREATMENT

Introduction

EDTA is widely used as a complexing agent in the plating and metal finishing industry as well as other chemical cleaning processes (Yating, Bin et al. 2008). Although EDTA is non-toxic to mammals at low concentrations, a higher dosage is still considered hazardous, which may lead to weight loss and kidney problems (Reuber and Schmieler 1962). Free EDTA can be hard to treat. The photo-oxidation of free dissolved EDTA at pH 7 has a measured half-life of 36 years for an initial hydroxyl radical concentration of 5×10^{-6} mM and a 12-hour daylight duration (WHO 2004). Once EDTA is released into an aquatic environment, its speciation will depend on the water quality and the presence of trace metals with which it can combine. It is a powerful hexadentate chelating ligand capable of combining stoichiometrically with virtually every metal in the periodic table in the chelating form of metal-EDTA (Gerike, Fischer et al. 1979). Although the stability constants for different metal-EDTA complexes vary considerably, many metals that are capable of forming a strong complex with EDTA will last for a long time in nature. These EDTA chelates are hard to decompose by normal processes. Although currently EDTA in wastewater has not been regulated in both US and China, concerns over the impacts of EDTA have already been widely expressed. The concern of the EDTA in wastewater and its impact on the environment may lead to new guidelines and regulations in the near future.

EDTA is resistant to many bacterial biodegradation processes. Therefore, most of the conventional biological methods are ineffective for EDTA treatment (Madsen and

Alexander 1985, Bolton, Li et al. 1993, Allard, Renberg et al. 1996). However, recent studies have demonstrated that EDTA can be degraded by specially enriched bacterial cultures, with which wastewater treatment plants could achieve a lower concentration of EDTA in the effluents (Palumbo, Lee et al. 1994, Nörtemann and biotechnology 1999, Witschel, Egli et al. 1999, Bucheli-Witschel and Egli 2001). However, biological treatment systems for EDTA were usually low efficient. Therefore, the operating tanks of the biological treatment systems were often in large sizes (Henneken, Nörtemann et al. 1998, Alkaim and Hussein 2012).

EDTA degradation has been attempted by diverse advanced oxidation processes (AOP) including hydroxyl radical-based (direct O_3 or O_3/H_2O_2, UV/TiO_2 photolysis, Fenton or Fenton-like reaction), sulfate radical-based, and ozonation-based. The oxidation reactions rely on the oxidation potentials of the reactive chemicals. The essential roles in the AOPs are the reactive hydroxyl radicals (· OH), ozone (O_3), and persulfate ($S_2O_8^{2-}$). Their standard oxidation potentials (E^o) are 2.80, 2.07, and 2.01 V, respectively (Weast, Astle et al. 1988, Huang, Dong et al. 1993, Tchobanoglous, Burton et al. 2003, Deng and Zhao 2015).

Hydroxyl radical is capable of independent existence and possesses an unpaired electrons (Gomes, Fernandes et al. 2005). With the highest oxidation potential, it is a strong oxidant and can be used to oxidize and degrade various organic species (Tai, Gu et al. 2002, Tchobanoglous, Burton et al. 2003). Hydroxyl radicals attack organic pollutants mainly through four pathways: radical addition, hydrogen abstraction, electron transfer, and radical combination (Deng and Zhao 2015). Their reactions with organic

compounds produce carbon-centered radicals (R· or R-OH). With O_2, these carbon-center radicals may be transformed into organic peroxyl radicals (ROO·). All these radicals further react with the formation of more reactive species such as H_2O_2 and superoxide ($O_2^{\bullet-}$), leading to chemical degradation. Because hydroxyl radicals have a very short lifetime, they are only in situ produced during application through many different methods, including a combination of oxidizing agents (such as H_2O_2 and O_3), UV light, and catalysts (such as Fe^{2+} and TiO_2). Many studies have attempted to investigate the role of hydroxyl radical in the decolorization of dyes, the cleavage of naphthalene and benzene rings, the oxidation of organic compounds, the remediation of As^{3+} contaminated water, and decompose pollutants like cyanide and EDTA (Lee, Yoon et al. 2004, Dutta, Pehkonen et al. 2005, Song, Xu et al. 2007, Li, Crittenden et al. 2009, Wang, Xu et al. 2012, Yang, Shan et al. 2016).

The titanium dioxide photocatalysis (UV/TiO_2) process has been successfully applied for EDTA reduction for years. Electron vacancies may be produced inside TiO_2 when exposed to UV light. These electrons can be adsorbed by hydroxylated surface species on TiO_2, leading to the formation of hydroxyl radicals (Sillanpaa and Pirkanniemi 2001, Ahmed, Rasul et al. 2011, Alkaim and Hussein 2012). Studies have revealed that TiO_2 photocatalysis is an effective method to degrade dissolved EDTA (Low, McEvoy et al. 1991, Davis, Green et al. 1999, Krapfenbauer, Getoff et al. 1999, Vohra and Davis 2000). An advantage of the application of TiO_2 is the adsorbed compounds can be stripped from the media surface and the catalyst can be reused. Unfortunately, the photocatalytic oxidation applied for nickel-EDTA complexes can be

very limited due to the slow reaction kinetics (Xue, Sigg et al. 1995, Sillanpaa and Pirkanniemi 2001).

H_2O_2 as a strong oxidant is widely utilized to treat various inorganic and organic pollutants. Still, H_2O_2 alone is not effective for degrading recalcitrant contaminants like EDTA because of low rates of reaction. Transition metal salts (e.g. iron salts) and UV-light can be used to react with or activate H_2O_2 to produce hydroxyl radicals, which is a much stronger oxidant than H_2O_2 (Venkatadri, Peters et al. 1993, Neyens and Baeyens 2003). The UV/H_2O_2 process has been applied successfully to the EDTA treatment in many cases (Ku, Wang et al. 1998, Sörensen, Zurell et al. 1998, Jiraroj, Unob et al. 2006). Both the removal and mineralization rates of EDTA increase with the UV light intensity, due to the increased generation rate of hydroxyl radicals (Ku, Wang et al. 1998). The use of H_2O_2 in conjunction with Fe^{2+}/Fe^{3+} to produce hydroxyl radicals (Equation 27) to oxidize target compounds is better known as Fenton Reactions, a well-established AOP (Pera-Titus, García-Molina et al. 2004, García-Montaño, Pérez-Estrada et al. 2008, Shin, Yoon et al. 2008, Wang, Xu et al. 2012). It is known to be very effective in the destruction of many hazardous organic pollutants in water including EDTA and metal-EDTA complexes (Kitis, Adams et al. 1999, Yoon, Lee et al. 2001, Neyens and Baeyens 2003, Ghiselli, Jardim et al. 2004, Fu, Chen et al. 2006, Pirkanniemi, Metsärinne et al. 2007). The optimal pH condition of the Fenton treatment system was around 2.5 to 3. Therefore, for the wastewaters in near-neutral pH (pH=6-7), the Fenton treatment may not be as effective (Neyens and Baeyens 2003).

$$Fe^{2+} + H_2O_2 \rightarrow Fe^{3+} + \cdot OH + OH^- \quad (29)$$

The applicability of ozonation for EDTA removal has also been widely studied (Gilbert and Hoffmann-Glewe 1990, Arslan, Balcioglu et al. 1999, Rodríguez, Mutis et al. 1999). A significant portion of EDTA could be destroyed during water treatment by ozonation, where other oxidants like chlorine were not effective (Sillanpaa and Pirkanniemi 2001). In the process of ozonation, the decomposition of ozone (O_3) could release intermediate products that could react with hydroxide ions (OH^-) to produce hydroxyl radicals. The formation of hydroxyl radicals can be artificially accelerated by increasing the pH or alkalinity of the system (Von Gunten 2003). Uncomplexed or weakly-complexed EDTA with calcium (Ca^{2+}) and cadmium (Cd^{2+}) ions could be more readily eliminated than strong-complexed EDTA with ferrous (Fe^{3+}) and nickel ions (Gilbert and Hoffmann-Glewe 1990, Korhonen, Metsärinne et al. 2000).

Persulfate ($S_2O_8^{2-}$) itself is a strong oxidant that can form more powerful sulfate radicals ($SO_4^{\cdot-}$, E^o=2.6 V), which can initiate the oxidation process (Farhataziz and Ross 1977, Glaze and technology 1987). The activation process of sulfate radicals can be by heat, UV irradiation, transitional metals, or elevated pH. Similar to hydroxyl radicals, sulfate radicals are highly reactive but with a short lifespan, though both radical species have different reaction patterns. Hydroxyl radicals usually add to C=C bonds or abstract H from the C-H bonds of the organic compounds. Sulfate radicals, compared to that, prefer to remove electrons from the molecules that are subsequently transformed into radical cations.

However, in the treatment of electroplating wastewater containing strong metal-EDTA complexes, both traditional and advanced processes have their limitations. A

specialized method is needed to deal with the treatment challenge. Therefore, developing and investigating specialized methods is needed in order to fully handle the treatment of EDTA.

The effectiveness of ZVI-related processes for metal removals is a well-established (Huang, Zhang et al. 2003, Huang, Tang et al. 2012). Laboratory experiments and field pilot tests of the AIM technology result in remarkable efficiency of removing various heavy metals, metalloids, and nitrate from mining, electric power, and refinery wastewaters (Huang, Peddi et al. 2014). Little has been reported about the potential of ZVI for EDTA treatment. The removal and breakdown of EDTA involve primarily the oxidation process. The understood that ZVI-based processes have a chance of generating radicals that might contribute to EDTA breakdown.

In this chapter, we aim to explore the potential of the AIM system for EDTA treatment. Developing and investigating specialized methods is needed in order to fully handle the treatment of EDTA.

Materials and Methods

Materials

All regent solutions were prepared by analytical reagent grade chemicals DI water and stored in the anaerobic chamber. Disodium Ethylenediaminetetraacetic acid dihydrate [$Na_2EDTA \cdot 2H_2O$, $(NaOOCCH_2)_2NCH_2CH_2N(CH_2COOH)_2 \cdot 2H_2O$, Honeywell], iminodiacetic acid [IMDA, $HN(CH_2COOH)_2$, Alfa Aesar], nitrilotriacetic acid [NTA, $N(CH_2COOH)_3$, Alfa Aesar], glycine (NH_2CH_2COOH, J.T.Baker), ferrous chloride ($FeCl_2 \cdot 4H_2O$, J.T. Baker), ferric chloride ($FeCl_3 \cdot 6H_2O$, J.T. Baker), sodium

nitrate ($NaNO_3$, Alfa Aesar), and hydrogen peroxide (H_2O_2, 30% in water, Alfa Aesar) were used in this study. Oxygen and nitrogen supply were ultra-purity grades from Airgas. ZVI of 325-mesh (>99.2%, Johnson Matthey) has a specific surface area of 0.073 m^2/g by BET nitrogen absorption analysis (Autosorb-6, Quantachrome).

Batch experiment procedure

The procedure was similar to the procedure described in Chapter III.

Production of the AIM system

The nitrate-Fe^{2+} pretreatment method was used to convert original ZVI media into AIM. The detail of the pretreating process was described in Chapter II.

Analytical methods

EDTA, NTA, IMDA, and glycine concentration were measured using Liquid Chromatography/Mass Selective Detector (LC/MSD) (Agilent). LC/MSD streamlined analytical work by adding mass detection intuitively with OpenLAB Chromatography Data System. A Zorbax Eclipse Plus C18 Rapid Resolution column (Agilent) of length 150 mm, diameter 4.6 mm, and particle size 3.5 μm was used. The column temperature of 40 ˚C. Methanol was used as the mobile phase solvent, tetrabutylammonium bromide as the ion-pair reagent in acetic acid buffer solution at a flow rate of 0.2 mL/min. The mobile phase consisted of methanol/water (30/70) and 1 mM tetra-n-butylammonium bromide [$(C_4H_9)_4NBr$, TGI] and 1 mM acetic acid (CH_3COOH, Honeywell). For EDTA, NTA, and IMDA, analytes were detected as Fe^{3+} complexes by electrospray ionization tandem mass spectrometry (ESI-MS) operated in the negative ion mode. Glycine was detected directly without Fe^{3+}. The capillary voltage was set at 2.0 kV, corona current 1

uA, charging voltage 2.0 kV, vaporizer temperature 250 ◦C, drying gas temperature 300 ◦C, nebulizer pressure 40 psi, and drying gas flow 8 L/min. Precursor molecular anion of Fe(III)-EDTA, Fe(III)-NTA, Fe(III)-IDA, and glycine was 344, 244, 187, and 74 m/z. The detection limit was 0.1 to 10 mg/L.

Total organic carbon (TOC) was measured on Shimadzu Total Organic Carbon Analyzer TOC-L Series following Patented 680 ◦C Combustion Catalytic Oxidation/NDIR Detection Method (Method 5301B).

Dissolved Fe^{2+}, Fe^{3+}, and ammonia were tested on a UV-VIS spectrophotometer (T80, PG Instruments). Fe^{2+} and Fe^{3+} were measured colorimetrically using the 1,10-phenanthroline method at the wavelength of 510 nm (Method 3500-Fe-D). Ammonia was tested using the phenate method at the wavelength of 640 nm (Method 4500-NH_3-F). Nitrate was measured using the use IC (DX-500, Dionex) with IonPac AS22 (Method 4110 B). ORION pH meter was used for pH measurement.

Results and Discussions

Media and conditions comparison

Due to the photolysis effect of EDTA in the natural systems, we evaluate its stability and potential decomposability during both anoxic and oxic environments in no media, ZVI, and AIM systems. In the no media system, the EDTA concentration and TOC remained at 0.5 mM after 4 hours in both anoxic and oxic conditions. The result indicates the stability of EDTA in a dark environment.

Figure 23 shows the EDTA removals with an initial EDTA of 0.5 mM during the batch test for 4 hours. In the ZVI system, the EDTA concentration dropped from 0.5 mM

to 0.263 and 0.283 mM (removals of 43.4 % and 47.3 %) during the 4-hour experiment in anoxic and oxic conditions. The anoxic AIM system achieved comparable performance to the ZVI system. The final EDTA concentration declined to 0.238 mM (removals of 52.4 %), The oxic AIM system performed better. The final EDTA concentration was down to 0.096 mM (removal of 80.8 %).

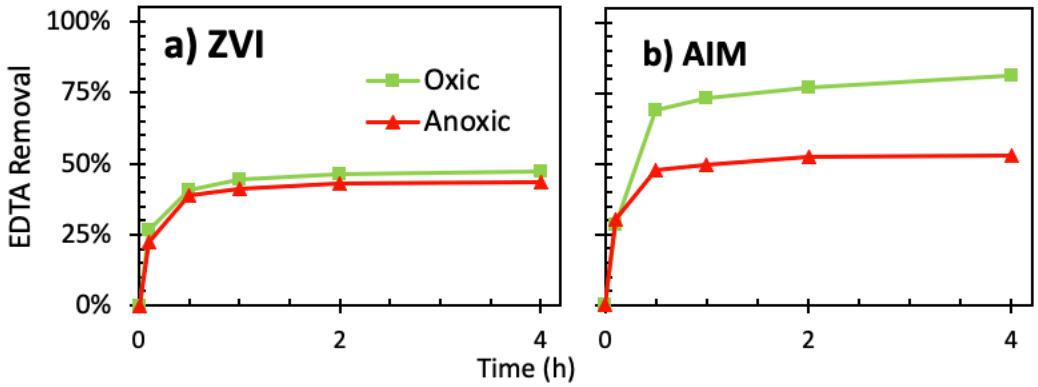

Figure 23. The EDTA removal percentages of a) ZVI and b) AIM batch system during anoxic and oxic conditions.

TOC decreased following the same trend as the EDTA concentration in the ZVI and anoxic AIM system. It declined from 62 mg/L to 32.4, 34.7, and 29.1 mg/L. The final TOC removal achieved 44.0 %, 47.7 %, and 53.1 %. However, in the oxic AIM system, it dropped slower. TOC removal was 58.5 % at 1 h, 64.2 % at 2h, and finally 69.5 % at 4 h.

TOC drops slower than the EDTA concentration in the oxic AIM system indicating the decomposition of EDTA to less-complex products. However, in the anoxic condition, the comparison experiments revealed similar removals of EDTA and TOC. This reveals that the removed EDTA may not be the decomposition during those conditions.

The adsorption process

It is worth noting that, in both the ZVI and AIM systems, the decline of EDTA concentration and TOC is following the same trend. They rapidly decrease at the first 30-min reaction, then slower. The first 30-min fast reaction contributes a significant part of the total removal. During this time, the removed EDTA could not be the break-down reaction to its shorter-chain compounds, nor volatilization. The EDTA molecules may be adsorbed to the iron media grains. Therefore, the anoxic batch test with EDTA dosage of 0.25, 0.5, and 1 mM in the ZVI and AIM system was conducted to evaluate the adsorption process. EDTA was added 0.5 mM in the first batch, twice of 0.25 mM at 0 and 1 hour in the second batch, three times of 0.1 mM at 0, 1, and 2 hours in the third batch. Figure 24 showed the removed EDTA concentration during the 4-hour experiment.

In the ZVI system, the removed EDTA in the one-time dosing batch increased to 0.219 mM in 4 hours. In the two-time dosing batch, it rose sequentially from 0.171 to 0.218 mM. In the three-time dosing batch, the removed EDTA improved from 0.089 to 0.169 and the final to 0.214 mM. In the AIM system, the one-time dosing batch resulted in 0.265 mM removed EDTA. The two- and three-time dosing batches performed similarly. The removed EDTA increased sequentially and finally to 0.267 and 0.261 mM.

Although the differences in the EDTA dosages and the remaining EDTA concentration, the removed EDTA was about the same for all three batches in both systems. Therefore, it pointed out that the similar adsorption ability of the same system

no matter the dosage EDTA. Due to the flexible structures, AIM has a higher adsorbing potential for EDTA molecules than ZVI.

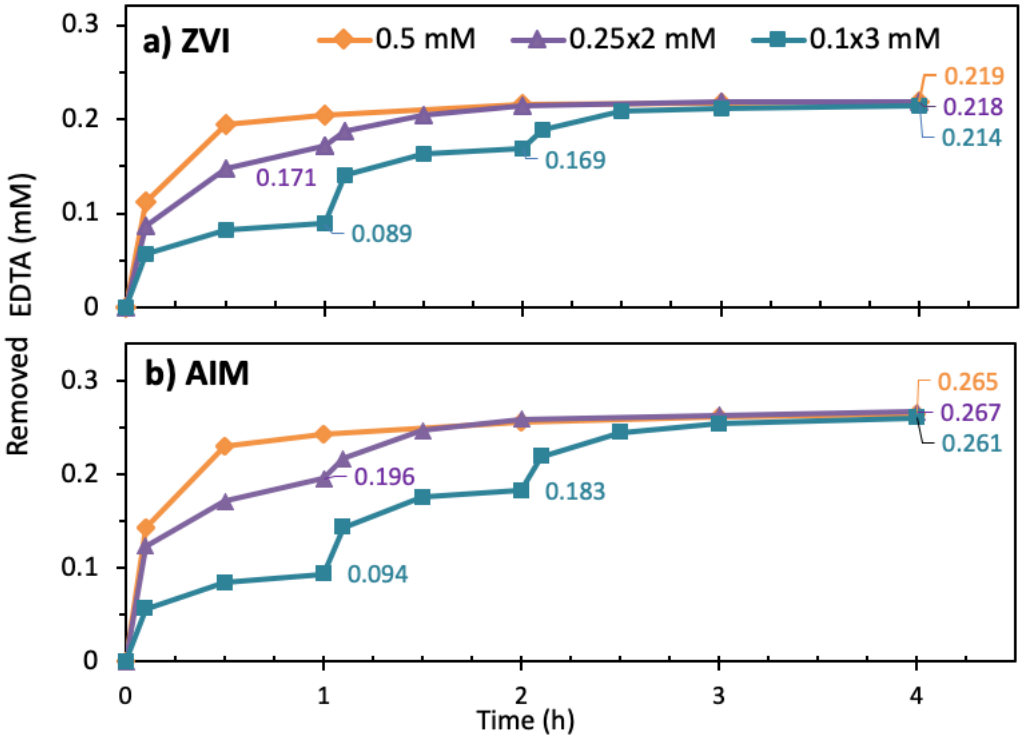

Figure 24. The removed EDTA concentration in the anoxic a) ZVI and b) AIM batch system.

Therefore, due to the limited surface loading of both media, only a fixed amount of EDTA can be adsorbed onto the iron media surface.

The oxidative degradation process

Most previous researchers have implemented EDTA treatment through different AOPs and found the formations of many intermediates (Gilbert and Hoffmann-Glewe 1990, Babey, Emilio et al. 2001, Ghiselli, Jardim et al. 2004, Zhou, Lim et al. 2010). These reported products include: (1) organic molecules with two nitrogen atoms, e.g. ethylenediaminetetraacetic acid (ED3A), ethylenediaminediacetic acid (EDDA or

ED2A), N-aminoethyl-eneglycine (EDMA), and ethylenediamine (EDA); (2) organic acids have one nitrogen atom, e.g. NTA, IMDA, and glycine; (3) simple organic acids, e.g. glyoxylic acid (GA), oxalic acid (OA), malonic acids, acetic acids, formic acid and formaldehyde; and (4) mineralization products such as carbonate, ammonia, and nitrate. These intermediates revealed the two possible EDTA degradation routes with AOPs: (1) EDTA → ED3A → ED2A → EDMA → EDA → glyoxylic acid ('amines pathway'), and (2) EDTA→ IMDA, NTA → glycine → glyoxylic acid ('glycines pathway') (Lockhart and Blakeley 1975, Madden, Datye et al. 1997, Sörensen, Zurell et al. 1998, Babey, Emilio et al. 2001, Xu, Shan et al. 2017).

Research has mentioned that during the hydroxyl radical-based AOPs, EDTA decomposed through the 'glycines pathway'. The intermediates of IMDA, NTA, and glycine can be detected. Some of these AOPs include the help of additional H_2O_2 (Venkatadri, Peters et al. 1993, Neyens and Baeyens 2003, Zhou, Lim et al. 2010). Therefore, batch experiments with an initial 0.5 mM EDTA were performed in the anoxic, oxic, and 10 mM H_2O_2 AIM system for 24 hours. Figure 25 shows the EDTA, IMDA, NTA, glycine, and ammonia concentration during the test.

In the anoxic environment, the EDTA concentration in the AIM system dropped from 0.5 mM to 0.286 mM in 0.5 h. Only a very small portion of EDTA was removed after that with the final concertation of 0.226 mM (54.8 % removal). No intermediate degradation products were detected. The ammonia concentration of 0.09 mM represents the same among in the blank test. The result demonstrated the removed EDTA was mostly contributed by the adsorption process of AIM.

When oxygen was introduced to the AIM system, the fate of EDTA was different. During the 0.5-h adsorption process, the EDTA concentration in the oxic AIM system declined to 0.157 mM. The final EDTA concentration was 0.053 mM (89.4 % removal), which is much lower than it in the anoxic AIM system. The IMDA, NTA, and glycine concentrations began to emerge after 1 h. These intermediate EDTA degradation products remain after 24 hours at about 0.04 mM with 0.16 mM of ammonia.

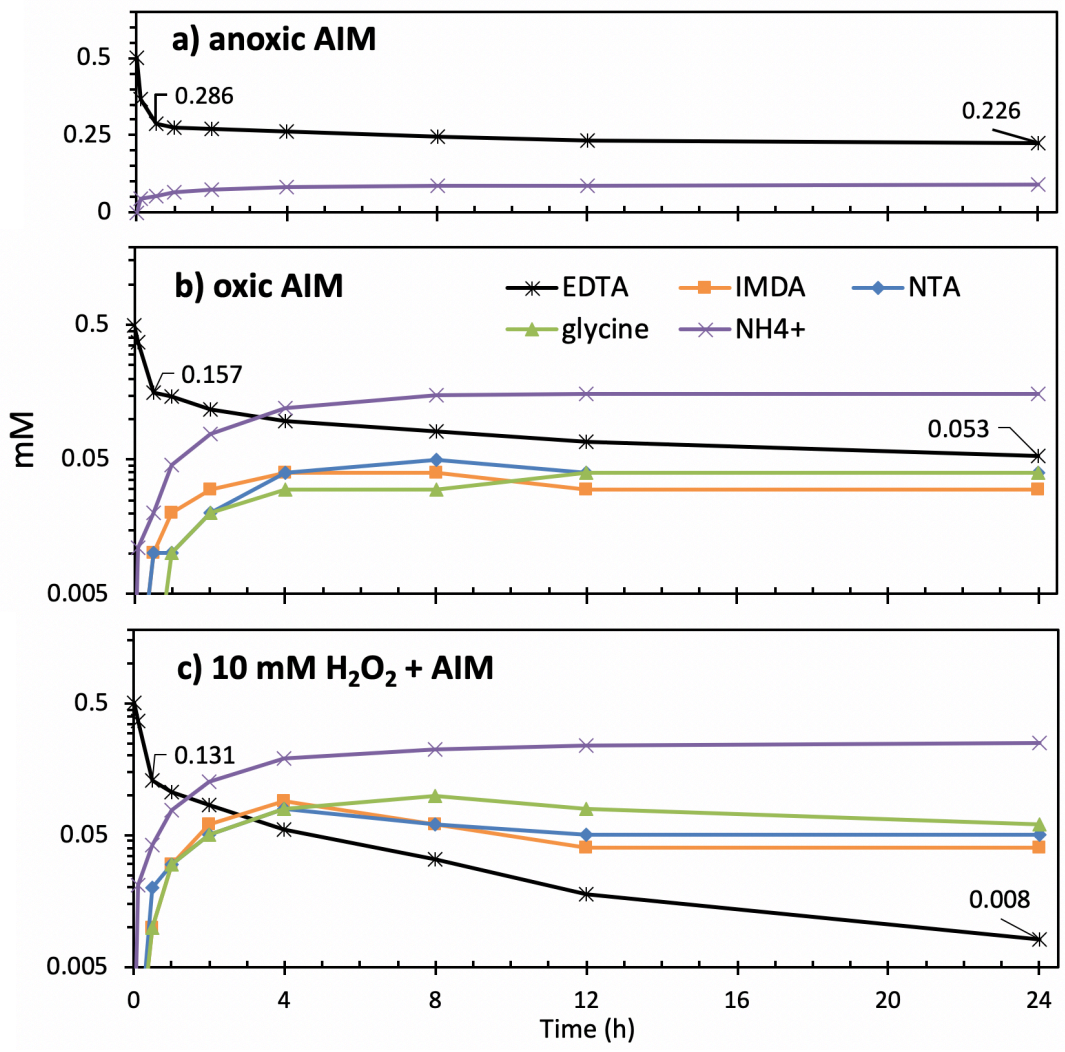

Figure 25. The concentration profile of EDTA, IMDA, NTA, and glycine in the a) anoxic, b) oxic, and c) 10 mM H_2O_2 AIM batch system.

With an additional 10 mM of H_2O_2 initially in the oxic AIM system, EDTA was removed faster. From 0.5 to 0.131 mM in 30 mins, it decreased rapidly to 0.008 mM at the end (98.4 % removal). The IMDA, NTA, and glycine concentrations were about 0.08 mM. The ammonia concentration was around 0.25 mM. The concentrations of the intermediates were higher than they in the oxic AIM system, indicating a faster EDTA decomposition process in the H_2O_2-AIM system.

The detection of IMDA, NTA, glycine, and ammonia during the oxidative process unveiled a possible 'glycines pathway' of EDTA degradation (Figure 26). It shows the ability of the oxic AIM system to decompose EDTA to IMDA and NTA, then to glycine and ammonia.

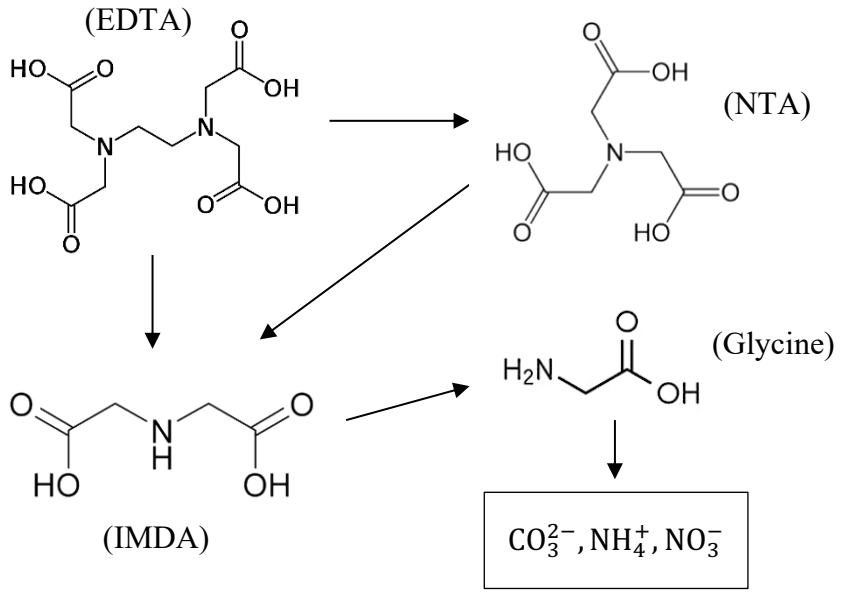

Figure 26. Possible degradation pathway of EDTA by hydroxyl radical-based AOPs.

System comparison

The additional H_2O_2 improves the decomposition of EDTA in the AIM system. To better understand the mechanism of the improvement and compare it with the traditional Fenton reaction, experiments with 0.5 mM EDTA and 10 mM H_2O_2 in a media system were implemented. Additional 0, 50, and 100 mg/L dissolved Fe^{2+} were added to the systems. EDTA, IMDA, NTA, glycine, and ammonia were monitored during the 4-hour tests (Figure 27).

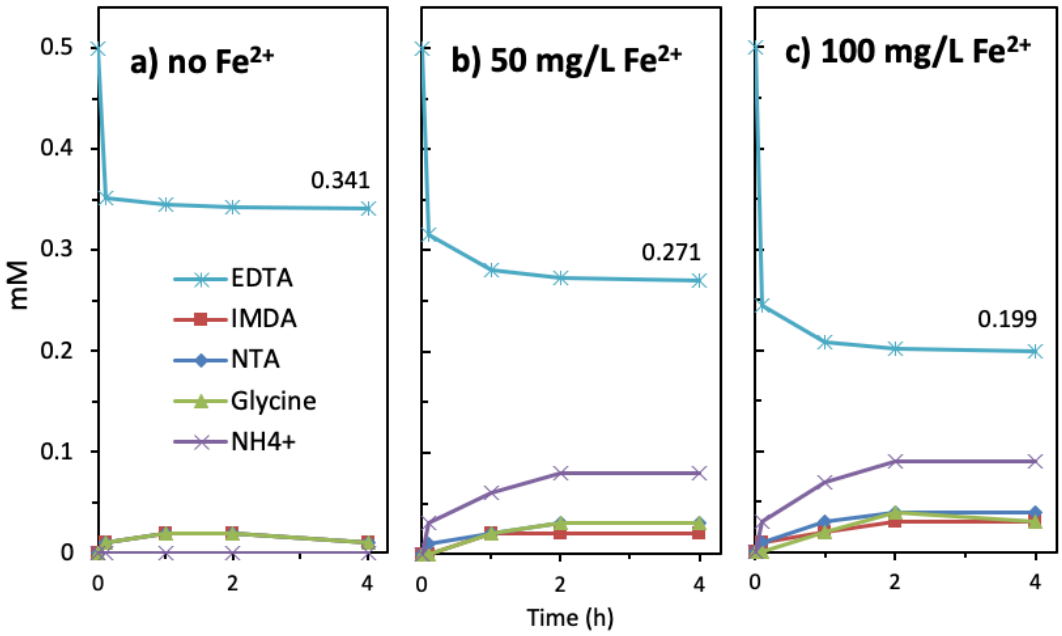

Figure 27. The concentration profile of EDTA, IMDA, NTA, glycine, and ammonia in 0.5 mM EDTA + 10 mM H_2O_2 no media batch system a) without Fe^{2+}, b) with 50 mg/L Fe^{2+}, and c) with 100 mg/L Fe^{2+}.

Without Fe^{2+}, EDTA concentration only dropped to about 0.34 mM with a small amount (0.02 mM) of IMDA, NTA, and glycine produced. No ammonia was detected. 10 mM of H_2O_2 only decomposed 0.16 mM of EDTA. With additional 50 and 100 mg/L dissolved Fe^{2+}, 0.23 and 0.30 mM of EDTA was removed (from 0.5 to 0.27 and 0.20

mM). The IMDA, NTA, and glycine concentration were at around 0.03 mM. Ammonia concentration was at about 0.9 mM.

According to the results, H_2O_2 can directly react with EDTA. However, only a small portion of EDTA transformed through the 'glycines pathway' to IMDA, NTA, and glycine. With dissolved Fe^{2+} in the system, H_2O_2 consumption efficiency was improved by the Fenton reactions. The hydroxyl radicals produced by the Fenton chain reactions break down more EDTA molecules than direct reaction with H_2O_2, which leads to more intermediates detected during the degradation.

Theoretically, to fully apply 10 mM H_2O_2 to producing hydroxyl radicals, 560 mg/L (10 mM) Fe^{2+} would be required (Equation 27). Therefore, to ensure the production of hydroxyl radicals and the EDTA treatment efficiency, the traditional Fenton-based AOPs would demand a high concentration of dissolved Fe^{2+}. In the H_2O_2-AIM system, the equilibrium between aqueous Fe^{2+} and $Fe^0/FeO_x/H_2O$ ensured an adequate amount of dissolved Fe^{2+}. Therefore, no additional Fe^{2+} is required for the treatment of EDTA.

Continuous batch experiments

A continuous batch experiment was conducted in order to further assess and compare the efficiency of the oxic AIM system with or without H_2O_2 (Figure 28). For each dosage, 0.5 mM EDTA was added. The next dose was added when the EDTA concentration was below 0.05 mM (90% was removed). An additional 10 mM H_2O_2 was introduced at each dosage in the H_2O_2-AIM system.

In the H_2O_2-AIM system, the ammonia concentration after the first dosage was 0.192 mM, higher than it in the AIM system (0.151 mM). The difference in ammonia concentration indicates higher oxidative degradation efficiency in the H_2O_2-AIM system. In the second dosage, EDTA was removed a lot slower in the AIM system. The total removed EDTA was 0.881 mM and produced ammonia was 0.206 mM during the 24-hour experiment. The 10 mM H_2O_2 AIM system, however, remains the removal efficiency in the second and third dosages. The total removed EDTA was 1.380 mM with 0.335 mM ammonia produced.

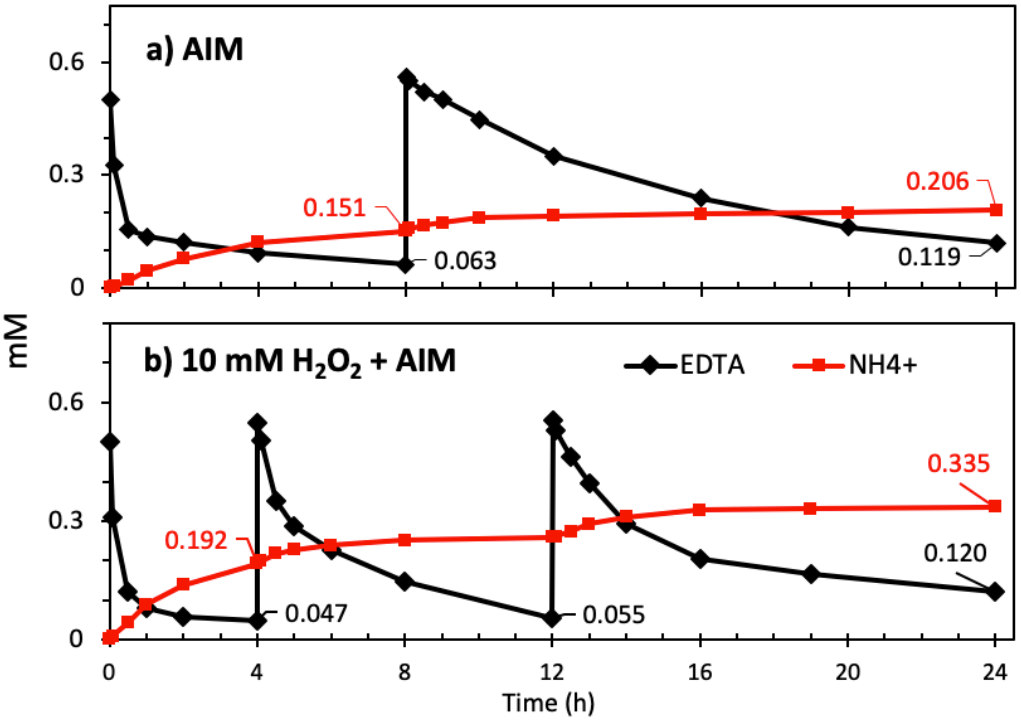

Figure 28. The EDTA and ammonia concentration of continuous AIM batch system a) without H_2O_2, b) with 10 mM H_2O_2.

Although the adsorption process performed well at the start of the experiment, the results indicated the oxidative degradation efficiency controls the EDTA treatment in the oxic AIM system. The additional H_2O_2 injection ensured the treatment reaction rate

by producing more hydroxyl radicals through Fenton reaction with dissolved Fe^{2+}. Therefore, the H_2O_2-AIM system can be a feasible and sustainable procedure for EDTA treatment.

Summary

We found EDTA can be removed by the adsorption process in both ZVI and AIM systems. In the anoxic environment, 0.22 and 0.27 mM EDTA can be adsorbed by 50 g/L of ZVI and AIM. However, due to the limited surface loading of both media, it is not sustainable and reliable.

EDTA treatment is more feasible in the oxidative degradation process provided in the oxic AIM system. Hydroxyl radicals, produced in the oxic AIM system, are able to break down EDTA to smaller molecule products. The detection of IMDA, NTA, glycine, and ammonia has proved that EDTA was degraded through the 'glycines pathway' during the process. For 0.5 mM of EDTA, the final removal was over 90%.

Additional H_2O_2 helped expedite the hydroxyl radicals by performing Fenton reactions with dissolved Fe^{2+} in the system, which leads to the efficiency improvement of the EDTA treatment. In the 10 mM of H_2O_2-AIM system, 0.5 mM EDTA can be treated to 0.008 mM (removal of >98%).

The continuous batch experiment proves the H_2O_2-AIM system has higher removal efficiency than AIM itself. Therefore, the H_2O_2-AIM system would be a possible treatment procedure for wastewater containing EDTA.

CHAPTER V. NICKEL-CYANIDE-EDTA MIXED SOURCE TREATMENT

Introduction

Electroplating and metal surface processing wastewaters are often reported with typically low pH (lower than 2) and a very complex contaminant matrix including metals like Cu^{2+}, Ni^{2+}, Zn^{2+}, and Cr^{6+}, nutrient elements such as nitrate and phosphate, cyanide, and various supplemental chemicals such as EDTA and citric acids to facilitate electroplating processes. The difficulties were illustrated in the previous chapters for the treatment of nickel, cyanide, and EDTA separately. The coexistence of these nutrients, supplements, and heavy metals extremely increases the treatment difficulty and limit the existing processes in two major ways:

1. The loss of effectiveness in heavy metals treatment. The nutrients and supplemental chemicals form chelating ligands with the heavy metals, which dramatically increase the metal solubility and the molecule size. These lead to the most chemical precipitation and adsorption treatment methods ineffective or ineligible (Madden, Datye et al. 1997, Botz, Mudder et al. 2005, Deng and Zhao 2015).

2. The limits in oxidation treatment. The cyanide and EDTA form strong chelating bonds with metals, which extraordinarily affect the rate of oxidation reactions. Because of that, both traditional and advanced oxidation processes have their limitations in handling metal complexes like nickel-cyanide and nickel-EDTA (Figure 29).

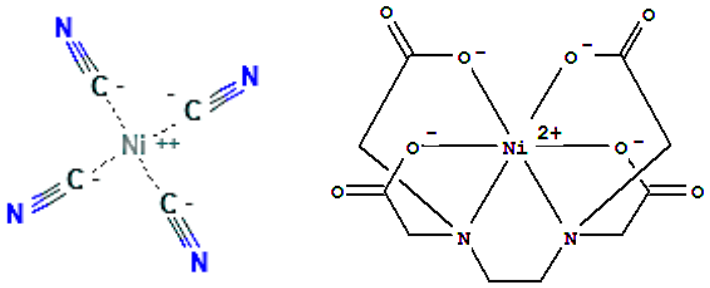

$Ni(CN)_4^{2-}$ $Ni(EDTA)^{2-}$

Figure 29. Schematic drawing of nickel-cyanide and nickel-EDTA in wastewater.

In this chapter, we evaluated the effectiveness of the AIM system for simultaneous removal of nickel, cyanide, and EDTA in a single treatment procedure. The operational conditions (pH, aeration intensity, nitrate dosage, and/or amount of H_2O_2), system configurations (one or multiple stage treatment systems), and required treatment time were needed to be determined in order to fully apply the AIM technologies to the electroplating wastewater treatment.

Materials and Methods

Materials

All regent solutions were prepared by analytical reagent grade chemicals DI water and stored in the anaerobic chamber. Nickel chloride ($NiCl_2 \cdot 6H_2O$, >99%, Alfa Aescar), sodium cyanide (NaCN, >98%, Acros), disodium Ethylenediaminetetraacetic acid dihydrate], disodium ethylenedinitrilotetraacetic acid ($Na_2EDTA \cdot 2H_2O$, Honeywell), ferrous sulfate ($FeSO_4 \cdot 4H_2O$, J.T. Baker), sodium nitrate ($NaNO_3$, Alfa Aesar), Oxygen and nitrogen supply were ultra-purity grade from Airgas. ZVI of 325-

mesh (>99.2%, Johnson Matthey) has a specific surface area of 0.073 m^2/g by BET nitrogen absorption analysis (Autosorb-6, Quantachrome).

Batch experiment procedure

The procedure was similar to the procedure described in Chapter III. The batch test results will determine the best condition and configuration for the CSTR treatment system.

CSTR experiment procedure

The CSTR experiments were conducted using a custom-designed bench-top multiple-stage reactor system (Figure 30). The reactor has an effective volume of 6 L. An overhead-motorized mixer (OS20-S overhead stirrer, Scilogex) with a propeller operated at 1500 rpm was used to fluidize the reactor. Within the reactor, an internal settling zone of about 3 L was designed to achieve solid/liquid separation and to retain reactive solids. A peristaltic pump (model 7528-30, Masterflex) transports the influent at the flow rate of 6 L/d (0.25 L/h). The corresponding hydraulic retention time of the reactor is 24 h. The initial ZVI concentration was controlled at 100 g/L. The reactor effluent was sampled and analyzed daily.

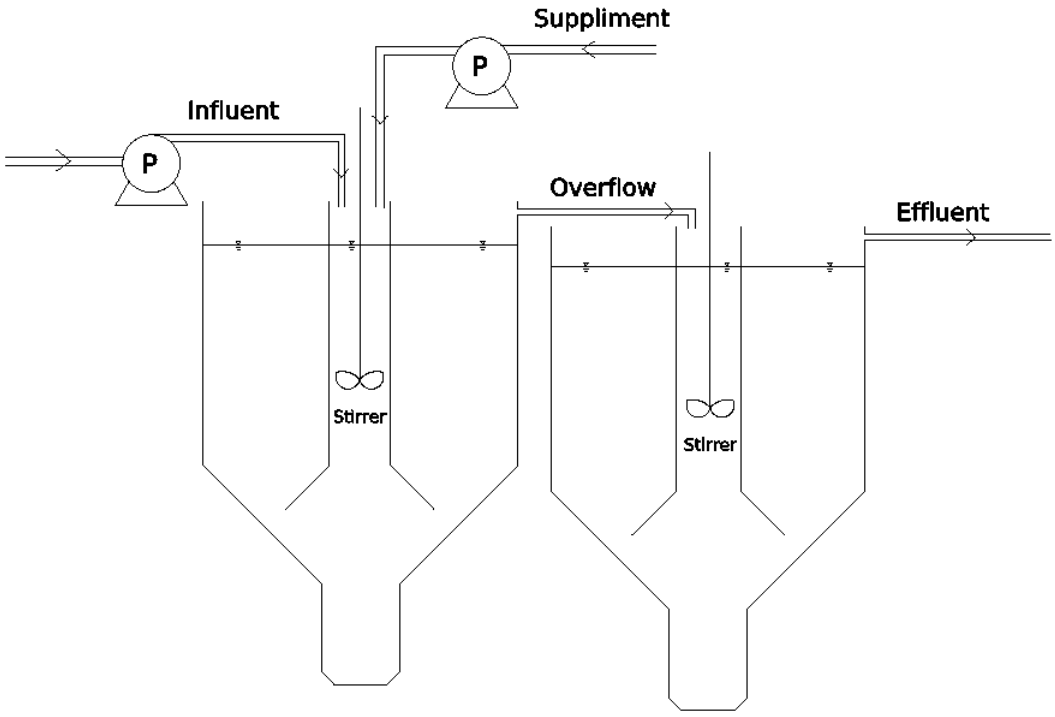

Figure 30. Schematic drawing of the multi-stage benchtop treatment system.

Production of the AIM system

The nitrate-Fe^{2+} pretreatment method was used to convert original ZVI media into AIM. The pretreating process was similar to the procedure described in Chapter II.

Analytical Methods

EDTA concentration was measured using Liquid Chromatography/Mass Selective Detector (LC/MSD) (Agilent). LC/MSD streamlined analytical work by adding mass detection intuitively with OpenLAB Chromatography Data System. A Zorbax Eclipse Plus C18 Rapid Resolution column (Agilent) of length 150 mm, diameter 4.6 mm, and particle size 3.5 μm was used. The column temperature of 50 ◦C. Methanol was used as the mobile phase solvent, tetrabutylammonium bromide as the ion-pair reagent in acetic acid buffer solution at a flow rate of 0.2 mL/min. The mobile

phase consisted of methanol/water (30/70) and 1 mM tetra-n-butylammonium bromide [$(C_4H_9)_4NBr$, TGI] and 1 mM acetic acid (CH_3COOH, Honeywell). For EDTA analytes were detected as Fe^{3+} complexes by electrospray ionization tandem mass spectrometry (ESI-MS) operated in the negative ion mode. Glycine was detected directly without Fe^{3+}. The capillary voltage was set at 2.0 kV, corona current 1 uA, charging voltage 2.0 kV, vaporizer temperature 250 ˚C, drying gas temperature 300 ˚C, nebulizer pressure 40 psi and drying gas flow 8 L/min. Precursor molecular anion of Fe(III)-EDTA was 344, 244, 187 and 74 m/z. The detection limit was 0.1 to 10 mg/L.

Total organic carbon (TOC) was measured on Shimadzu Total Organic Carbon Analyzer TOC-L Series following Patented 680°C Combustion Catalytic Oxidation/NDIR Detection Method (Method 5301B).

Dissolved nickel concentration was determined using ICP-MS (Agilent). Free cyanide was tested using the chloramine-T and pyridine-barbituric method at the wavelength of 580 nm (Method 4500-CN-C). Ferrocyanide [$Fe(CN)_6^{4-}$] was measured using the direct ultraviolet spectrophotometric method at 215 nm wavelengths (Method 9015). EDTA and its degradation products concentration were measured using Liquid Chromatography/Mass Selective Detector (LC/MSD) (Agilent). Dissolved Fe^{2+}, Fe^{3+}, and ammonia were tested on a UV-VIS spectrophotometer (T80, PG Instruments). Fe^{2+} and Fe^{3+} were measured colorimetrically using the 1,10-phenanthroline method at the wavelength of 510 nm (Method 3500-Fe-D). Ammonia was tested using the phenate method at the wavelength of 640 nm (Method 4500-NH_3-F). Nitrate was measured using

the use IC (DX-500, Dionex) with IonPac AS22 (Method 4110 B). ORION pH meter was used for pH measurement.

Results and Discussions

Mixed source comparison

According to the previous chapters, the AIM system showed promising results in treating nickel, cyanide, and EDTA separately. Therefore, mixed sources of nickel-cyanide, nickel-EDTA were tested in the oxic AIM system in order to compare the removal efficiency of the three contaminants. Figure 31 showed the concentration of nickel, total cyanide, and EDTA in the oxic AIM batch system for 24 hours. The initial nickel, cyanide, and EDTA for the batches were 50 mg/L, 20 mg/L, and 0.5 mM.

The nickel concentration in the nickel-only batch dropped from 50 mg/L to 0.19 mg/L after 24 hours. While in the nickel-cyanide mixed batch, it decreased slightly slower with comparable efficiency (50 to 0.28 mg/L). This indicates the cyanide chelated bonds with nickel may not affect the nickel treatment efficiency. Both Ni^{2+} and Fe^{2+} would form metal-complex with CN^-, the stability constant (Log K) of ferrocyanide $[Fe(CN)_6^{4-}]$ (~47) is larger than tetracyanonickelate(II) $[Ni(CN)_4^{2-}]$ (~22) (Caruso 1975, Kyle 1997, Broekaert 2015). Therefore, cyanide tends to free itself from the original nickel-cyanide bond-forming ferrous-cyanide bond with Fe^{2+} instead. This chelation tendency frees up nickel ions, which ensures the nickel removal efficiency in the nickel-cyanide mixed batch. However, the nickel concentration in the nickel-EDTA mix batch shows a different situation. Nickel concentration declined slower than the nickel-only batch, the final concentration after 24 hours was 2.12 mg/L. According to the stability

constant data of chelating reagents, the stability constant of Fe(II)-EDTA (~14) is smaller than Ni(II)-EDTA (~18.5) (Standards, Technology. Gaithersburg et al. 2004, Anderegg 2013, Broekaert 2015). Nickel in the nickel-EDTA is too stable to be replaced by aqueous Fe^{2+} ions, which leads to a slower nickel treatment process.

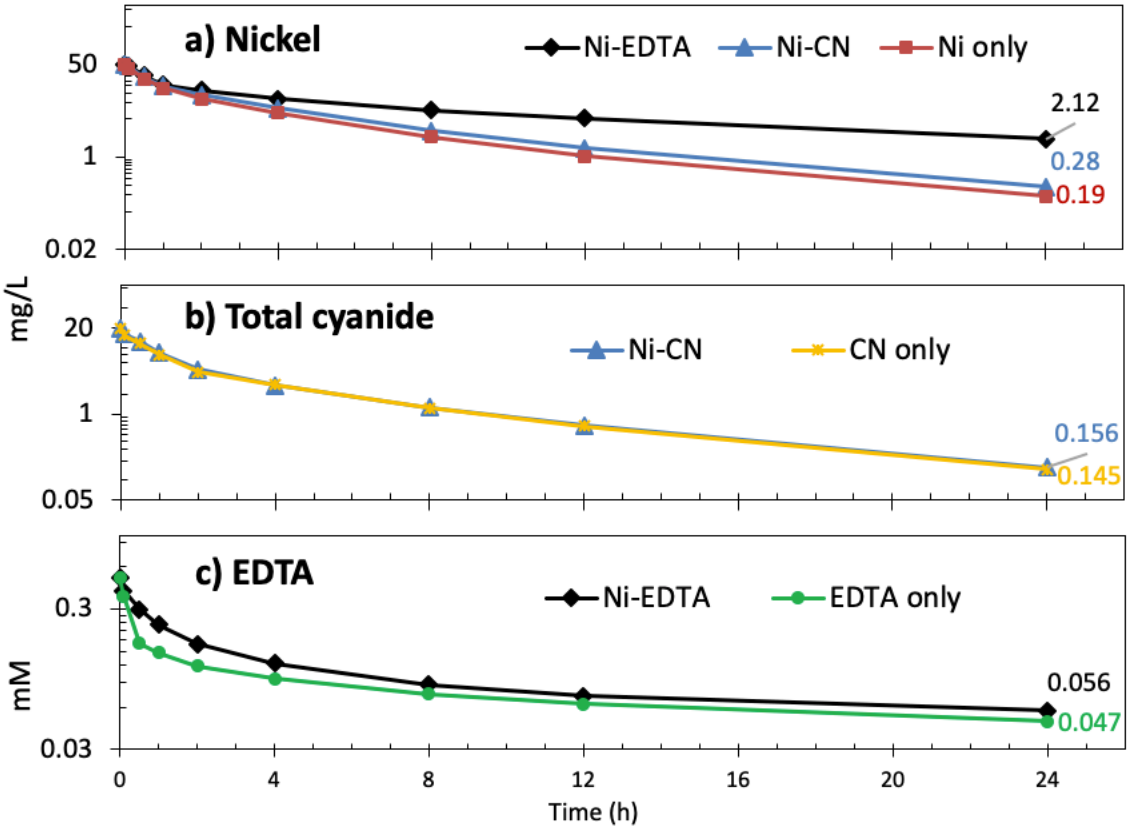

Figure 31. The concentration profile of a) nickel, b) total cyanide, and c) EDTA in the oxic AIM batch system for nickel-cyanide and nickel-EDTA, in compared with nickel, cyanide, and EDTA only.

Due to the same chelation tendency, cyanide treatment for the nickel-cyanide batch is analogical to the cyanide-only batch. As Figure 31b showed, the final total cyanide concentration of the nickel-cyanide batch was 0.156 mg/L, similar to the cyanide-only batch of 0.145 mg/L.

The EDTA concentration of the nickel-EDTA batch dropped a little slower than the EDTA-only batch during the first two hours. Due to the larger molecule size of nickel-EDTA than EDTA itself, the adsorption process is less effective. The treatment efficiency of the mixed batch is not as good as the EDTA-only batch. The final EDTA concentration was 0.073 mM, higher than it in the EDTA-only batch (0.047 mM). The EDTA treatment in the mixed batch may have been affected by the nickel chelation effect.

Comparing the result of the mixed source batch experiments, the treatment efficiency of cyanide was not affected. The mixing cyanide did not impact the nickel reduction, either. However, the treatment of nickel and EDTA in nickel-EDTA was limited due to their strong chelating effect. Therefore, increasing the EDTA treatment efficiency in the mixed source may lead to a better nickel reduction.

Optimal condition of mixed source treatment

According to the previous research, additional H_2O_2 injection expedited the hydroxyl radical's production in the oxic AIM system, which improved the EDTA treatment efficiency. Therefore, we conducted batch experiments for the mixed nickel-cyanide-EDTA source in the oxic AIM system is compared with the H_2O_2-AIM system. Figure 32 showed the result of the batch tests for initial nickel of 50 mg/L, cyanide of 20 mg/L, and EDTA of 0.5 mM in the three systems.

In the oxic AIM system, the nickel treatment was similar to the nickel-EDTA mix batch. The same chelation effect influences the nickel treatment efficiency, leads to the final nickel concentration of 2.92 mg/L in the 24-h test. The treatment of cyanide and

EDTA appeared to be a little slower than the nickel-cyanide and nickel-EDTA mix batches. Due to the degradation needs for both cyanide and EDTA, the limited production of hydroxyl radicals leads to slower treatment efficiency, resulting in higher final concentrations. The final total cyanide and EDTA concentrations were 0.192 mg/L and 0.091 mM.

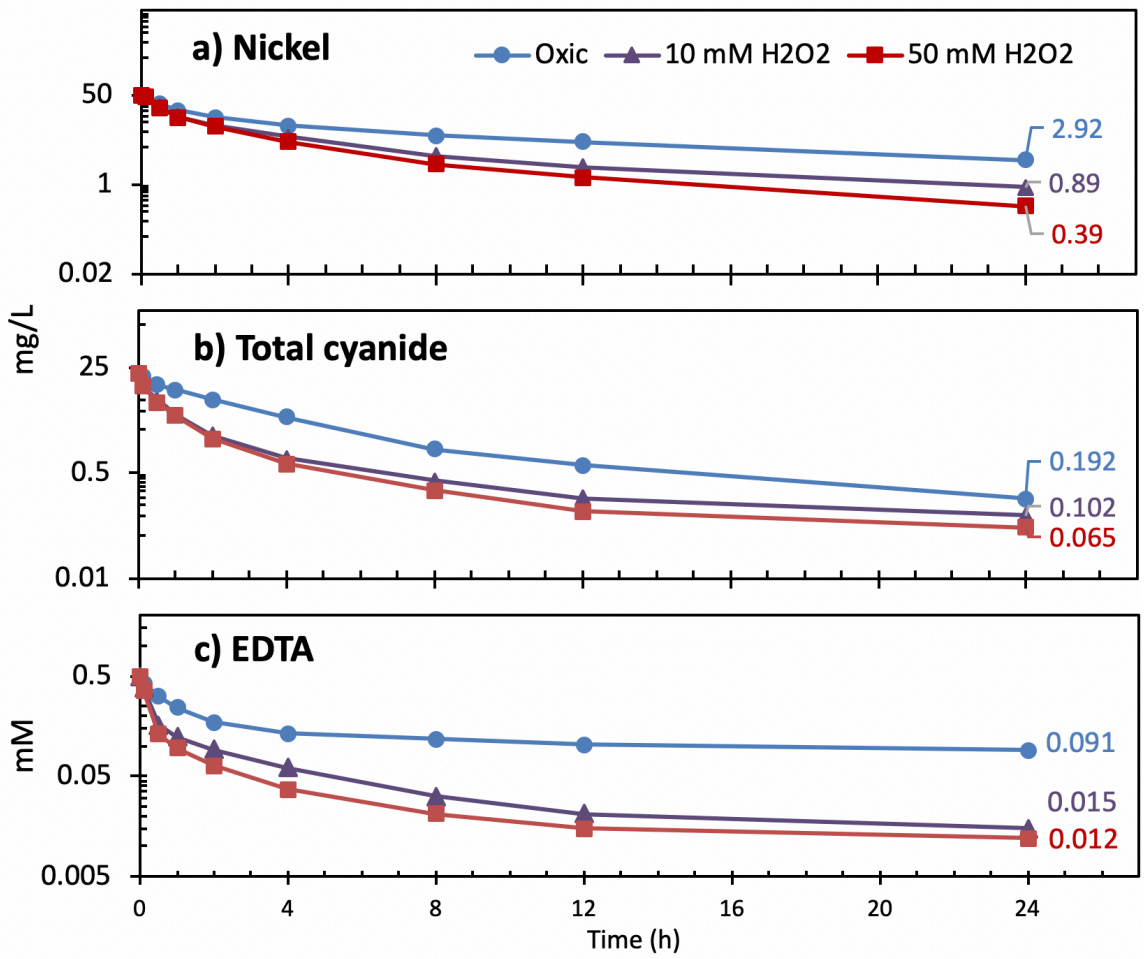

Figure 32. The concentration profile of a) nickel, b) total cyanide, and c) EDTA of nickel-cyanide-EDTA mixed source in three AIM batch systems.

However, with additional H_2O_2 in the system, the removal of nickel, cyanide, and EDTA increased. The nickel concentration decreased to 3.51 mg/L at 8 h with the help

of 10 mM H_2O_2, while the oxic system required more than 20 h. When H_2O_2 injection increased to 50 mM, it dropped to 2.42 mg/L at 8 h. The nickel concentration eventually decreased to 0.89 and 0.39 mg/L for the H_2O_2-AIM system. The total cyanide concentration also dropped faster than the oxic system. It declined to 0.197 and 0.120 mg/L in 12 h and finally to 0.102 and 0.065 mg/L. EDTA concentration in the 50 mM H_2O_2 batch declined faster than the 10 mM batch. It decreased to 0.061 and 0.037 mM in 4 hours, 0.021 and 0.015 in 12 hours, and finally to 0.015 and 0.012 mM.

The injection of EDTA leads to faster production of hydroxyl radicals through Fenton reactions in the AIM system. Hydroxyl radicals ensure the fast treatment of cyanide and EDTA, which consequently improve nickel treatment efficiency.

Continuous batch experiments

We then conducted the continuous batch experiment with different amounts of additional H_2O_2. For each batch dosage, 50 mg/L nickel, 20 mg/L cyanide, and 0.5 mM EDTA were added. The next dose was added when the nickel concentration was below the EPA's limit (2.6 mg/L). Additional 10 and 50 mM of H_2O_2 was added with each batch. The concentration of nickel, total cyanide, and EDTA was also monitored during the 36-h experiment (Figure 33).

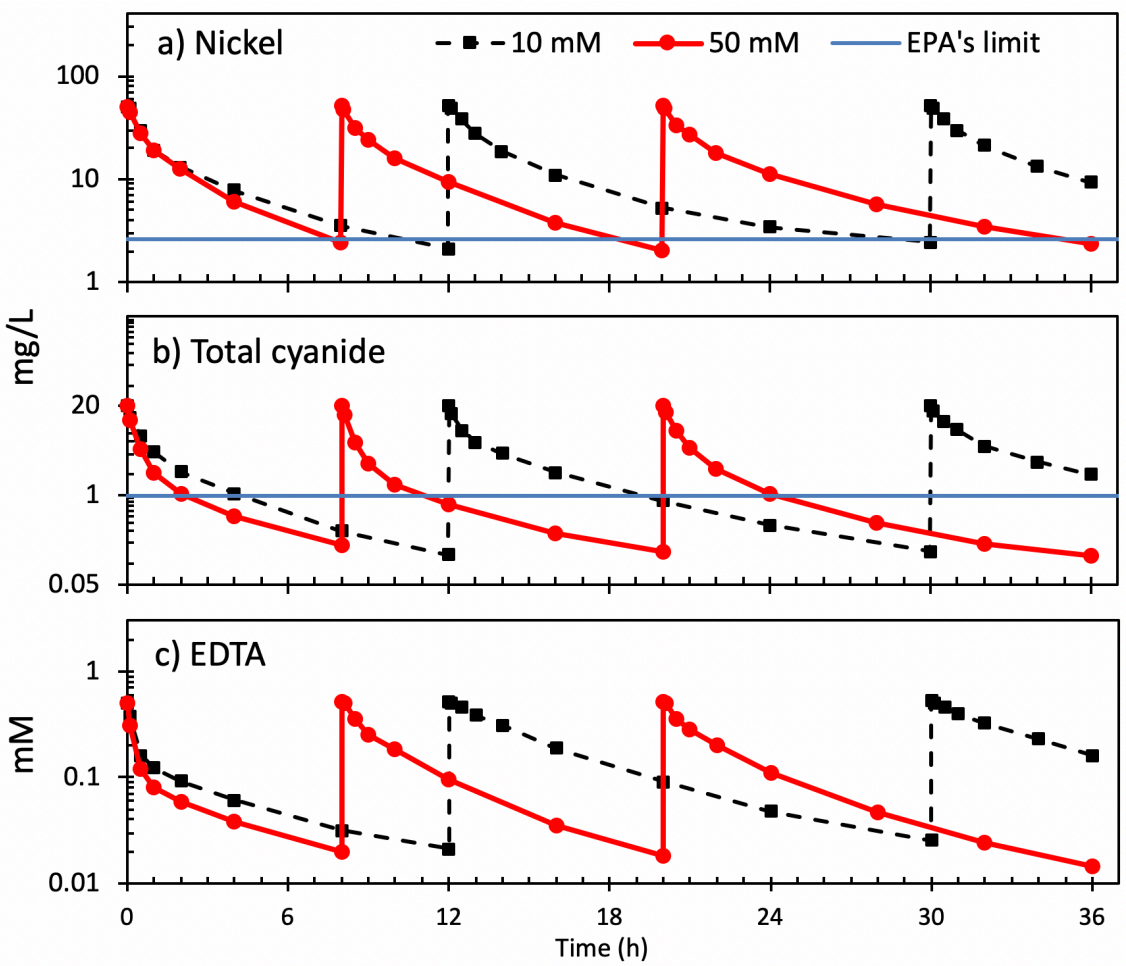

Figure 33. The concentration profile of a) nickel, b) total cyanide, and c) EDTA for nickel-cyanide-EDTA mixed source in 10 and 50 mM H_2O_2-AIM continuous batch system.

The 10 mM H_2O_2-AIM system was able to treat 2 batches with the final nickel concentration of 9.34 mg/L. More than 140 mg/L of nickel was removed in 36 h. The 50 mM H_2O_2-AIM system has removed 3 batches, resulting in the reduction of ~147 mg/L of nickel (final nickel concentration of 2.35 mg/L).

The total cyanide concentration was dropped fast below 1 mg/L in each batch for both systems. The total cyanide of 58.0 and 59.9 mg/L was removed in the two

experiments. The EDTA concentration declined below 0.02 mM at the end of each batch for both systems, resulting in the decomposition of 1.34 and 1.49 mM EDTA.

More H_2O_2 in the system leads to a faster reduction of EDTA, resulting in the more efficient treatment of nickel. Therefore, the overall performance of the 50 mM H_2O_2-AIM system is better than 10 mM H_2O_2.

CSTR experiments

The CSTR was conducted using a two-stage reactor. the Influent of 50 mg/L nickel, 20 mg/L of cyanide, and 0.5 mM of EDTA was transported into the first stage reactor at the flowrate of 6 L/d. The TOC of influent is around 62 mg/L. The retention time was 24 h for each reactor. According to the previous research, the limitation of hydroxyl radicals was the constrain of the mixed source treatment. Therefore, H_2O_2 of 50 mM was injected at a flow rate of 0.635 mL/h (from 30% H_2O_2 stock solution) in the first stage reactor to ensure the decomposition of cyanide and EDTA which chelated with nickel. Additional nitrate of 20 mg/L was included in the second stage reactor at a flow rate of 2.5 mL/h (from 1000 mg/L $NaNO_3$ stock solution) in order to accelerate and maintain nickel treatment efficiency by reforming and reactivating the passivated iron media. Dissolved Fe^{2+} and nitrate, and pH were analyzed to ensure the system stability, besides nickel, total cyanide, EDTA, and TOC concentrations (Figure 34).

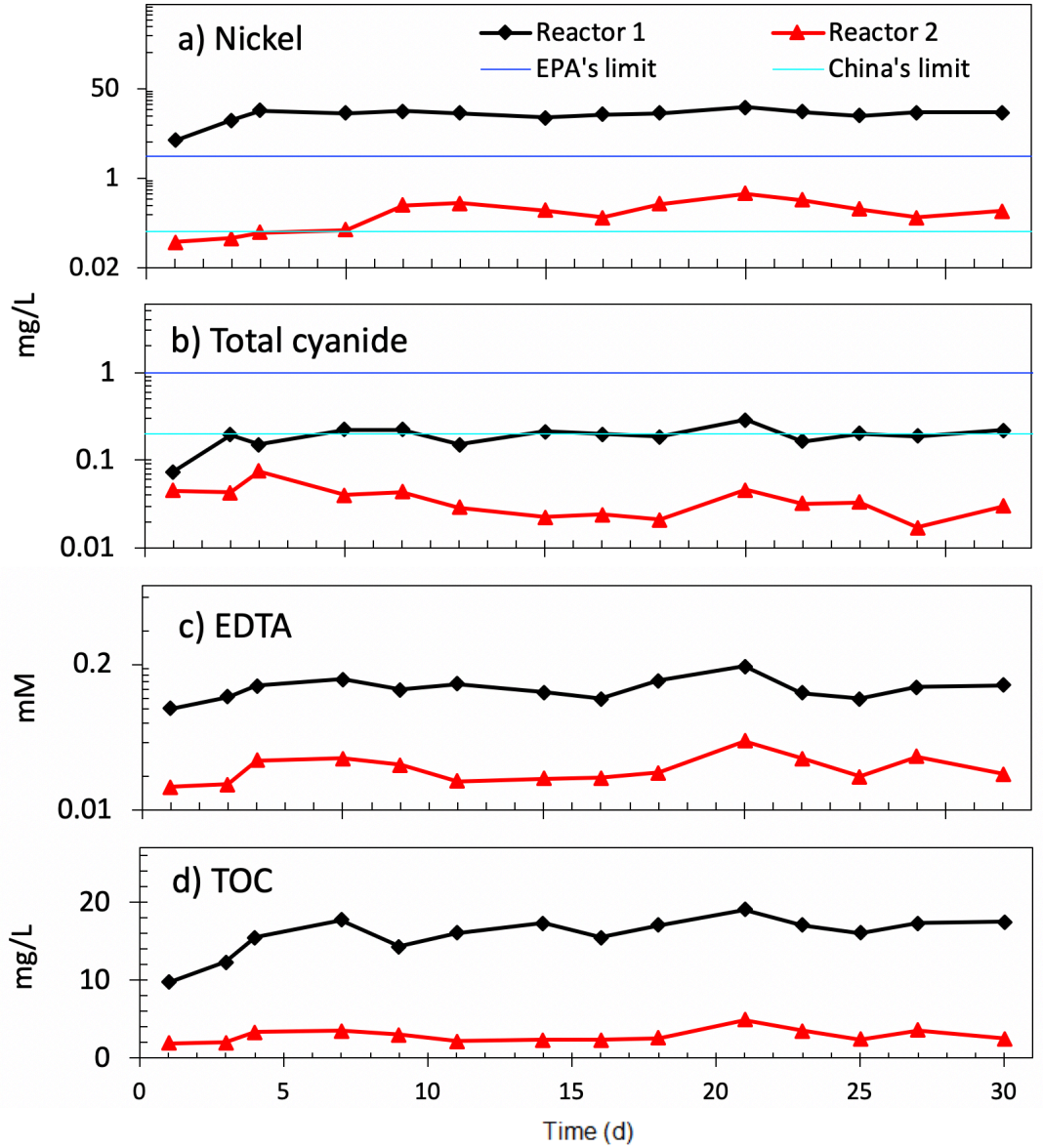

Figure 34. The concentration profile of a) nickel, b) total cyanide, and c) EDTA for nickel-cyanide-EDTA mixed source in the two-stage H_2O_2-AIM CSTR system.

In the first stage (Reactor 1), with the help of the 50 mM H_2O_2, total cyanide and EDTA concertation in the effluent was decreased from 20 mg/L and 0.5 mM to around 0.2 mg/L and 0.15 mM. Nearly 99% of cyanide and 70% of EDTA were decomposed during the first-stage reaction. The declined TOC of 73% (from 62 to near 17 mg/L) basically represents the treated cyanide and EDTA. Due to the removal of cyanide and

EDTA, nickel treatment was effective. For it dropped to the range of 16 to 20 mg/L, over 60% of nickel was removed during the 24-hour first-stage H_2O_2-AIM process.

In the second stage (Reactor 2), the additional 20 mg/L nitrates accelerate the reformation and reactivation of the reacted AIM, leading to the fast reduction of nickel. After this stage, the dissolved nickel concentration of the effluent was below 0.5 mg/L, achieving a total nickel removal of over 99%. The total cyanide concentration after the two-stage treatment was under 0.07 mg/L, reaching the cyanide removal over 99.6%. The EDTA was also removed to the concentration of about 0.03 mM, resulting in the removal of over 94%. The effluent TOC concentration was only an average of 2.8 mg/L, decreased over 95.4%.

The final effluent compiles the EPA's discharge limit for nickel and cyanide during the 30-day experiment. Therefore, the H_2O_2-AIM continuous reacting system can be a feasible, sustainable, and reliable treatment process for simultaneous treatment of nickel, cyanide, and EDTA in wastewater.

Summary

We found the reduction of cyanide was nearly not affected when they combined with nickel. However, the nickel and EDTA treatment in the mixed was limited by the strong chelation. The addition of H_2O_2 accelerates the decomposition of cyanide and EDTA, which consequently improves nickel treatment. In the H_2O_2-AIM system, the dissolved nickel concentration dropped from 50 to 3.51 mg/L in 8 h with 10 mM H_2O_2, to 2.42 mg/L with 50 mM H_2O_2, while the AIM only system required more than 20 h.

The continuous batch experiment proves the H_2O_2-AIM system can simultaneously treatment of nickel, cyanide, and EDTA. The total of 140 and 147 mg/L nickel, 58.0 and 59.9 mg/L cyanide, 1.34 and 1.49 mM EDTA were removed in the 10 and 50 mM H_2O_2-AIM system during the 36-h test.

The CSTR experiment achieved 99.5% nickel removal, 99.6% cyanide removal, and 94% EDTA removal. The effluent compiles the EPA's discharge limit during the whole time. Therefore, the H_2O_2-AIM system can be a reliable and sustainable process for simultaneous treatment of nickel, cyanide, and EDTA in industrial wastewater.

CHAPTER VI. SUMMARIES AND DISCUSSIONS

We demonstrate the treatment of nickel, cyanide, and EDTA by two iron media systems in this study (the ZVI and AIM systems). Batch and CSTR experiments were conducted in both oxic and anoxic environments. Removal mechanisms and reasonable treatment procedures have been found. The summaries of all the results and conclusions are as follows.

Nickel treatment

For both the ZVI and AIM systems, nickel removal is possible. The removal mechanism in the ZVI system is mostly contributed by the reductive reaction. Fe^0 on the iron particle surface reduces the dissolved Ni^{2+} ions to insoluble Ni^0, while it was oxidized and released as Fe^{2+}. In the AIM system, it is the lattice substitution reaction that dominates the removal mechanism. The labile Fe(II) from surface CPs are substituted by dissolved Ni^{2+} ions resulting in the change of the FeO_x structure.

The XPS and XRD spectra of the sediments indicated the detection of Ni^0 in the ZVI system and the formation of $NiFe_2O_4$ in the AIM system. These pieces of evidence support the reductive and substitution mechanisms.

The results of the continuous batch and CSTR experiment show that the AIM system was more efficient, reliable, and sustainable than the ZVI system. And therefore, would be a suitable process for nickel removal.

Cyanide treatment

The removal of cyanide was not preferable in anoxic conditions. In the iron-precipitation process, cyanide forms ferrocyanide with dissolved Fe^{2+} and further to

insoluble ferrous ferrocyanide. However, the process is reversible and the sediments are unstable. The anion exchange procedure allows cyanide ions to exchange with ions in iron media, which reduced the aqueous cyanide concentration. The cyanide ions, whereas, can be exchanged back by ions with higher binding affinity. Therefore, this process is hard to operate and maintained.

In the oxic environment, the AIM system becomes an oxidizing reactive system with highly reactive radicals. The oxygen consumption in the AIM system and the difference of the aqueous Fe^{3+} in the blank and inhibited system indicated the production of the hydroxyl radicals.

The oxidizing reactive AIM system made it feasible for cyanide treatment. Cyanide and iron-chelated cyanide can be converted to nitrogen gas step by step in the oxic AIM system. With the quantification of the intermediate products (ferricyanide, cyanate, and ammonia) and comparison of the inhibited system, the AIM system was tested in removing cyanide irreversibly with no other reagent needed.

The continuous batch test further implied the reliability, efficiency, and sustainability of the system. Therefore, the oxic AIM system would be a trustworthy treatment procedure for cyanide-containing wastewater.

EDTA treatment

EDTA can be removed by the adsorption process in both ZVI and AIM systems. In the anoxic environment, around 0.22 and 0.27 mM EDTA was adsorbed by 50 g/L of ZVI and AIM. However, due to the limited surface loading of both media, it is not sustainable and reliable.

EDTA treatment is feasible in the oxic AIM system by the oxidative process. Hydroxyl radicals, produced in the oxic AIM system, are able to break down the long-chain EDTA molecule to the smaller molecule products. The detection of IMDA, NTA, glycine, and ammonia has proved that EDTA can degrade through the 'glycines pathway' during the process. Additional H_2O_2 performs Fenton reactions with dissolved Fe^{2+} in the system, which expedites the hydroxyl radical's production. The treatment efficiency of EDTA was improved in the H_2O_2-AIM system, with increased removal.

The continuous batch experiment also implied the H_2O_2-AIM has higher removal efficiency than AIM itself. Therefore, the H_2O_2-AIM system would be a possible treatment procedure for wastewater containing EDTA.

Mixed source treatment

The reduction of cyanide was nearly unaffected when they combined with nickel. However, due to the strong chelating effect, the nickel and EDTA treatment was limited. The addition of H_2O_2 accelerates the decomposition of cyanide and EDTA, which consequently improves nickel treatment. In the H_2O_2-AIM system, the dissolved nickel concentration dropped even faster than it in the AIM-only system.

The continuous batch and CSTR experiment proved the H_2O_2-AIM system can simultaneously treatment of nickel, cyanide, and EDTA to the discharge limits. Therefore, the H_2O_2-AIM system can be a reliable and sustainable process for simultaneous treatment of nickel, cyanide, and EDTA in industrial wastewater.

Discussions

The different results between ZVI and AIM in terms of radical generation suggest that the FeO_x phase in the AIM plays a key role in a radical generation. The role of Fe^0 in AIM cannot be neglected, however. In the absence of Fe^0, FeO_x could be quickly fully oxidized to become a stable FeOOH or Fe_2O_3 and lost its reactivity. Likely, the presence of Fe^0 and its redox interactions with FeO_x, possibly with the involvement of aqueous Fe^{2+} or surface-bound Fe(II), help maintain the mixed-valence status of Fe and a flexible structure in the FeO_x phase, thus enabling its reactivity with O_2 to produce radicals.

Concerning the detailed mechanism, many questions remain open. For example, while we attribute cyanide oxidation to hydroxyl radicals, as is often the case in many iron-media-supported advanced oxidative systems, it is still possible that other reactive radical species might be involved. Although the consumptions of O_2 were evaluated in the studies, the rate of radical generation could not be quantified. Future tests will be performed to assess the quantitative relationship among O_2 dosage, Fe^0 consumed and radical generation, which will help assess chemical consumptions and economy if the AIM system is applied as an alternative advanced oxidation treatment in real world application. We suspect labile Fe(II) on the FeO_x surface or within the structure might play a key role in initiating the key radical generation reaction loops, a detailed picture will not be available without further tests with innovative methods/tools to track the changes occurring at nano-scale. Nonetheless, it is rational to postulate that labile Fe(II) interacts with O_2 and be oxidized to Fe(III) could be among the initial reactions to

trigger ·OH generation. Reduction of Fe(III) by Fe^0 via FeO_x-mediated solid-state chemistry could be essential to replenish labile Fe(II) and complete the reaction loops for sustained radical production.

Mixed valent Fe(II)/Fe(III) oxides are common in nature. For example, many biogenic iron oxides consisted of mixed Fe(II)/Fe(III) oxides including green rusts (Pantke, Obst et al. 2012, Kiskira, Papirio et al. 2019). The finding that such FeO_x is highly efficient in producing radicals by just exposing them to O_2 implies understanding the fate of many pollutants in nature. The role of UV light in initiating radical production and thus helping degrade many environmental pollutants has been well recognized (Wang, Xu et al. 2012, Attri, Kim et al. 2015). In light of the current study, we should examine the role of iron minerals and the Fe(II)/Fe(III) redox cycle on the fate and transport of contaminants by including the potential of radical generation and the impacts. As for cyanide removal applications, the current mainstream industrial practice of using chlorination is well established and considered sufficiently cost-effective. A potential advantage of the AIM lies in the fact that AIM is particularly effective in removing various heavy metals, thus it could be used as a final polishing process to ensure compliance with stringent limits for not only total cyanides, but also heavy metals such as Cr, Cu, Zn, and Ni, all tightly regulated pollutants for metal polishing and electroplating industries.

REFERENCES

Adams, M. (1992). "The removal of cyanide from aqueous solution by the use of ferrous sulphate." Journal of the Southern African Institute of Mining and Metallurgy **92**(1): 17-25.

Ahmed, S., et al. (2011). "Advances in heterogeneous photocatalytic degradation of phenols and dyes in wastewater: a review." **215**(1-4): 3-29.

Ahn, K.-H., et al. (1999). "Removal of ions in nickel electroplating rinse water using low-pressure nanofiltration." **122**(1): 77-84.

Ajmal, M., et al. (2000). "Adsorption studies on Citrus reticulata (fruit peel of orange): removal and recovery of Ni (II) from electroplating wastewater." **79**(1-2): 117-131.

Akita, S., et al. (1999). "Separation of Co (II)/Ni (II) via micellar-enhanced ultrafiltration using organophosphorus acid extractant solubilized by nonionic surfactant." **162**(1-2): 111-117.

Al-Shannag, M., et al. (2015). "Heavy metal ions removal from metal plating wastewater using electrocoagulation: kinetic study and process performance." Chemical Engineering Journal **260**: 749-756.

Alkaim, A. F. and F. H. J. I. J. o. C. S. Hussein (2012). "Photocatalytic degradation of EDTA by using TiO2 suspension." **10**(1): 586-598.

Allard, A.-S., et al. (1996). "Absence of 14CO2 evolution from 14C-labelled EDTA and DTPA and the sediment/water partition ratio." **33**(4): 577-583.

Alyüz, B. and S. J. J. o. H. M. Veli (2009). "Kinetics and equilibrium studies for the removal of nickel and zinc from aqueous solutions by ion exchange resins." **167**(1-3): 482-488.

Anderegg, G. (2013). Critical Survey of Stability Constants of EDTA Complexes: Critical Evaluation of Equilibrium Constants in Solution: Stability Constants of Metal Complexes, Elsevier.

Annachhatre, A. and A. J. W. e. r. Amornkaew (2001). "Upflow anaerobic sludge blanket treatment of starch wastewater containing cyanide." **73**(5): 622-632.

Argun, M. E. J. J. o. H. M. (2008). "Use of clinoptilolite for the removal of nickel ions from water: kinetics and thermodynamics." **150**(3): 587-595.

Arslan, I., et al. (1999). "Advanced oxidation of synthetic dyehouse effluent by O3, H2O2/O3 and H2O2/UV processes." **20**(9): 921-931.

Attri, P., et al. (2015). "Generation mechanism of hydroxyl radical species and its lifetime prediction during the plasma-initiated ultraviolet (UV) photolysis." Scientific reports **5**: 9332.

Babey, P., et al. (2001). "Kinetics and mechanisms of EDTA photocatalytic degradation with TiO2." Water Science and technology **44**(5): 179-185.

Barakat, M. and E. J. D. Schmidt (2010). "Polymer-enhanced ultrafiltration process for heavy metals removal from industrial wastewater." **256**(1-3): 90-93.

Barakat, M. J. A. j. o. c. (2011). "New trends in removing heavy metals from industrial wastewater." **4**(4): 361-377.

Bartzas, G., et al. (2006). "Laboratory evaluation of Fe0 barriers to treat acidic leachates." Minerals Engineering **19**(5): 505-514.

Bhatnagar, A. and M. Sillanpää (2010). "Utilization of agro-industrial and municipal waste materials as potential adsorbents for water treatment—a review." Chemical Engineering Journal **157**(2-3): 277-296.

Blais, J., et al. (2008). "Metals precipitation from effluents." **12**(3): 135-149.

Bolton, H., et al. (1993). "Biodegradation of synthetic chelates in subsurface sediments from the southeast coastal plain." **22**(1): 125-132.

Borbély, G. and E. J. D. Nagy (2009). "Removal of zinc and nickel ions by complexation–membrane filtration process from industrial wastewater." **240**(1-3): 218-226.

Botz, M., et al. (2005). "Cyanide treatment: physical, chemical and biological processes." 672-700.

Bougeard, C. M., et al. (2010). "Comparison of the disinfection by-product formation potential of treated waters exposed to chlorine and monochloramine." water research **44**(3): 729-740.

Britigan, B. E., et al. (1989). "Neutrophil degranulation inhibits potential hydroxyl-radical formation. Relative impact of myeloperoxidase and lactoferrin release on hydroxyl-radical production by iron-supplemented neutrophils assessed by spin-trapping techniques." Biochemical Journal **264**(2): 447-455.

Broekaert, J. A. (2015). "Daniel C. Harris: Quantitative chemical analysis." Analytical and bioanalytical chemistry **407**(30): 8943-8944.

Bucheli-Witschel, M. and T. J. F. m. r. Egli (2001). "Environmental fate and microbial degradation of aminopolycarboxylic acids." **25**(1): 69-106.

Buxton, G. V., et al. (1988). "Critical review of rate constants for reactions of hydrated electrons, hydrogen atoms and hydroxyl radicals (· OH/· O− in aqueous solution." **17**(2): 513-886.

Caruso, S. (1975). "The chemistry of cyanide compounds and their behavior in the aquatic environment." **4400**.

Chen, G. (2004). "Electrochemical technologies in wastewater treatment." Separation and purification Technology **38**(1): 11-41.

Chiang, P.-C., et al. (2010). "Evaluating and elucidating the formation of nitrogen-contained disinfection by-products during pre-ozonation and chlorination." Chemosphere **80**(3): 327-333.

Coman, V., et al. (2013). "Nickel recovery/removal from industrial wastes: A review." **73**: 229-238.

Danis, U. and C. J. J. o. h. m. Aydiner (2009). "Investigation of process performance and fouling mechanisms in micellar-enhanced ultrafiltration of nickel-contaminated waters." **162**(2-3): 577-587.

Dash, R. R., et al. (2008). "Treatment of metal cyanide bearing wastewater by simultaneous adsorption and biodegradation (SAB)." Journal of hazardous materials **152**(1): 387-396.

Dash, R. R., et al. (2009). "Cyanide in industrial wastewaters and its removal: a review on biotreatment." **163**(1): 1-11.

Davis, A. P., et al. (1999). "Photocatalytic oxidation of cadmium-EDTA with titanium dioxide." **33**(4): 609-617.

Dąbrowski, A., et al. (2004). "Selective removal of the heavy metal ions from waters and industrial wastewaters by ion-exchange method." **56**(2): 91-106.

Deng, Y. and R. J. C. P. R. Zhao (2015). "Advanced oxidation processes (AOPs) in wastewater treatment." **1**(3): 167-176.

Desai, J., et al. (1998). "Microbial degradation of cyanides and its commercial applications." **57**(8): 441-453.

Dong, H., et al. (2016). "Chromate removal by surface-modified nanoscale zero-valent iron: Effect of different surface coatings and water chemistry." Journal of colloid and interface science **471**: 7-13.

Dries, J., et al. (2005). "Effect of humic acids on heavy metal removal by zero-valent iron in batch and continuous flow column systems." water research **39**(15): 3531-3540.

Dutta, P. K., et al. (2005). "Photocatalytic oxidation of arsenic (III): evidence of hydroxyl radicals." **39**(6): 1827-1834.

Dzombak, D., et al. (1996). Removal of cyanide from spent potlining leachate by iron cyanide precipitation. Proc. Water Environ. Fed. 69th Annu. Conf. Exposition, Dallas, Tex.

Farhataziz, P. and A. J. N. B. o. S. Ross, Washington, DC, NSDRS-NBS59 (1977). "Selected specific rates of radicals of transients from water in aqueous solutions."

Figueira, M. M., et al. (1996). "Cyanide degradation by an Escherichia coli strain." **42**(5): 519-523.

Fleet, M. (1981). "The structure of magnetite." Acta Crystallographica Section B: Structural Crystallography and Crystal Chemistry **37**(4): 917-920.

Fu, F., et al. (2006). "Application of a novel strategy—coordination polymerization precipitation to the treatment of Cu2+-containing wastewaters." **52**(2): 388-393.

Fu, F. and Q. J. J. o. e. m. Wang (2011). "Removal of heavy metal ions from wastewaters: a review." **92**(3): 407-418.

Gallerani, P. A., J. Lord, K. Klink. (2001). "Capsule Report: Managing Cyanide in Metal Finishing." **EPA/625/R-99/009**.

García-Montaño, J., et al. (2008). "Pilot plant scale reactive dyes degradation by solar photo-Fenton and biological processes." Journal of Photochemistry and Photobiology A: Chemistry **195**(2-3): 205-214.

Gerike, P., et al. (1979). "A correlation study of biodegradability determinations with various chemicals in various tests." **3**(2): 159-173.

Ghaedi, M., et al. (2015). "Modeling of competitive ultrasonic assisted removal of the dyes–Methylene blue and Safranin-O using Fe3O4 nanoparticles." Chemical Engineering Journal **268**: 28-37.

Ghiselli, G., et al. (2004). "Destruction of EDTA using Fenton and photo-Fenton-like reactions under UV-A irradiation." **167**(1): 59-67.

Ghosh, R. S., et al. (1999). "Equilibrium precipitation and dissolution of iron cyanide solids in water." **16**(4): 293-313.

Giannopoulou, I. and D. J. H. Panias (2008). "Differential precipitation of copper and nickel from acidic polymetallic aqueous solutions." **90**(2-4): 137-146.

Gilbert, E. and S. J. W. r. Hoffmann-Glewe (1990). "Ozonation of ethylenediaminetetraacetic acid (EDTA) in aqueous solution, influence of pH value and metal ions." **24**(1): 39-44.

Given, B., et al. (1998). "Combined aerobic and anaerobic biological treatment of tailings solution at the Nickel Plate Mine." 391-421.

Glaze, W. H. J. E. s. and technology (1987). "Drinking-water treatment with ozone." **21**(3): 224-230.

Gomes, A., et al. (2005). "Fluorescence probes used for detection of reactive oxygen species." **65**(2-3): 45-80.

Gorter, E. W. (1954). "Saturation magnetization and crystal chemistry of ferrimagnetic oxides. I. II. Theory of ferrimagnetism." Philips Res. Rep. **9**: 295-320,321-365.

Griffith, W. (1962). "Cyanide complexes of the transition metals." Quarterly Reviews, Chemical Society **16**(2): 188-207.

Hanson, J. (1979). Development document for existing source pretreatment standards for the electroplating point source category. Development document for existing source pretreatment standards for the electroplating point source category, NTIS.

Harbour, J. R. and S. L. Issler (1982). "Involvement of the azide radical in the quenching of singlet oxygen by azide anion in water." Journal of the American Chemical Society **104**(3): 903-905.

Haseloff, R. F., et al. (1990). "Hydroxyl radical scavenging and antipsoriatic activity of benzoic acid derivatives." **9**(2): 111-115.

Henneken, L., et al. (1998). "Biological degradation of EDTA: Reaction kinetics and technical approach." **73**(2): 144-152.

Huang, C., et al. (1993). "Advanced chemical oxidation: its present role and potential future in hazardous waste treatment." **13**(5-7): 361-377.

Huang, Y. H., et al. (2013). "Hybrid zero-valent iron process for removing heavy metals and nitrate from flue-gas-desulfurization wastewater." **118**: 690-698.

Huang, Y. H., et al. (2014). Field demonstration of the activated iron technology for removing heavy metals from flue-gas-desulfurization wastewater, Pittsburgh, USA: Engineers Society of Western Pennsylvania.

Huang, Y. H., et al. (2012). "Removing molybdate from water using a hybridized zero-valent iron/magnetite/Fe (II) treatment system." **200**: 257-263.

Huang, Y. H. and T. C. Zhang (2005). "Effects of dissolved oxygen on formation of corrosion products and concomitant oxygen and nitrate reduction in zero-valent iron systems with or without aqueous Fe2+." Water research **39**(9): 1751-1760.

Huang, Y. H., et al. (2003). "Effects of oxide coating and selected cations on nitrate reduction by iron metal." Journal of Environmental Quality **32**(4): 1306-1315.

Ingles, J. and J. Scott (1987). State-of-the-art of Processes for the Treatment of Gold Mill Effluents, Mining and Milling Section, Mining, Mineral and Metallurgical Processes Division, Industrial Programs Branch, Conservation and Protection, Environment Canada.

Ipek, U. J. D. (2005). "Removal of Ni (II) and Zn (II) from an aqueous solutionby reverse osmosis." **174**(2): 161-169.

Jiraroj, D., et al. (2006). "Degradation of Pb–EDTA complex by a H2O2/UV process." **40**(1): 107-112.

Kandah, M. I. and J.-L. J. J. o. h. m. Meunier (2007). "Removal of nickel ions from water by multi-walled carbon nanotubes." **146**(1-2): 283-288.

Kasprzak, K. S., et al. (2003). "Nickel carcinogenesis." Mutation Research/Fundamental and Molecular Mechanisms of Mutagenesis **533**(1): 67-97.

Keenan, C. R., et al. (2008). "Factors affecting the yield of oxidants from the reaction of nanoparticulate zero-valent iron and oxygen." **42**(4): 1262-1267.

Kim, K.-W., et al. (2005). "The electrolytic decomposition mechanism of ammonia to nitrogen at an IrO2 anode." **50**(22): 4356-4364.

Kiskira, K., et al. (2019). "Mineral characterization of the biogenic Fe (III)(hydr) oxides produced during Fe (II)-driven denitrification with Cu, Ni and Zn." Science of the total environment **687**: 401-412.

Kitis, M., et al. (1999). "The effects of Fenton's reagent pretreatment on the biodegradability of nonionic surfactants." **33**(11): 2561-2568.

Klein, G. W., et al. (1975). "Reaction of hydroxyl radicals with benzoic acid. Isomer distribution in the radical intermediates." **79**(17): 1767-1774.

Korhonen, M. S., et al. (2000). "Removal of ethylenediaminetetraacetic acid (EDTA) from pulp mill effluents by ozonation."

Krapfenbauer, K., et al. (1999). "Comparative studies of photo-and radiation-induced degradation of aqueous EDTA. Synergistic effects of oxygen, ozone and TiO2 (acronym: CoPhoRaDe/EDTA)." **55**(4): 385-393.

Ku, Y., et al. (1998). "Decomposition of EDTA in aqueous solution by UVy HO process." **2**(2): 60.

Kurepin, V. A., et al. (2002). Thermodynamic Modelling of Fe-Cr-Ni-Spinel Formation at the Light-Water Reactor Conditions, Paul Scherrer Inst.

Kurniawan, T. A., et al. (2006). "Physico–chemical treatment techniques for wastewater laden with heavy metals." **118**(1-2): 83-98.

Kyle, J. (1997). "Stability of metal–cyanide and hydroxide complexes." Publications of the Australasian Institute of Mining and Metallurgy (World Gold '97): 163-169.

Laetsch, T. and R. Downs (2006). Software for identification and refinement of cell parameters from powder diffraction data of minerals using the RRUFF Project and American Mineralogist Crystal Structure Databases. 19th General Meeting of the International Mineralogical Association, Kobe, Japan.

Lee, C., et al. (2004). "Application of photoactivated periodate to the decolorization of reactive dye: reaction parameters and mechanism." **165**(1-3): 35-41.

Lee, T.-Y., et al. (2004). "Oxidative treatment of cyanide in wastewater using hydrogen peroxide and homogeneous catalyst." **39**(3): 787-801.

Li, K., et al. (2009). "Computerized pathway elucidation for hydroxyl radical-induced chain reaction mechanisms in aqueous phase advanced oxidation processes." **43**(8): 2831-2837.

Li, M., et al. (2001). "Quenching of Singlet Molecular Oxygen (1O2) by Azide Anion in Solvent Mixtures¶." Photochemistry and photobiology **74**(6): 760-764.

Li, X.-q. and W.-x. Zhang (2006). "Iron nanoparticles: the core− shell structure and unique properties for Ni (II) sequestration." Langmuir **22**(10): 4638-4642.

Li, Y., et al. (2016). "Catalytic debromination of tetrabromobisphenol A by Ni/nZVI bimetallic particles." Chemical Engineering Journal **284**: 1242-1250.

Li, Z., et al. (2017). "Enhanced removal of Ni (II) by nanoscale zero valent iron supported on Na-saturated bentonite." Journal of colloid and interface science **497**: 43-49.

Ling, L. and W.-x. Zhang (2014). "Reactions of nanoscale zero-valent iron with Ni (II): three-dimensional tomography of the "hollow out" effect in a single nanoparticle." Environmental Science & Technology Letters **1**(3): 209-213.

Liu, D., et al. (2014). "Recycled chitosan nanofibril as an effective Cu (II), Pb (II) and Cd (II) ionic chelating agent: adsorption and desorption performance." Carbohydrate polymers **111**: 469-476.

Lockhart, H. B. and R. V. Blakeley (1975). "Aerobic photodegradation of iron (III)-(ethylenedinitrilo) tetraacetate (ferric EDTA). Implications for natural waters." Environmental Science & Technology **9**(12): 1035-1038.

Low, G. K., et al. (1991). "Formation of nitrate and ammonium ions in titanium dioxide mediated photocatalytic degradation of organic compounds containing nitrogen atoms." **25**(3): 460-467.

Lowry, G. V. and K. M. Johnson (2004). "Congener-specific dechlorination of dissolved PCBs by microscale and nanoscale zerovalent iron in a water/methanol solution." Environmental science & technology **38**(19): 5208-5216.

Madden, T. H., et al. (1997). "Oxidation of metal− EDTA complexes by TiO2 photocatalysis." **31**(12): 3475-3481.

Madsen, E. and M. J. A. E. M. Alexander (1985). "Effects of chemical speciation on the mineralization of organic compounds by microorganisms." **50**(2): 342-349.

Martín-Lara, M., et al. (2014). "New treatment of real electroplating wastewater containing heavy metal ions by adsorption onto olive stone." **81**: 120-129.

Mavrov, V., et al. (2003). "Study of new integrated processes combining adsorption, membrane separation and flotation for heavy metal removal from wastewater." **157**(1-3): 97-104.

Mohammad, A. W., et al. (2004). "Potential use of nanofiltration membranes in treatment of industrial wastewater from Ni-P electroless plating." **168**: 241-252.

Mohsen-Nia, M., et al. (2007). "Removal of Cu2+ and Ni2+ from wastewater with a chelating agent and reverse osmosis processes." **217**(1-3): 276-281.

Molinari, R., et al. (2008). "Selective separation of copper (II) and nickel (II) from aqueous media using the complexation–ultrafiltration process." **70**(3): 341-348.

Morgan, B. and O. Lahav (2007). "The effect of pH on the kinetics of spontaneous Fe (II) oxidation by O2 in aqueous solution–basic principles and a simple heuristic description." Chemosphere **68**(11): 2080-2084.

Mudder, T. I., et al. (2001). "Chemistry and treatment of cyanidation wastes."

Murthy, Z. and L. B. J. J. o. h. m. Chaudhari (2008). "Application of nanofiltration for the rejection of nickel ions from aqueous solutions and estimation of membrane transport parameters." **160**(1): 70-77.

Neyens, E. and J. J. J. o. H. m. Baeyens (2003). "A review of classic Fenton's peroxidation as an advanced oxidation technique." **98**(1-3): 33-50.

Norcross, R. (1996). New developments in Caro's acid technology for cyanide destruction. Proceedings of Randol Gold Forum.

Noubactep, C. (2008). "A critical review on the process of contaminant removal in Fe0–H2O systems." Environmental technology **29**(8): 909-920.

Noubactep, C. (2013). "Relevant reducing agents in remediation Fe0/H2O systems." Clean–Soil, Air, Water **41**(5): 493-502.

Nörtemann, B. J. A. m. and biotechnology (1999). "Biodegradation of EDTA." **51**(6): 751-759.

Palumbo, A. V., et al. (1994). "The effect of media composition on EDTA degradation byAgrobacterium sp." **45**(1): 811-822.

Pantke, C., et al. (2012). "Green rust formation during Fe (II) oxidation by the nitrate-reducing Acidovorax sp. strain BoFeN1." Environmental science & technology **46**(3): 1439-1446.

Patil, Y. and K. J. P. B. Paknikar (2000). "Development of a process for biodetoxification of metal cyanides from waste waters." **35**(10): 1139-1151.

Patterson, J. W. (1985). "Industrial wastewater treatment technology."

Pera-Titus, M., et al. (2004). "Degradation of chlorophenols by means of advanced oxidation processes: a general review." Applied Catalysis B: Environmental **47**(4): 219-256.

Pirkanniemi, K., et al. (2007). "Degradation of EDTA and novel complexing agents in pulp and paper mill process and waste waters by Fenton's reagent." **147**(1-2): 556-561.

Pohl, C. A., et al. (1997). "Factors controlling ion-exchange selectivity in suppressed ion chromatography." **789**(1-2): 29-41.

Pohlandt, C. (1985). "Chromatographic separation and determination of stable metal cyanide complexes in gold processing solutions." South African Journal of Chemistry **38**(3): 110-114.

Popuri, S. R., et al. (2009). "Adsorptive removal of copper and nickel ions from water using chitosan coated PVC beads." **100**(1): 194-199.

Priya, P. G., et al. (2009). "Recovery and reuse of Ni (II) from rinsewater of electroplating industries." **163**(2-3): 899-909.

Qin, J.-J., et al. (2002). "A feasibility study on the treatment and recycling of a wastewater from metal plating." **208**(1-2): 213-221.

Reguera, E., et al. (1999). "The existence of ferrous ferricyanide." Transition Metal Chemistry **24**(6): 648-654.

Repo, E., et al. (2013). "Aminopolycarboxylic acid functionalized adsorbents for heavy metals removal from water." water research **47**(14): 4812-4832.

Reuber, M. D. and G. C. J. A. o. E. H. A. I. J. Schmieler (1962). "Edetate kidney lesions in rats." **5**(5): 430-436.

Robie, R. A. and B. S. Hemingway (1995). Thermodynamic properties of minerals and related substances at 298.15 K and 1 bar (105 Pascals) pressure and at higher temperatures, US Government Printing Office.

Rodríguez, J., et al. (1999). "Chemical degradation of EDTA and DTPA in a totally chlorine free (TCF) effluent." **40**(11-12): 267-272.

Ross, F. and A. B. Ross (1977). Selected specific rates of reactions of transients from water in aqueous solution. III. Hydroxyl radical and perhydroxyl radical and their radical ions, Notre Dame Univ., IN (USA). Radiation Lab.

Salcedo, A. F. M., et al. (2016). "Nickel recovery from synthetic Watts bath electroplating wastewater by homogeneous fluidized bed granulation process." Separation and Purification Technology **169**: 128-136.

Shannon, R. D. (1976). "Revised effective ionic radii and systematic studies of interatomic distances in halides and chalcogenides." Acta crystallographica section A: crystal physics, diffraction, theoretical and general crystallography **32**(5): 751-767.

Sharma, V. K., et al. (1998). "Ferrate (VI) oxidation of aqueous cyanide." **32**(17): 2608-2613.

Shin, S., et al. (2008). "Polymer-encapsulated iron oxide nanoparticles as highly efficient Fenton catalysts." Catalysis Communications **10**(2): 178-182.

Sillanpaa, M. and K. J. E. t. Pirkanniemi (2001). "Recent developments in chelate degradation." **22**(7): 791-801.

Sist, C. and G. P. J. J. Demopoulos (2003). "Nickel hydroxide precipitation from aqueous sulfate media." **55**(8): 42-46.

Smith, F. N., et al. (2015). "Technetium incorporation into goethite (α-FeOOH): An atomic-scale investigation." Environmental science & technology **49**(22): 13699-13707.

Smith, F. N., et al. (2016). "Computational investigation of technetium (IV) incorporation into inverse spinels: Magnetite (Fe3O4) and trevorite (NiFe2O4)." Environmental science & technology **50**(10): 5216-5224.

Sohn, K., et al. (2006). "Fe (0) nanoparticles for nitrate reduction: stability, reactivity, and transformation." Environmental science & technology **40**(17): 5514-5519.

Song, S., et al. (2007). "Mechanism of the photocatalytic degradation of CI Reactive Black 5 at pH 12.0 using SrTiO3/CeO2 as the catalyst." **41**(16): 5846-5853.

Standards, N. I. o., et al. (2004). NIST Critically Selected Stability Constants of Metal Complexes: Version 8.0, NIST.

Sörensen, M., et al. (1998). "Degradation Pathway of the Photochemical Oxidation of Ethylenediaminetetraacetate (EDTA) in the UV/H2O2-process." **26**(2): 109-115.

Tai, C., et al. (2002). "A new simple and sensitive fluorometric method for the determination of hydroxyl radical and its application." **58**(4): 661-667.

Tang, C., et al. (2016). "Rapid removal of selenate in a zero-valent iron/Fe3O4/Fe2+ synergetic system." Applied Catalysis B: Environmental **184**: 320-327.

Tchobanoglous, G., et al. (2003). "Wastewater Engineering: Treatment and Reuse. Metcalf & Eddy Inc." **10**: 0070418780.

US, D. o. I. (2001). Cyanide Fact Sheet. Bureau of Reclamation, Technical Service Center, Water Treatment Engineering and Research Group.

Venkatadri, R., et al. (1993). "Chemical oxidation technologies: ultraviolet light/hydrogen peroxide, Fenton's reagent, and titanium dioxide-assisted photocatalysis." **10**(2): 107-149.

Vohra, M. S. and A. P. J. W. R. Davis (2000). "TiO2-assisted photocatalysis of lead–EDTA." **34**(3): 952-964.

Von Gunten, U. J. W. r. (2003). "Ozonation of drinking water: Part I. Oxidation kinetics and product formation." **37**(7): 1443-1467.

Wang, J. L., et al. (2012). "Advanced oxidation processes for wastewater treatment: formation of hydroxyl radical and application." **42**(3): 251-325.

Weast, R. C., et al. (1988). CRC handbook of chemistry and physics, CRC press Boca Raton, FL.

Wedl, D. J. and R. J. J. M. F. Fulk (1991). "Cyanide destruction in plating sludges by hot alkaline chlorination." **89**(11): 33-37.

Wen, N. and M. H. J. C. j. o. c. Brooker (1994). "Rate constants for cyanate hydrolysis to urea: A Raman study." **72**(4): 1099-1106.

Whittig, L. and W. Allardice (1986). "X-ray diffraction techniques." Methods of Soil Analysis: Part 1—Physical and Mineralogical Methods(methodsofsoilan1): 331-362.

WHO (2004). Guidelines for drinking-water quality, World Health Organization.

Williams, H. E. (1948). "Cyanogen compounds."

Witschel, M., et al. (1999). "Transport of EDTA into cells of the EDTA-degrading bacterial strain DSM 9103." **145**(4): 973-983.

Xu, Z., et al. (2010). "Sensors for the optical detection of cyanide ion." Chemical Society Reviews **39**(1): 127-137.

Xu, Z., et al. (2017). "Decomplexation of Cu (II)-EDTA by UV/persulfate and UV/H2O2: efficiency and mechanism." Applied Catalysis B: Environmental **200**: 439-447.

Xue, H., et al. (1995). "Speciation of EDTA in natural waters: exchange kinetics of Fe-EDTA in river water." **29**(1): 59-68.

Yang, Z., et al. (2016). "Temporospatial evolution and removal mechanisms of As (V) and Se (VI) in ZVI column with H2O2 as corrosion accelerator." water research **106**: 461-469.

Yating, W., et al. (2008). "Artificial neural network modelling of plating rate and phosphorus content in the coatings of electroless nickel plating." **205**(1-3): 207-213.

Yoon, J., et al. (2001). "Investigation of the reaction pathway of OH radicals produced by Fenton oxidation in the conditions of wastewater treatment." **44**(5): 15-15.

Yurlova, L., et al. (2002). "Removal of Ni (II) ions from wastewater by micellar-enhanced ultrafiltration." **144**(1-3): 255-260.

Zafar, M. N., et al. (2009). "Removal of nickel onto alkali treated rice bran." **197**(1-4): 361-370.

Zaidi, A. and L. J. R. o. W. T. C.-E. C. Whittle, Burlington, Canada (1987). "Evaluation of the full scale alkaline chlorination treatment plant at Giant Yellowknife Mines Ltd."

Zaidi, S. and J. Carey (1984). Ultraviolet irradiation for removing iron cyanide from gold mill effluents. Proc. of the Conf. on Cyanide and Environment, Colorado State Univ., Fort Collins, Colo.

Zhang, T. C. and Y. H. Huang (2006). "Profiling iron corrosion coating on iron grains in a zerovalent iron system under the influence of dissolved oxygen." Water research **40**(12): 2311-2320.

Zhou, T., et al. (2010). "The role and fate of EDTA in ultrasound-enhanced zero-valent iron/air system." Chemosphere **78**(5): 576-582.

APPENDIX A

ORIGINAL DATA ASSOCIATED WITH CHAPTER 2

Table 1 for Figure 3. Dissolved Fe^{2+} concentration and pH in the blank anoxic ZVI and AIM system.

Media	T (h)	pH	Fe^{2+} (mg/L)
ZVI	0	7.50	0.0
ZVI	1	7.19	13.7
ZVI	4	7.08	14.8
ZVI	8	6.58	15.2
ZVI	19	6.55	16.1
ZVI	24	6.64	16.3
ZVI	48	6.48	16.2
ZVI	72	6.50	16.1

Media	T (h)	pH	Fe^{2+} (mg/L)
AIM	0	7.50	0.0
AIM	1	7.31	7.9
AIM	4	7.28	9.7
AIM	8	7.18	10.0
AIM	19	6.95	11.2
AIM	24	6.94	12.9
AIM	48	6.88	13.1
AIM	72	6.90	13.0

Table 2 and 3 for Figure 4 and 6. pH, dissolved Fe^{2+}, and nickel concentration in the anoxic and oxic ZVI system.

Anoxic Batch										
Media	T (h)	pH			Fe^{2+} (mg/L)			Ni^{2+} (mg/L)		
ZVI	0	7.50	7.50	7.50	0.0	0.0	0.0	50.0	100.0	200.0
ZVI	0.5	7.42	7.52	7.36	8.7	13.3	25.6	37.3	63.6	153.6
ZVI	1	7.17	7.19	7.15	16.0	16.8	41.9	25.2	51.2	111.2
ZVI	4	7.01	7.00	6.91	27.5	45.6	81.1	12.4	26.3	67.3
ZVI	8	6.81	6.88	6.76	37.8	64.3	113.2	4.84	12.5	37.5
ZVI	19	6.73	6.83	6.63	42.8	84.1	150.1	0.760	1.80	8.42
ZVI	29	6.65	6.78	6.55	46.4	87.5	159.6	0.278	0.720	2.72
ZVI	49	6.60	6.71	6.49	47.6	89.2	161.5	0.161	0.384	1.36
ZVI	72	6.60	6.70	6.47	47.7	88.7	161.9	0.159	0.370	1.30

Oxic Batch										
Media	T (h)	pH			Fe^{2+} (mg/L)			Ni^{2+} (mg/L)		
ZVI	0	7.50	7.50	7.50	0.0	0.0	0.0	50.0	100.0	200.0
ZVI	0.5	7.42	7.36	7.25	9.1	10.9	21.9	36.2	69.1	161.1
ZVI	1	7.17	7.05	6.98	16.2	24.3	51.8	27.9	53.9	128.4
ZVI	4	7.01	6.81	6.59	21.4	40.8	86.7	15.1	28.4	69.4
ZVI	8	6.81	6.66	6.45	23.5	63.2	126.0	6.32	13.5	38.9
ZVI	19	6.73	6.53	6.39	46.9	90.8	136.6	1.21	2.97	9.56
ZVI	29	6.65	6.45	6.34	50.1	98.2	159.1	0.412	1.16	3.79
ZVI	49	6.63	6.39	6.28	50.9	99.3	169.7	0.192	0.472	1.92
ZVI	72	6.61	6.37	6.26	51.7	100.3	172.1	0.161	0.372	1.38

Table 4 and 5 for Figure 7 and 10. pH, dissolved Fe^{2+}, Fe^{3+}, and nickel concentration in the anoxic and oxic AIM system.

Anoxic Batch													
Media	T (h)	pH			Fe^{2+} (mg/L)			Fe^{3+} (mg/L)			Ni^{2+} (mg/L)		
AIM	0	7.50	7.50	7.50	0	0	0	0	0	0	50.0	100.0	200.0
AIM	0.5	7.25	7.15	7.05	16.7	32.1	44.3	1.2	1.4	2.2	27.2	57.1	130.1
AIM	1	6.98	6.93	6.88	22.7	40.8	74.0	1.3	2.0	3.0	17.9	42.9	90.9
AIM	4	6.59	6.46	6.39	29.1	56.4	105.3	1.4	2.2	3.2	7.41	15.4	35.2
AIM	8	6.45	6.35	6.25	33.1	62.5	125.0	1.3	2.3	3.3	2.32	5.5	15.4
AIM	19	6.39	6.26	6.12	34.4	68.4	133.0	1.3	2.4	3.3	0.210	0.461	2.06
AIM	29	6.34	6.2	6.08	34.4	69.1	134.6	1.4	2.3	3.2	0.121	0.242	1.24
AIM	49	6.28	6.14	5.98	34.2	68.8	134.9	1.3	2.4	3.3	0.080	0.191	0.721
AIM	72	6.25	6.12	5.95	34.3	69.0	134.7	1.3	2.4	3.2	0.070	0.162	0.690

Oxic Batch													
Media	T (h)	pH			Fe^{2+} (mg/L)			Fe^{3+} (mg/L)			Ni^{2+} (mg/L)		
AIM	0	7.50	7.50	7.50	0	0	0	0	0	0	50.0	100.0	200.0
AIM	0.5	6.96	7.05	6.83	16.2	36.1	36.8	0.7	0.8	1.2	37.88	75.7	141.5
AIM	1	6.56	6.83	6.63	20.1	50.4	66.3	1.4	3.0	4.3	27.19	54.3	108.7
AIM	4	6.39	6.38	6.21	24.5	58.6	110.1	3.2	5.2	7.4	16.16	28.3	56.6
AIM	8	6.28	6.22	5.74	23.1	62.0	143.7	5.0	7.2	10.3	7.92	15.8	31.7
AIM	19	6.16	6.20	5.45	29.4	82.4	159.4	5.6	8.6	12.3	2.21	5.23	10.4
AIM	29	6.33	6.17	5.35	31.4	91.4	160.1	6.2	9.4	13.4	0.841	1.98	4.56
AIM	49	6.23	6.10	5.22	37.7	90.9	167.2	6.8	10.0	14.3	0.180	0.660	1.72
AIM	72	6.21	6.11	5.25	41.4	92.4	170.1	7.4	10.7	15.3	0.105	0.331	0.961

Table 6 and 7 for Figure 11. pH, dissolved Fe^{2+}, and nickel concentration of the continuous batch ZVI and AIM system.

Media	T (h)			pH			Fe^{2+} (mg/L)			Ni^{2+} (mg/L)		
ZVI	0	0	0	7.50	7.50	7.50	0	0	0	50.0	100.0	200.0
ZVI	1	1	1	7.15	7.25	7.00	16.7	32.1	44.3	24.42	40.23	84.36
ZVI	3	3	3	6.93	6.98	6.45	22.7	40.8	74.0	9.96	16.72	32.10
ZVI	6	6	6	6.46	6.59	6.35	29.1	56.4	105.3	5.32	6.87	17.58
ZVI	9	10	10	6.35	6.45	6.22	33.1	62.5	125.0	3.43	3.18	10.41
ZVI	12	15	16	6.26	6.39	6.25	34.4	68.4	133.0	2.50	2.36	6.10
ZVI	12.01	15.01	22	6.32	6.34	6.15	34.4	68.5	134.6	52.50	102.36	3.88
ZVI	13	16	28	6.24	6.28	6.12	38.2	72.8	136.9	27.34	61.31	2.57
ZVI	15	18	28.01	6.22	6.25	6.08	40.8	79.0	136.9	17.74	34.93	202.57
ZVI	19	23	29	6.12	6.15	5.98	46.8	81.9	144.0	8.52	11.92	175.40
ZVI	22	28	32	6.08	6.12	5.95	56.4	81.1	145.3	5.12	6.75	97.53
ZVI	27	34	36	5.98	6.08	5.45	62.5	93.2	155.0	3.66	4.24	43.18
ZVI	31	39	41	5.95	5.98	5.39	68.4	100.1	153.0	2.93	3.11	22.82
ZVI	36	42	48	6.01	5.95	5.34	69.1	103.2	154.6	2.49	2.58	11.21
ZVI	36.01	42.01	55	5.91	5.45	5.28	69.0	103.5	154.9	52.49	102.58	6.03
ZVI	37	43	62	6.13	5.39	5.25	65.8	112.3	154.7	39.73	87.29	4.63
ZVI	40	45	72	6.05	5.34	5.25	69.4	114.2	154.7	28.42	74.21	3.25
ZVI	48	50	80	6.11	5.28	5.39	70.6	115.7	150.4	18.97	54.27	2.79
ZVI	56	60	86	6.02	5.25	5.34	65.8	116.2	158.9	13.18	37.86	2.53
ZVI	63	70	86.01	5.73	5.25	5.34	69.4	118.5	159.5	9.93	29.41	202.53
ZVI	70	82	87	5.65	5.39	5.35	70.6	120.1	160.8	7.84	26.13	182.30
ZVI	80	96	90	5.60	5.34	5.36	70.7	120.5	160.6	5.72	25.05	142.97
ZVI	96		96	5.76		5.37	71.7		161.6	4.66		120.3

Media	T (h)			pH			Fe^{2+} (mg/L)			Ni^{2+} (mg/L)		
AIM	0	0	0	7.5	7.5	7.5	0	0	0	50.0	100.0	200.0
AIM	1	1	1	7.15	7.25	7.01	16.7	32.1	44.3	21.84	42.22	83.10
AIM	3	3	3	6.93	6.98	6.43	22.7	40.8	74.0	8.70	15.17	29.21
AIM	5	6	6	6.46	6.59	6.10	29.1	56.4	105.3	4.43	4.70	10.98
AIM	8	9	10	6.35	6.45	6.06	33.1	62.5	125.0	2.64	2.82	5.42
AIM	8.01	12	15	6.26	6.39	6.03	33.4	68.4	133.0	52.64	2.26	2.92
AIM	9	12.01	20	6.32	6.34	5.99	37.4	68.8	134.6	30.13	102.26	2.19
AIM	11	13	20.01	6.24	6.28	5.96	38.2	76.8	136.9	15.34	57.93	202.19
AIM	13	15	21	6.22	6.25	5.92	40.8	79.0	139.7	8.30	27.19	97.23
AIM	16	19	24	6.12	6.15	5.89	46.8	81.9	144.0	4.52	8.29	48.40
AIM	19	24	30	6.08	6.12	5.85	56.4	81.1	145.3	3.12	3.98	15.53
AIM	22.5	27	36	5.98	6.08	5.82	62.5	93.2	155.0	2.56	3.02	8.28
AIM	22.51	32	42	5.95	5.98	5.84	62.8	100.1	153.0	52.56	2.51	5.12
AIM	23.5	32.01	52	6.01	5.95	5.63	69.1	100.3	154.6	32.25	102.51	3.21
AIM	25	33	60	5.91	5.45	5.77	68.8	106.2	154.9	16.23	82.29	2.63
AIM	28	36	60.01	6.13	5.39	5.68	65.8	106.8	154.7	7.37	52.83	202.63
AIM	32	40	62	6.05	5.34	5.64	69.4	107.2	154.7	4.24	31.21	137.25
AIM	38	48	66	6.11	5.28	5.49	70.6	108.4	150.4	2.97	12.27	72.79
AIM	42	55	70	6.02	5.25	5.47	65.8	110.2	158.9	2.48	7.26	43.53
AIM	42.01	62	78	5.73	5.25	5.43	66.0	111.2	160.5	52.48	4.91	19.52
AIM	44	72	88	5.65	5.39	5.43	70.6	113.2	160.8	34.84	3.13	10.30
AIM	48	80	96	5.60	5.34	5.44	70.7	120.1	160.6	20.17	2.55	7.97
AIM	52	80.01		5.66	5.34		71.7	120.3		12.66	102.6	
AIM	60	82		5.62	5.35		72.1	128.2		7.49	92.1	
AIM	70	88		5.68	5.36		72.7	135.2		4.8512	72.8	
AIM	82	96		5.54	5.37		72.9	141.9		3.13	60.9	
AIM	96			5.40			72.7			2.57		

Table 8 for Figure 12. pH and the concentration profile of dissolved nickel, nitrate, and dissolved Fe^{2+} in the anoxic CSTR ZVI and AIM system.

Media	T (d)	pH	Fe^{2+} (mg/L)	NO_3^- (mg/L)	Ni^{2+} (mg/L)
ZVI	1	7.31	67.8	0.02	2.37
ZVI	2	6.21	70.1	0.02	2.52
ZVI	3	6.61	76.6	0.02	2.43
ZVI	4	6.55	83	0.02	2.98
ZVI	5	6.65	84.4	0.02	3.12
ZVI	7	6.87	78.9	0.02	4.27
ZVI	8	6.60	77.5	0.08	2.92
ZVI	9	6.17	74.7	0.12	2.50
ZVI	10	6.41	77.2	0.02	1.82
ZVI	11	6.47	76.9	0.01	2.04
ZVI	12	6.28	76.0	0.04	1.84
ZVI	13	6.74	75.9	0.02	2.91
ZVI	14	6.94	75.6	0.24	3.29
ZVI	15	6.97	79.5	0.01	3.37
ZVI	16	6.93	77.7	0.04	2.70
ZVI	17	6.02	77.7	0.02	3.02
ZVI	18	6.79	77.3	0.01	2.91
ZVI	20	6.32	77.8	0.01	2.54
ZVI	21	6.08	78.0	0.01	2.53
ZVI	22	6.13	76.9	0.24	1.38
ZVI	23	6.19	77.1	0.17	1.34
ZVI	24	6.54	75.8	0.05	1.42
ZVI	25	6.62	75.3	0.06	1.39
ZVI	27	6.68	75.7	0.03	1.57
ZVI	29	6.34	78.4	0	1.68
ZVI	30	6.48	85.3	0.02	1.94
ZVI	31	6.68	86.2	0.02	2.28
ZVI	32	6.54	74.8	0.01	2.33
ZVI	34	6.48	79.3	0.09	1.46
ZVI	35	6.01	80.2	0.11	1.37
ZVI	36	6.00	75.5	0.12	1.38
ZVI	38	6.08	75.7	0.01	2.32
ZVI	39	6.80	76.4	0.02	1.77
ZVI	41	6.88	79.1	0.02	1.89
ZVI	43	6.94	80.9	0.02	2.08
ZVI	44	6.84	78.3	0.02	3.66
ZVI	46	6.65	75.7	0.02	9.08
ZVI	48	6.92	67.1	0.02	44.8
ZVI	49	7.05	53.0	0.02	72.1
ZVI	50	7.29	35.0	0.02	70.8

Media	T (d)	pH	Fe^{2+} (mg/L)	NO_3^- (mg/L)	Ni^{2+} (mg/L)
AIM	1	6.03	2.0	1.20	0.310
AIM	2	6.21	1.5	1.02	0.341
AIM	3	5.67	0.2	0.23	0.352
AIM	4	5.82	0.2	0.20	0.310
AIM	5	5.73	0.2	0.18	0.289
AIM	7	5.79	0.2	0.18	0.351
AIM	8	5.75	0.1	0.20	0.290
AIM	9	5.76	0	0.16	0.210
AIM	10	5.80	1.5	0.84	0.061
AIM	11	5.11	1.3	1.20	0.170
AIM	12	5.28	0.7	0.52	0.090
AIM	13	5.80	1.3	0.23	0.112
AIM	14	5.97	3.5	0.20	0.133
AIM	15	6.45	0.3	0.18	0.121
AIM	16	6.27	2.8	0.18	0.125
AIM	17	6.21	3.2	0.20	0.162
AIM	18	6.36	3.0	0.16	0.272
AIM	20	6.64	2.4	0.84	0.191
AIM	21	6.60	2.8	0.41	0.273
AIM	22	6.56	1.0	0.24	0.324
AIM	23	6.33	0.3	0.15	0.351
AIM	24	6.52	0.2	0.41	0.252
AIM	25	6.31	0	0.21	0.317
AIM	27	6.14	0	0.37	0.379
AIM	28	6.08	0	0.10	0.170
AIM	29	6.25	0.4	0.40	0.088
AIM	31	6.47	0	0.08	0.109
AIM	32	6.51	0	0.10	0.442
AIM	34	6.64	0	0.07	0.234
AIM	35	6.31	0	0.86	0.107
AIM	36	6.74	0	0.42	0.327
AIM	38	6.41	0	0.48	0.352
AIM	39	6.73	0	0.57	0.254
AIM	41	6.78	0	0.30	0.314
AIM	43	6.03	0	0.04	0.384
AIM	44	6.21	0	0.03	0.172
AIM	46	6.67	0	0.18	0.314
AIM	48	6.82	0	0.36	0.387
AIM	49	6.73	0	0.57	0.175
AIM	50	6.79	0	0.85	0.282

APPENDIX B

ORIGINAL DATA ASSOCIATED WITH CHAPTER 3

Table 9 for Figure 13 and 15. The concentration profile of free cyanide and ferrocyanide in the anoxic Fe^{2+}-enriched AIM system.

Media	T (h)	CN^- (mM)		$Fe(CN)_6^{4-}$ (mM)	
AIM	0	0.769	1.538	0	0
AIM	0.1	0.019	0.111	0.419	0.819
AIM	0.5	0.003	0.020	0.127	0.277
AIM	1	0.001	0.008	0.043	0.093
AIM	2	0.001	0.005	0.018	0.048
AIM	4	ND	0.002	0.010	0.018
AIM	8	ND	0.001	0.005	0.009
AIM	16	ND	0.001	0.003	0.006
AIM	16.1	ND	0.001	0.004	0.008
AIM	17	0.001	0.002	0.036	0.049
AIM	19	ND	0.001	0.034	0.045
AIM	22	ND	0.001	0.031	0.037
AIM	27	ND	0.001	0.025	0.032
AIM	32	ND	ND	0.017	0.024

Table 10 for Figure 16. The concentration profile of anion exchange test in the pH-controlled anoxic AIM system.

Media	T (h)	Cl^- (mM)	SO_4^{2-} (mM)	CN^- (mM)	$Fe(CN)_6^{4-}$ (mM)
AIM	0	0.02	0	0.769	0.001
AIM	0.1	0.163	0	0.465	0.015
AIM	0.5	0.276	0	0.165	0.022
AIM	1	0.415	0	0.081	0.023
AIM	2	0.554	0	0.013	0.024
AIM	4	0.666	0	0.005	0.022
AIM	8	0.706	1.5	0.004	0.022
AIM	8.1	0.71	1.42	0.023	0.022
AIM	9	0.725	1.315	0.283	0.024
AIM	10	0.732	1.262	0.423	0.023
AIM	12	0.746	1.175	0.662	0.023
AIM	16	0.751	1.148	0.715	0.023

Table 11 for Figure 17. pH and the concentration profile of dissolved Fe^{2+} and Fe^{3+} in the blank oxic ZVI, AIM, azide-AIM, and benzoic-AIM systems.

Media	T (h)	pH	Fe^{2+} (mg/L)	Fe^{3+} (mg/L)
ZVI	0	7.5	0	0
ZVI	0.1	6.12	1.3	0.2
ZVI	1	7.19	6.7	0.3
ZVI	2.5	7.28	9.7	0.4
ZVI	4	7.18	11.2	0.5
ZVI	8	6.95	14.3	0.5
ZVI	16	6.54	17.4	0.5
ZVI	24	6.48	17.9	0.5
ZVI	48	6.50	17.8	0.5
ZVI	72	6.52	17.5	0.5

Media	T (h)	pH	Fe^{2+} (mg/L)	Fe^{3+} (mg/L)
AIM+AZ	0	7.5	0	0
AIM+AZ	0.1	6.83	1.8	0.1
AIM+AZ	1	6.63	10.2	1.1
AIM+AZ	2.5	6.21	16.5	3.0
AIM+AZ	4	5.74	20.8	4.1
AIM+AZ	8	5.45	21.6	4.7
AIM+AZ	16	5.35	22.6	5.1
AIM+AZ	24	5.22	23.4	5.2
AIM+AZ	48	5.25	23.5	4.9
AIM+AZ	72	5.27	23.7	4.8

Media	T (h)	pH	Fe^{2+} (mg/L)	Fe^{3+} (mg/L)
AIM	0	7.5	0	0
AIM	0.1	6.73	1.3	0.1
AIM	1	6.53	8.9	1.2
AIM	2.5	6.41	15.5	3.4
AIM	4	6.04	18.4	4.6
AIM	8	5.55	20.3	6.1
AIM	16	5.45	21.4	7.3
AIM	24	5.42	21.5	7.2
AIM	48	5.43	21.6	7.3
AIM	72	5.39	21.5	7.3

Media	T (h)	pH	Fe^{2+} (mg/L)	Fe^{3+} (mg/L)
AIM+BA	0	7.5	0	0
AIM+BA	0.1	6.73	1.02	0
AIM+BA	1	6.53	12.2	0.4
AIM+BA	2.5	6.41	17.3	0.5
AIM+BA	4	6.04	23.5	0.6
AIM+BA	8	5.55	26.8	0.9
AIM+BA	16	5.45	27.3	0.9
AIM+BA	24	5.42	28.1	0.9
AIM+BA	48	5.43	28.5	0.7
AIM+BA	72	5.39	28.7	0.8

Table 12 for Figure 18. The gas pressure of the headspace in the blank AIM system.

Media	T (h)	Pressure (atm)
AIM	0	1.00
AIM	0.5	0.85
AIM	1	0.72
AIM	2	0.50
AIM	4	0.22
AIM	8	0.04
AIM	8.01	1.00
AIM	8.5	0.86
AIM	9	0.76
AIM	10	0.54
AIM	12	0.32
AIM	16	0.04

Table 13 for Figure 19. The concentration profile of cyanide, ferrocyanide, cyanate, and ammonia in the oxic AIM system with 0.769- and 1.538-mM initial cyanide concentration.

Media	T (h)	CN^- (mM)		$Fe(CN)_6^{4-}$ (mM)		OCN^- (mM)		NH_4^+ (mM)	
AIM	0	0.769	1.538	0	0	0	0	0	0
AIM	0.1	0.215	0.425	0.419	0.919	0.055	0.085	0.025	0.236
AIM	0.5	0.018	0.078	0.427	0.927	0.092	0.169	0.062	0.293
AIM	1	0.003	0.028	0.223	0.523	0.186	0.266	0.076	0.321
AIM	2	0.002	0.017	0.104	0.304	0.203	0.340	0.129	0.536
AIM	3	0.002	0.013	0.062	0.262	0.170	0.369	0.212	0.736
AIM	4	0.001	0.010	0.027	0.173	0.086	0.286	0.388	1.079
AIM	6	0.006	0.006	0.012	0.082	0.036	0.116	0.658	1.402
AIM	8	0.002	0.005	0.006	0.026	0.020	0.068	0.743	1.443
AIM	12	ND	0.003	0.004	0.004	0.008	0.028	0.736	1.426
AIM	16	ND	0.003	0.003	0.003	0.003	0.003	0.674	1.274
AIM	20	ND	0.002	0.002	0.002	0.003	0.002	0.534	1.034
AIM	24	ND	0.002	0.003	0.003	0.002	0.003	0.475	0.879
AIM	30	ND	0.001	0.002	0.001	0.001	0.001	0.344	0.744
AIM	36	ND	0.001	0.003	0.001	0.001	0.001	0.291	0.691
AIM	48	ND	ND	0.002	0.001	0.001	0.001	0.274	0.571

Table 14 for Figure 20. the concentration profile of no media system and ZVI system under oxic condition.

Media	T (h)	pH	Fe^{2+} (mg/L)	Fe^{3+} (mg/L)	CN- (mM)	$Fe(CN)_6^{4-}$ (mM)	NH_4^+ (mM)
ZVI	0	7.50	0	0	1.538	0	0
ZVI	0.1	10.78	0	0	1.522	0	0
ZVI	1	10.63	0	0	1.431	0.021	0
ZVI	2	10.56	0	0	1.302	0.135	0.011
ZVI	4	10.36	0	0	1.179	0.314	0.035
ZVI	8	10.12	0.1	0	0.999	0.583	0.043
ZVI	12	9.23	0.2	0.1	0.772	0.732	0.032
ZVI	24	8.48	0.5	0.8	0.473	0.931	0.041
Non	0	7.50	0	0	1.538	0	0
Non	0.1	8.50	0	0	1.538	0	0
Non	1	8.27	0	0	1.538	0	0
Non	2	8.33	0	0	1.538	0	0
Non	4	8.37	0	0	1.538	0	0
Non	8	8.28	0	0	1.538	0	0
Non	12	8.13	0	0	1.538	0	0
Non	24	8.18	0	0	1.538	0	0

Table 15 for Figure 21. the concentration profile of azide-AIM and benzoic-AIM system.

Media	T (h)	pH	Fe^{2+} (mg/L)	Fe^{3+} (mg/L)	CN- (mM)	OCN- (mM)	$Fe(CN)_6^{4-}$ (mM)	NH_4^+ (mM)
AIM+azide	0	7.50	0	0	1.538	0	0	0
AIM+azide	0.1	10.02	0.6	0.3	1.288	0.004	0.121	0.031
AIM+azide	0.5	9.52	3.1	0.7	0.338	0.025	0.720	0.135
AIM+azide	1	8.76	3.1	0.7	0.120	0.083	0.712	0.321
AIM+azide	2	7.02	3.0	0.1	0.085	0.112	0.427	0.513
AIM+azide	4	6.59	5.7	0.4	0.065	0.106	0.323	0.932
AIM+azide	8	6.31	8.0	1.1	0.025	0.076	0.210	1.121
AIM+benzoic	0	7.50	0	0	1.538	0	0	0
AIM+benzoic	0.1	10.50	0.8	2.2	1.196	0	0.332	0
AIM+benzoic	0.5	9.96	3.0	1.0	0.849	0	0.572	0
AIM+benzoic	1	8.15	3.0	1.0	0.462	0	0.992	0
AIM+benzoic	2	7.30	2.8	0.1	0.144	0	1.321	0
AIM+benzoic	4	6.43	10.6	0.1	0.085	0	1.363	0
AIM+benzoic	8	6.24	8.5	2.2	0.043	0	1.421	0

Table 16 for Figure 22. the total cyanide and ammonia concentration profile of continuous batch oxic AIM system with initial cyanide of 0.769 and 1.538 mM.

Media	T (h)		pH		Fe^{2+} (mg/L)		CN- (mM)		$Fe(CN)_6^{4-}$ (mM)		Total cyanide (mM)		NH_4^+ (mM)	
AIM	0	0	7.5	7.5	0	0	0.769	1.538	0	0	0.769	1.538	0	0
AIM	0.1	0.1	9.00	10.11	0.9	0.9	0.41	1.012	0.265	0.315	0.675	1.327	0.06	0.12
AIM	1	1	8.11	9.54	0.7	0.7	0.049	0.282	0.262	0.41	0.311	0.692	0.17	0.34
AIM	3	3	7.31	8.16	1	1.0	0.016	0.032	0.091	0.329	0.107	0.361	0.25	0.5
AIM	5	6	6.95	7.96	2.5	2.5	0.009	0.078	0.043	0.11	0.052	0.188	0.48	0.96
AIM	7	8	6.45	7.02	3.9	3.9	0.005	0.03	0.028	0.063	0.033	0.093	0.66	1.32
AIM	7.01	10	8.88	6.88	0.4	3.4	0.774	0.005	0.028	0.022	0.802	0.027	0.67	1.44
AIM	8	10.01	8.29	10.21	0.6	0.6	0.501	1.543	0.101	0.022	0.602	1.565	0.76	1.49
AIM	10	11	7.34	9.41	1.4	0	0.109	1.098	0.218	0.176	0.327	1.274	0.88	1.76
AIM	13	13	6.84	8.21	5.2	0.2	0.029	0.432	0.118	0.391	0.147	0.823	1.01	2.02
AIM	15	16	6.27	8.12	8.3	0.3	0.016	0.218	0.075	0.277	0.091	0.495	1.19	2.38
AIM	17	19	6.11	7.73	10.4	2.4	0.009	0.11	0.048	0.142	0.057	0.252	1.29	2.58
AIM	20	22	6.19	7.34	12.8	5.8	0.005	0.052	0.03	0.077	0.035	0.129	1.36	2.72
AIM	20.01	25	8.90	7.18	0.3	9.3	0.764	0.019	0.04	0.043	0.804	0.062	1.38	2.86
AIM	21	27	8.06	6.80	1.2	13.2	0.471	0.004	0.172	0.035	0.643	0.039	1.42	2.96
AIM	23	27.01	7.68	10.67	3.8	1.8	0.221	1.542	0.224	0.035	0.445	1.577	1.53	3.06
AIM	25	28	7.12	9.53	17.9	1.9	0.122	1.208	0.192	0.137	0.314	1.345	1.64	3.28
AIM	28	30	6.89	8.64	21.8	1.8	0.054	0.746	0.133	0.346	0.187	1.092	1.76	3.52
AIM	31	34	6.64	8.02	24.6	4.6	0.023	0.22	0.081	0.543	0.104	0.763	1.90	3.8
AIM	35	38	6.59	7.55	29.4	9.4	0.021	0.126	0.031	0.338	0.052	0.464	2.01	4.02
AIM	38	42	6.45	7.45	30.6	13.6	0.013	0.074	0.015	0.182	0.028	0.256	2.06	4.12
AIM	38.01	46	8.89	6.83	0.9	14.2	0.776	0.021	0.021	0.112	0.797	0.133	2.09	4.28
AIM	39	50	8.20	6.45	1.2	21.4	0.502	0.011	0.195	0.043	0.697	0.054	2.11	4.42
AIM	42	52	7.86	6.35	2.3	23.2	0.121	0.005	0.413	0.021	0.534	0.026	2.24	4.58
AIM	45	52.01	7.28	10.22	2.5	1.8	0.102	1.543	0.3	0.021	0.402	1.564	2.31	4.62
AIM	50	53	6.98	9.32	5.6	2.5	0.073	1.286	0.214	0.17	0.287	1.456	2.37	4.74
AIM	55	56	6.79	8.46	10.2	4.2	0.032	0.864	0.16	0.323	0.192	1.187	2.42	4.84
AIM	60	60	6.61	7.82	23.5	5.5	0.012	0.604	0.092	0.275	0.104	0.879	2.49	4.98
AIM	65	65	6.59	7.42	31.2	12.2	0.007	0.314	0.048	0.279	0.055	0.593	2.59	5.18
AIM	68	70	6.3	7.31	34.2	14.8	0.002	0.174	0.03	0.249	0.032	0.423	2.61	5.25
AIM	68.01	75	8.86	7.09	1.1	13.2	0.771	0.054	0.03	0.2	0.801	0.254	2.61	5.32
AIM	70	80	8.18	7.01	1.2	16.2	0.621	0.024	0.11	0.147	0.731	0.171	2.63	5.46
AIM	75	85	7.68	6.72	1.6	20.5	0.403	0.016	0.199	0.081	0.602	0.097	2.73	5.56
AIM	80	90	7.39	6.82	4.2	26.9	0.213	0.014	0.31	0.031	0.523	0.045	2.86	5.72
AIM	85	96	7.14	6.56	6.3	34.1	0.179	0.004	0.288	0.019	0.467	0.023	2.98	5.96
AIM	90		6.89		12.4		0.137		0.288		0.425		3.12	
AIM	96		6.50		21.6		0.101		0.267		0.368		3.22	

APPENDIX C

ORIGINAL DATA ASSOCIATED WITH CHAPTER 4

Table 17 and 18 for Figure 23. Removal percentage of EDTA and TOC in ZVI and AIM system during anoxic and oxic conditions.

Anoxic					
Media	T (h)	TOC (mg/L)	TOC removal	EDTA (mM)	EDTA removal
AIM	0	62.0	0.0%	0.5	0.0%
AIM	0.1	43.2	30.3%	0.357	28.6%
AIM	0.5	32.3	47.9%	0.269	46.2%
AIM	1	31.2	49.7%	0.257	48.6%
AIM	2	29.6	52.3%	0.243	51.4%
AIM	4	29.1	53.1%	0.238	52.4%
ZVI	0	62.0	0.0%	0.5	0.0%
ZVI	0.1	48.1	22.4%	0.388	22.3%
ZVI	0.5	37.3	39.8%	0.305	39.0%
ZVI	1	36.3	41.5%	0.295	41.0%
ZVI	2	34.9	43.7%	0.284	43.2%
ZVI	4	34.7	44.0%	0.283	43.4%

Oxic					
Media	T (h)	TOC (mg/L)	TOC removal	EDTA (mM)	EDTA removal
AIM	0	62.0	0.0%	0.5	0.0%
AIM	0.1	44.5	28.2%	0.361	27.8%
AIM	0.5	29.1	53.1%	0.157	68.6%
AIM	1	25.7	58.5%	0.136	72.8%
AIM	2	22.2	64.2%	0.118	76.5%
AIM	4	18.9	69.5%	0.096	80.8%
ZVI	0	62.0	0.0%	0.5	0.0%
ZVI	0.1	45.1	27.3%	0.368	26.4%
ZVI	0.5	36.3	41.5%	0.296	40.8%
ZVI	1	34.1	45.0%	0.277	44.6%
ZVI	2	32.9	46.9%	0.268	46.4%
ZVI	4	32.4	47.7%	0.263	47.3%

Table 19 and 20 for Figure 24. the removed EDTA concentration in the anoxic ZVI and AIM system.

Media	T (h)	EDTA (mM)	Removed EDTA (mM)
AIM	0.0	0.1	0.000
AIM	0.1	0.043	0.057
AIM	0.5	0.015	0.085
AIM	1.0	0.006	0.094
AIM	1.01	0.106	0.094
AIM	1.1	0.056	0.144
AIM	1.5	0.024	0.176
AIM	2.0	0.017	0.183
AIM	2.01	0.117	0.183
AIM	2.1	0.080	0.220
AIM	2.5	0.055	0.245
AIM	3.0	0.045	0.255
AIM	4.0	0.039	0.261
AIM	0.0	0.25	0.000
AIM	0.1	0.126	0.124
AIM	0.5	0.079	0.171
AIM	1.0	0.054	0.196
AIM	1.01	0.304	0.196
AIM	1.1	0.283	0.217
AIM	1.5	0.253	0.247
AIM	2.0	0.241	0.259
AIM	3.0	0.236	0.264
AIM	4.0	0.233	0.267
AIM	0.0	0.5	0.000
AIM	0.1	0.357	0.143
AIM	0.5	0.269	0.231
AIM	1.0	0.257	0.243
AIM	2.0	0.243	0.257
AIM	3.0	0.238	0.262
AIM	4.0	0.235	0.265

Media	T (h)	EDTA (mM)	Removed EDTA (mM)
ZVI	0.0	0.1	0.000
ZVI	0.1	0.044	0.056
ZVI	0.5	0.018	0.082
ZVI	1.0	0.011	0.089
ZVI	1.01	0.111	0.089
ZVI	1.1	0.059	0.141
ZVI	1.5	0.037	0.163
ZVI	2.0	0.031	0.169
ZVI	2.01	0.131	0.169
ZVI	2.1	0.111	0.189
ZVI	2.5	0.092	0.208
ZVI	3.0	0.088	0.212
ZVI	4.0	0.086	0.214
ZVI	0.0	0.25	0.000
ZVI	0.1	0.163	0.087
ZVI	0.5	0.103	0.147
ZVI	1.0	0.079	0.171
ZVI	1.01	0.329	0.171
ZVI	1.1	0.313	0.187
ZVI	1.5	0.296	0.204
ZVI	2.0	0.286	0.214
ZVI	3.0	0.282	0.218
ZVI	4.0	0.282	0.218
ZVI	0.0	0.5	0.000
ZVI	0.1	0.388	0.112
ZVI	0.5	0.305	0.195
ZVI	1.0	0.295	0.205
ZVI	2.0	0.284	0.216
ZVI	3.0	0.283	0.217
ZVI	4.0	0.281	0.219

Table 21, 22, and 23 for Figure 25. The concentration profile of EDTA, IMDA, NTA, and glycine in the anoxic, oxic, and with 10 mM H_2O_2-AIM condition.

Anoxic									
Media	T (h)	pH	Fe^{2+} (mg/L)	Fe^{3+} (mg/L)	EDTA (mM)	IMDA (mM)	NTA (mM)	NH_4^+ (mM)	Glycine (mM)
AIM	0	7.5	0	0	0.5	0	0	0	0
AIM	0.1	7.41	2.2	0.6	0.368	0	0	0	0
AIM	0.5	7.32	1.3	1.0	0.286	0	0	0	0
AIM	1	7.33	0.9	0.8	0.277	0	0	0	0
AIM	2	6.92	0.9	1.0	0.269	0	0	0	0
AIM	4	6.87	1.4	0.5	0.260	0	0	0	0
AIM	8	6.92	2.1	0.7	0.245	0	0	0	0
AIM	12	7.05	3.5	0.8	0.235	0	0	0	0
AIM	24	6.88	3.1	0.5	0.226	0	0	0	0

Oxic									
AIM	0	7.5	0	0	0.5	0	0	0	0
AIM	0.1	6.95	4.3	0.8	0.371	0	0	0.011	0
AIM	0.5	6.5	9.7	4.5	0.157	0.01	0.01	0.020	0
AIM	1	6.53	7.7	3.6	0.146	0.02	0.01	0.045	0.01
AIM	2	6.35	6.9	3.5	0.118	0.03	0.02	0.078	0.02
AIM	4	6.47	7.5	1.2	0.096	0.04	0.04	0.121	0.03
AIM	8	6.36	8.2	2.1	0.082	0.04	0.05	0.151	0.03
AIM	12	6.27	9.5	2.3	0.067	0.03	0.04	0.154	0.04
AIM	24	6.31	8.6	2.8	0.053	0.03	0.04	0.155	0.04

10 mM H_2O_2									
AIM	0	7.5	0	0	0.5	0	0	0	0
AIM	0.1	6.95	3.2	0.5	0.365	0	0	0.020	0
AIM	0.5	6.53	15.3	3.6	0.131	0.01	0.02	0.042	0.01
AIM	1	6.45	22.3	3.0	0.105	0.03	0.03	0.078	0.03
AIM	2	5.76	25.3	4.0	0.084	0.06	0.05	0.127	0.05
AIM	4	5.87	27.4	4.6	0.055	0.09	0.08	0.192	0.08
AIM	8	5.66	28.2	3.1	0.033	0.06	0.06	0.226	0.10
AIM	12	5.47	24.5	4.3	0.018	0.04	0.05	0.240	0.08
AIM	24	5.81	28.6	4.8	0.008	0.04	0.05	0.249	0.06

Table 24, 25, and 26 for Figure 27. The concentration profile of EDTA, IMDA, NTA, glycine, and ammonia in 0.5 mM EDTA + 10 mM H_2O_2 without Fe^{2+}, with 50 mg/L Fe^{2+}, and with 100 mg/L Fe^{2+}.

10 mM H_2O_2 without Fe^{2+}						
Media	T (h)	EDTA (mM)	IMDA (mM)	NTA (mM)	NH_4^+ (mM)	Glycine (mM)
no media	0	0.5	0	0	0	0
no media	0.1	0.352	0.01	0.01	0	0.01
no media	1	0.345	0.02	0.02	0	0.02
no media	2	0.342	0.02	0.02	0	0.02
no media	4	0.341	0.01	0.01	0	0.01

10 mM H_2O_2 + 50 mg/L Fe^{2+}						
no media	0	0.500	0	0	0	0
no media	0.1	0.316	0	0.01	0.031	0
no media	1	0.280	0.02	0.02	0.062	0.02
no media	2	0.273	0.02	0.03	0.084	0.03
no media	4	0.271	0.02	0.03	0.081	0.03

10 mM H_2O_2 + 100 mg/L Fe^{2+}						
no media	0	0.500	0	0	0	0
no media	0.1	0.244	0.01	0.01	0.032	0
no media	1	0.208	0.02	0.03	0.075	0.02
no media	2	0.201	0.03	0.04	0.097	0.04
no media	4	0.199	0.03	0.04	0.095	0.03

Table 27 for Figure 28. The concentration profile of continuous batch AIM system with and without 10 mM H_2O_2.

Continuous AIM																			
Additions		T (h)		pH		Fe^{2+} (mg/L)		Fe^{3+} (mg/L)		EDTA (mM)		IMDA (mM)		NTA (mM)		NH_4^+ (mM)		Glycine (mM)	
-	10 mM H_2O_2	0	0	7.50	7.50	0	0	0	0	0.50	0.50	0	0	0	0	0	0	0	0
-	10 mM H_2O_2	0.1	0.1	7.30	7.60	7.1	6.3	2.2	2.3	0.326	0.311	0.004	0.009	0	0.01	0	0.010	0	0
-	10 mM H_2O_2	0.5	0.5	6.37	5.86	5.1	15.0	3.0	4.7	0.156	0.120	0.020	0.042	0.01	0.01	0.020	0.022	0	0.01
-	10 mM H_2O_2	1	1	6.65	5.96	7.2	16.1	2.4	5.4	0.137	0.080	0.045	0.088	0.03	0.03	0.031	0.032	0.01	0.01
-	10 mM H_2O_2	2	2	6.14	5.77	11.5	28.1	4.2	5.3	0.121	0.058	0.078	0.137	0.06	0.05	0.052	0.054	0.03	0.03
-	10 mM H_2O_2	4	4	6.16	5.87	13.5	29.4	5.2	4.0	0.093	0.047	0.121	0.192	0.04	0.06	0.052	0.078	0.03	0.05
-	10 mM H_2O_2	8	4.01	6.18	6.53	13.5	27.2	4.5	6.3	0.063	0.547	0.151	0.192	0.04	0.06	0.051	0.060	0.03	0.05
-	10 mM H_2O_2	8.01	4.1	6.88	6.53	18.5	27.2	2.8	6.3	0.563	0.505	0.151	0.198	0.04	0.07	0.052	0.082	0.05	0.08
-	10 mM H_2O_2	8.1	4.5	6.88	6.20	18.5	29.2	2.8	5.9	0.551	0.352	0.158	0.217	0.04	0.06	0.052	0.064	0.07	0.10
-	10 mM H_2O_2	8.5	5	6.63	6.07	25.7	31.2	1.7	5.4	0.522	0.286	0.167	0.227	0.04	0.08	0.053	0.085	0.08	0.11
-	10 mM H_2O_2	9	6	6.59	6.18	26.2	37.3	1.4	5.3	0.503	0.226	0.173	0.239	0.04	0.07	0.051	0.097	0.08	0.12
-	10 mM H_2O_2	10	8	6.46	6.18	31.9	37.3	2.3	5.3	0.448	0.146	0.187	0.252	0.04	0.08	0.054	0.071	0.08	0.13
-	10 mM H_2O_2	12	12	6.46	8.02	31.9	7.5	2.3	6.7	0.352	0.055	0.192	0.259	0.03	0.09	0.041	0.046	0.08	0.15
-	10 mM H_2O_2	16	12.01	6.32	7.29	26.8	8.2	1.1	4.9	0.239	0.555	0.196	0.259	0.03	0.06	0.045	0.068	0.09	0.15
-	10 mM H_2O_2	20	12.1	6.46	7.29	31.0	8.2	1.3	4.9	0.162	0.530	0.200	0.261	0.03	0.07	0.042	0.082	0.08	0.14
-	10 mM H_2O_2	24	12.5	6.32	6.75	36.8	21.8	2.1	4.0	0.119	0.462	0.206	0.273	0.03	0.06	0.036	0.061	0.09	0.13
-	10 mM H_2O_2	24.01	13	7.23	6.59	29.9	18.1	2.9	6.9	0.919	0.395	0.150	0.293	0.04	0.08	0.041	0.084	0.08	0.15
-	10 mM H_2O_2	24.1	14	7.23	6.73	29.9	20.5	2.9	5.2	0.912	0.294	0.157	0.311	0.05	0.07	0.042	0.097	0.08	0.16
-	10 mM H_2O_2	24.5	16	6.66	6.57	42.9	34.4	3.5	4.2	0.891	0.204	0.157	0.328	0.04	0.08	0.057	0.076	0.10	0.14
-	10 mM H_2O_2	25	19	6.50	6.48	26.0	34.3	2.7	3.3	0.864	0.164	0.159	0.331	0.05	0.08	0.061	0.084	0.11	0.15
-	10 mM H_2O_2	26	24	6.49	6.52	39.6	27.5	3.0	5.7	0.832	0.120	0.158	0.335	0.05	0.06	0.052	0.061	0.12	0.16
-	10 mM H_2O_2	28		6.69		36.7		2.2		0.785		0.155		0.05		0.064		0.11	
-	10 mM H_2O_2	32		6.89		31.7		3.2		0.733		0.195		0.05		0.041		0.11	
-	10 mM H_2O_2	36		6.72		26.8		3.1		0.676		0.200		0.06		0.058		0.10	

APPENDIX D

ORIGINAL DATA ASSOCIATED WITH CHAPTER 5

Table 28 for Figure 31. Concentration profile of nickel, total cyanide, and EDTA in the oxic AIM system for nickel-cyanide and nickel-EDTA batches, in compared with nickel, cyanide, and EDTA only.

Media	T (h)	Ni^{2+} in Ni-EDTA (mg/L)	Ni^{2+} in Ni-CN (mg/L)	Ni^{2+} in Ni only (mg/L)	Total cyanide in Ni-CN (mg/L)	Total cyanide in CN only (mg/L)	EDTA in Ni-EDTA (mM)	EDTA in EDTA only (mM)
AIM	0	50.0	50.0	50.0	20.0	20.0	0.50	0.50
AIM	0.1	47.61	45.57	42.10	16.368	15.480	0.403	0.371
AIM	0.5	31.03	29.16	27.20	12.590	11.764	0.297	0.171
AIM	1	21.12	19.58	17.90	8.544	7.902	0.231	0.146
AIM	2	16.52	11.64	11.48	4.729	4.358	0.168	0.118
AIM	4	12.55	6.93	6.41	2.728	2.802	0.123	0.096
AIM	8	7.83	2.93	2.32	1.276	1.226	0.087	0.074
AIM	12	5.29	1.45	1.04	0.672	0.669	0.072	0.063
AIM	24	2.12	0.28	0.19	0.156	0.145	0.056	0.047

Table 29 for Figure 32. Concentration profile of nickel, total cyanide, and EDTA of mixed source in oxic, 10, and 50 mM H_2O_2-AIM batch system.

Media	T (h)	EDTA (mM)			Total cyanide (mM)			Ni^{2+} (mg/L)		
		-	10 mM H_2O_2	50 mM H_2O_2	-	10 mM H_2O_2	50 mM H_2O_2	-	10 mM H_2O_2	50 mM H_2O_2
AIM	0	0.50	0.50	0.50	20.0	20.0	20.0	50.0	50.0	50.0
AIM	0.1	0.423	0.378	0.355	17.499	12.393	12.480	47.88	48.28	45.10
AIM	0.5	0.312	0.162	0.131	12.885	7.441	6.764	33.84	29.46	28.20
AIM	1	0.221	0.123	0.095	10.670	4.213	4.102	25.30	19.17	18.90
AIM	2	0.172	0.092	0.064	7.505	1.982	1.758	18.72	13.04	12.48
AIM	4	0.133	0.061	0.037	3.899	0.858	0.702	13.11	7.87	6.51
AIM	8	0.097	0.032	0.021	1.195	0.369	0.256	8.44	3.51	2.42
AIM	12	0.082	0.021	0.015	0.658	0.196	0.120	6.39	2.12	1.34
AIM	24	0.063	0.015	0.012	0.192	0.102	0.065	2.92	0.89	0.39

Table 30 for Figure 33. Concentration profile of nickel, total cyanide, and EDTA for nickel-cyanide-EDTA mixed source in 10 and 50 mM H_2O_2-AIM continuous batch system.

Media	50 mM H_2O_2				10 mM H_2O_2			
	T (h)	Ni^{2+} (mg/L)	EDTA (mM)	Total cyanide (mg/L)	T (h)	Ni^{2+} (mg/L)	EDTA (mM)	Total cyanide (mg/L)
AIM	0	50	0.500	20	0	50	0.5	20
AIM	0.1	45.1	0.311	12.48	0.1	48.28	0.378	13.393
AIM	0.5	28.2	0.120	4.764	0.5	29.46	0.162	7.441
AIM	1	18.9	0.080	2.102	1	19.17	0.123	4.213
AIM	2	12.48	0.058	1.058	2	13.04	0.092	2.182
AIM	4	6.01	0.038	0.502	4	7.87	0.061	1.058
AIM	8	2.42	0.020	0.186	8	3.51	0.032	0.299
AIM	8.01	52.42	0.520	20.186	12	2.12	0.021	0.136
AIM	8.1	47.33	0.505	14.899	12.01	52.12	0.521	20.136
AIM	8.5	31.32	0.352	5.736	12.1	49.41	0.503	15.723
AIM	9	23.82	0.256	2.888	12.5	38.25	0.458	8.839
AIM	10	16.13	0.186	1.423	13	27.76	0.386	5.909
AIM	12	9.31	0.095	0.723	14	18.66	0.312	4.028
AIM	16	3.74	0.035	0.281	16	10.92	0.188	2.167
AIM	20	2.05	0.018	0.153	20	5.25	0.091	0.822
AIM	20.01	52.05	0.518	20.153	24	3.42	0.048	0.364
AIM	20.1	48.33	0.495	15.899	30	2.46	0.025	0.153
AIM	20.5	33.32	0.352	8.736	30.01	52.46	0.525	20.153
AIM	21	26.82	0.286	4.888	30.1	49.33	0.503	16.723
AIM	22	18.13	0.199	2.423	30.5	38.32	0.458	11.839
AIM	24	11.31	0.109	1.063	31	29.82	0.399	9.109
AIM	28	5.74	0.046	0.401	32	21.13	0.323	5.228
AIM	32	3.42	0.024	0.193	34	13.31	0.229	3.067
AIM	36	2.35	0.015	0.131	36	9.34	0.161	1.992

Table 31 for Figure 34. Concentration profile of a) nickel, b) total cyanide, and c) EDTA for nickel-cyanide-EDTA mixed source in the two-stage H_2O_2-AIM CSTR system.

T (d)	Fe^{2+} (mg/L)		Ni^{2+} (mg/L)		Total cyanide (mg/L)		EDTA (mM)		TOC (mg/L)		NH_4^+ (mM)	
	R1	R2	R1	R2	R1	R2	R1	R2	R1	R2	R1	R2
1	46.8	0.6	5.28	0.06	0.074	0.045	0.081	0.016	9.7	1.95	1.04	0.26
3	58.3	0.3	12.72	0.07	0.194	0.042	0.102	0.017	12.4	2.04	2.34	0.52
4	70.1	0.2	19.55	0.09	0.150	0.075	0.128	0.028	15.5	3.37	1.76	0.44
7	83.4	0.3	17.39	0.11	0.222	0.040	0.147	0.029	17.7	3.48	2.29	0.38
9	77.5	0.7	18.81	0.31	0.224	0.044	0.119	0.025	14.3	3.04	1.84	0.46
11	84.2	0.2	17.52	0.34	0.152	0.029	0.133	0.018	16.1	2.18	1.55	0.39
14	76.8	0.6	14.34	0.25	0.212	0.022	0.112	0.019	17.4	2.29	2.43	0.61
16	76.4	0.6	16.45	0.18	0.198	0.024	0.098	0.019	15.5	2.32	2.25	0.75
18	64.3	0.3	17.22	0.33	0.186	0.021	0.142	0.021	17.1	2.57	2.33	0.58
21	70.1	0.2	22.23	0.51	0.289	0.045	0.192	0.041	19.1	4.94	2.26	0.56
23	53.4	0.2	18.56	0.39	0.165	0.032	0.110	0.029	17.1	3.48	1.76	0.44
25	57.5	0.7	15.52	0.26	0.202	0.033	0.098	0.020	16.1	2.40	2.29	0.33
27	64.1	0.9	17.87	0.18	0.189	0.017	0.124	0.030	17.4	3.59	1.91	0.48
30	64.8	0.6	17.69	0.24	0.220	0.030	0.130	0.021	17.5	2.54	2.04	0.51